AGATA, Technical Proposal for an Advanced Gamma Tracking Array for the European Gamma Spectroscopy Community

D. Bazzacco, B. Cederwall, J. Cresswell, G. Duchêne, J. Eberth, W. Gast, J. Gerl, W. Korten, I. Lazarus, R.M. Lieder, et al.

AGATA

AGATA

Technical Proposal

for an

Advanced Gamma Tracking Array

for the

European Gamma Spectroscopy Community

Edited by J. Gerl and W. Korten

September 2001

This proposal has been written and edited by

D. Bazzacco (INFN Padova), B. Cederwall (Royal Inst. Tech. Stockholm), J. Cresswell (Univ. Liverpool), G. Duchêne (IRES Strasbourg), J. Eberth (Univ. Köln), W. Gast (FZ Jülich), J. Gerl (GSI Darmstadt), W. Korten (CEA Saclay), I. Lazarus (CLRC Daresbury), R.M. Lieder (FZ Jülich), J. Simpson (CLRC Daresbury) and D. Weisshaar (Univ. Köln).

Acknowledgements

This document was prepared with significant input of many scientists from the international nuclear structure community. It is based on R&D results from the European TMR Network Project *Development of γ-Ray Tracking Detectors for 4π γ-Ray Arrays* initiated by the EUROBALL collaboration, the Italian MARS project, and the GRETA project in the USA. Colleagues from 24 institutions provided advice, comments and suggestions resulting in a document that reflects the needs of a large community and a concurrent view of the best technical solution for the required next generation γ-spectrometer. The authors like to thank the following scientists and engineers for their contribution and apologize to everyone we failed to contact or who contributed and are inadvertently not listed below:

F. Azaiez (IPN Orsay), E. Badura (GSI, Darmstadt), F.A. Beck (IRES Strasbourg), M. Bellato (INFN Padova), P. v. Brentano (Univ. Köln), A. Boston (Univ. Liverpool), C. Bourgeois (IPN Orsay), P. Butler (Univ. Liverpool), B. Cahon (GANIL Caen), F. Camera (INFN Milano), P. Coleman-Smith (CLRC Daresbury), M. Descovich (Univ. Liverpool), G. de France (GANIL Caen), H. Emling (GSI Darmstadt), H. Essel (GSI Darmstadt), H. Geissel (GSI Darmstadt), M. Gorska (GSI Darmstadt), H. Grawe (GSI Darmstadt), D. Habs (Univ. München), F. Hannachi (CSNSM Orsay), K. Hauschild (CEA Saclay), M. Hellström (GSI, Darmstadt), B. Herskind (NBI Copenhagen), J. Hoffmann (GSI Darmstadt), H. Hübel (Univ. Bonn), J. Jolie (Univ. Köln), N. Karkour (CSNSM Orsay), I. Kojouharov (GSI Darmstadt), Y. Kopatsch (GSI Darmstadt), A. Korichi (CSNSM Orsay), T. Kröll (INFN Padova), N. Kurz (GSI, Darmstadt), D. Linget (CSNSM Orsay), J. Lisle (Univ. Manchester), S. Mandal (GSI Darmstadt), M. Maier (LBNL Berkeley), H. van der Marel (Univ. Stockholm), A. Lopez-Martens (CSNSM Orsay), P. Medina (IRES Strasbourg), I. Merlin (CSNSM Orsay), L. Mihailescu (FZ Jülich), B. Million (INFN Milano), P.J. Nolan (Univ. Liverpool), J. Nyberg (TSL Uppsala), C. Pearson (Univ. Surrey), Z. Podolyak (Univ. Surrey), V. Pucknell (CLRC Daresbury), B. Quintana Arnes (INFN Padova), N. Redon (IPN Lyon), P. Reiter (Univ. München), M. Rejmund (CEA Saclay), M. Richter (GSI Darmstadt), C. Ring (IRES Strasbourg), G. Ripamonti (PT Milano), E. Roeckl (GSI Darmstadt), M. Rossewij (FZ Jülich), C. Rossi-Alvarez (INF Padova), H. Schaffner (GSI Darmstadt), H. Scheit (MPI Heidelberg), C. Schlegel (GSI Darmstadt), G. Sletten (NBI Copenhagen), R. Schwengner (FZ Rossendorf), G. Smith (Univ. Manchester), H. J. Thomas (Univ. Köln), J. Thornhill (Univ. Liverpool), K. Vetter (LBNL Berkeley), R. Wadsworth (Univ. York), A. Wagner (FZ Rossendorf), O. Wieland (INFN Milano), H.J. Wollersheim (GSI Darmstadt).

Contents

Preamble

An Advanced GAmma-ray Tracking Array, AGATA, is proposed for high-resolution γ-ray spectroscopy with exotic beams. AGATA will employ highly segmented Ge detectors as well as fully digital electronics and relies on newly developed pulse-shape analysis and tracking methods. The array is being designed in a way that it provides optimal properties for nuclear structure experiments in a wide range of beam velocities (from stopped to v/c ≈ 50%), almost independent of beam quality and background conditions. Selectivity and sensitivity of AGATA will be superior to any existing γ-array by several orders of magnitude. Hence, it will be for a long time a rich source for nuclear structure physics providing the means for new discoveries and opening challenging new perspectives.

To build the AGATA array a European collaboration will be established. By joining together the leading European groups working in the different areas of γ-ray spectroscopy, the necessary strength and expertise to carry out the AGATA project will be provided. The principles of γ-ray tracking have been developed within the European TMR Network Project *Development of γ-Ray Tracking Detectors for 4π γ-Ray Arrays*, initiated by the EUROBALL collaboration, the Italian MARS project, and by the GRETA project in the USA. Valuable experience is also obtained from the new γ-ray spectrometers for radioactive-beam facilities currently being built from highly segmented Ge detectors (MINIBALL, EXOGAM and VEGA). AGATA will be realised based on this knowledge and experience. Following an initial design and development phase, for which a EU-IHP proposal has been submitted, the array is optimally built in steps. In this way sub-arrays of AGATA can already be used for nuclear structure experiments. The implementation of the full array is expected to take about eight years.

To maximise the physics output both qualitatively and quantitatively, AGATA needs to operate permanently and with a large variety of beams. To this end experimental campaigns with complementary physics programs at major European host facilities will be promoted by the collaboration, rendering AGATA a truly European initiative.

2. Introduction

2.1 Motivation

The nucleus is a unique strongly interacting quantum mechanical system. Consisting of a few to a few hundred nucleons, its structure combines the macroscopic features expected of nuclear matter in a bulk form with the microscopic properties associated with the motion of a finite number of fermions in a potential well. It represents a self-bound, complex system, which displays a rich variety of excitation modes governed by the interplay of nucleons in individual orbits and by their collective behaviour.

Understanding nuclear excitations is one of the principal goals of nuclear structure studies. The most powerful tool to investigate nuclear structure under extreme conditions is high precision γ-ray spectroscopy. The study of the γ-decay properties of the atomic nucleus has provided an enormous quantity of information on the behaviour of such a system, for example, under the influence of high temperatures, high spin or large deformations as well as for extreme isospin values (the proton-to-neutron ratio) and of the total nuclear mass. The decay of nuclei that are created in a nuclear reaction in a state of finite excitation energy, temperature and spin to the ground state is characterised by the emission of a certain number of γ rays. The information about how the nuclear structure changes during the decay as the nucleus loses energy and angular momentum is obtained by measuring the properties of these γ rays, such as their energy, the emission sequence and the time relationships as well as their electro-magnetic properties.

New challenges for nuclear spectroscopy are imminent at a time when high intensity radioactive ion beams are emerging in a wide energy range: from the Coulomb energy regime, typical for the European ISOL facilities (SPIRAL and the planned EURISOL), to the intermediate and relativistic energy regimes of fragmentation facilities, such as SIS/FRS and in particular the new GSI facility. In the Coulomb energy regime the classical reaction types (transfer, deep-inelastic or compound reactions) become available with intensities comparable to that of today's stable beams. At intermediate energies, i.e. between 50 and 200 MeV/u, Coulomb excitation can be employed to populate low-spin states; depending on the available beam energy highly excited states up to the giant resonances can be reached. For even higher energies secondary fragmentation becomes a powerful tool to create very exotic fragments that are excited to relatively high spins, i.e. in violent collisions spins of more than 30ħ can be reached [Pfü01]. Finally, the rarest species, i.e. close to the drip lines, can be studied using decay spectroscopy after implantation.

Exotic beams allow approaching and mapping the drip-line regions in order to answer the open questions in nuclear structure physics and to explore nuclear stability at the very limits. Nuclei far from stability allow amplifying and isolating particular aspects of the nuclear interaction and dynamics and may favour the occurrence of new symmetries. First and foremost, high-resolution γ-spectroscopic studies will open up unique possibilities allowing a very rich physics program to be addressed that covers the full range of topics in which the nuclear physics community is currently interested: The investigation of exotic nuclei will be aiming at essentially all *nuclear degrees of freedom*, such as (i) proton-rich nuclei at and beyond the proton drip line and the extension of the N=Z line, (ii) neutron-rich nuclei towards the drip line in medium heavy elements and (iii) the heaviest elements and towards new super-heavy elements. The *internal degrees freedom* of nuclei will be exploited by investigating (i) ultra-high spin states produced in extremely cold reactions, (ii) meta-stable states at

high spins and at very large deformation, (iii) Multi-Phonon Giant resonances as well as other high-temperature phenomena, such as quantum chaos.

An instrument of major importance for these studies is a high performance γ-ray spectrometer capable of disentangling the structure of exotic nuclei produced with extremely small cross section in an overwhelming background of less exotic nuclei and possibly under the constraint of severe Doppler effects. In the following section the requirements for such a spectrometer are discussed, naturally leading to a new type of instrument, the γ-tracking array. Finally, the worldwide developments, which have lead to the possibility of constructing this spectrometer, are summarised.

2.2 Requirements for AGATA

Even though radioactive beams from next generation facilities will often approach today's intensity of stable beams, the most exotic nuclei under investigation will always be produced with extremely low rates. A γ-ray spectrometer to study these nuclei must be a universal instrument capable of measuring γ radiation in a large energy range (from a few tens keV up to 10 MeV and more), with the largest possible efficiency and with a very good spectral response. The nuclei of interest are often rarely produced, but can be accompanied by much more abundant, less exotic species. The radiation can be emitted by fast moving sources and in a hostile environment of high background radioactivity (Bremsstrahlung, neutrons and charged particles, etc.). This requires the simultaneous optimisation of several and sometimes conflicting properties:

- The ***full energy*** or photopeak ***efficiency*** (ε_{fe}), i.e. the probability to detect the total energy of any emitted photon individually, must be maximised (for both low and high γ-ray multiplicity) in order to identify the weakest reaction channels.

- A very good spectral response measured by the ***peak-to-total ratio*** (P/T), i.e. the ratio of full energy efficiency to the total interaction efficiency, must be obtained in order to preserve good spectrum quality also for high-fold coincidences.

- A very good ***angular resolution*** for the emission direction of the detected γ-quanta must be achieved in order to sufficiently reduce the strong Doppler effects of radiation sources moving with velocities up to v/c ~ 0.5.

- The system must be capable of high ***event rates***, either because the background radioactivity might dominate for very low intensity radioactive beams or because a very high luminosity is needed in order to populate the weakest reaction channels.

- A suitable free inner space must be available in order to allow for additional detection systems inside the Ge ball that allow to better select the nuclei of interest, i.e. ***ancillary detectors*** to measure light charged particles, heavy ions, etc.

These features can only be simultaneously achieved by a new generation of spectrometers built from a close-packed arrangement of γ-ray tracking detectors and resembling a 4π shell of large segmented Ge crystals. The individual interaction points of the γ quanta have to be disentangled by numerical (*tracking*) algorithms (see chapter 3). In the following we will explain the basic properties of such a system, called the **A**dvanced **GA**mma **T**racking **A**rray (**AGATA**), and deduce its possible performance. In table 2.1 the properties of AGATA, as it

Table 2.1: *Basic properties as required for AGATA and compared to an ideal Ge shell of 9 cm thickness and an inner free radius of 150 mm.*

Detector properties specified for		Ideal Ge-shell	AGATA
Efficiency (P_{fe})	E_γ = 0.1 MeV, M_γ = 1, $0 < \beta < 0.5$	100 %	> 70 %
	E_γ = 1 MeV, M_γ = 1, $0 < \beta < 0.5$	72 %	~ 50 %
	E_γ = 10 MeV, M_γ = 1, $0 < \beta < 0.5$	15 %	~ 10 %
	E_γ = 1 MeV, M_γ = 30, $0 < \beta < 0.5$	36 %	~ 25 %
Peak-to-total ratio (P/T)	E_γ = 1 MeV, M_γ = 1	85 %	60 – 70 %
	E_γ = 1 MeV, M_γ =30	60 %	40 – 50 %
Angular resolution ($\Delta\theta_\gamma$)	$\Delta E/E < 1\%$	—	better than 1°
Maximum event rates	M_γ = 1	—	3 MHz
	M_γ = 30	—	0.3 MHz
Inner free space (R_i)		150 mm	170 mm

will be derived in the following chapters, is summarised and compared to the properties of an ideal shell using the same amount of Ge material as has been employed for EUROBALL. The ideal shell provides a suitable and easy to generate reference to compare properties of detector designs. With the properties anticipated for AGATA several orders of magnitude improvement in resolving power will be obtained making the advanced γ-tracking array extremely more powerful than all current or near future arrays.

The ***total full energy efficiency*** (P_{fe}) for a single γ ray is essentially determined by the amount of Ge material that can be placed around the radiation source since it depends on the probability that the total energy is absorbed by the detector. The ideal shell represents the optimal performance for a given mass of germanium material surrounding the radiation source. Using the best techniques available today for constructing closely packed arrays of Ge detectors, i.e. composite detectors of encapsulated Ge crystals (see chapter 2.3), close to 80% of the total solid angle can be covered with active Ge material. In that way a maximum total full energy efficiency above 70% can be obtained for low-energy γ rays (around 100 keV) that have a much smaller interaction length compared to the length of the detectors.

For higher energy γ rays the thickness of the Ge shell becomes very important. With Ge crystals of 10 cm length a total full energy efficiency close to 50% should be possible (at an energy of 1 MeV), compared to the best high-spin spectrometers for stable beams (P_{fe} ~ 10%) and current high-efficiency spectrometers for radioactive beams (P_{fe} ~ 20%). With this choice of crystals it will be possible to achieve ~ 10% efficiency even for 10 MeV γ rays, while using even longer crystals will increase the costs dramatically.

For a higher γ-ray multiplicity it must be ensured that different γ rays do not deposit energy in the same detection element. To optimise this "single-hit probability" the number of detection elements must be very large compared to the total number of interactions in the detector.

Simulations have shown that each detection element should not cover a solid angle larger than 10^{-3} of 4π, which together with a suitable segmentation in depth leads to a total number of detection elements of the order of 6000-8000. In this situation the full energy efficiency will be essentially determined by the effectiveness of the tracking algorithms in reconstructing the tracks of the γ-rays. Realistic simulations of the tracking performance (see chapter 3.3) indicate that an efficiency of ~25% for an energy of 1 MeV and at $M_\gamma = 30$ can be reached. The superiority of AGATA in every domain of γ-ray spectroscopy is clearly demonstrated by a comparison with the best high-spin spectrometers for stable beams ($P_{fe} \sim 6$ % at $M_\gamma = 30$).

The ***peak-to-total ratio*** describes the spectral response of the detector. In a tracking spectrometer the P/T ratio can be optimised by the tracking algorithms (see chapter 3.2). In this way a P/T ratio up to 70% can be reached for individual 1 MeV γ-rays. Even at multiplicity $M_\gamma = 30$ a very good P/T ratio of 50% can be achieved. When the tracking is optimised to obtain highest efficiency a P/T ratio of 60% can still be realised at low multiplicity, which compares favourably with conventional γ-ray spectrometers using escape-suppressed detectors.

An optimal ***position resolution*** is also assured by the high granularity of AGATA, since the segments are sufficiently small in order to determine the interaction position(s) within one segment with very high precision (see chapter 3). This key feature of AGATA allows to determine the emission direction of all detected γ-quanta within an opening angle smaller than 1°, corresponding to an array with an "effective granularity" of $\sim 10^5$ elements. In this way an energy resolution better than 0.5 % is ensured for transitions emitted by nuclei at velocities up to v/c = 50 %. This value is comparable to current spectrometers used at 10 times smaller recoil velocities and is only a factor of 2 larger than the intrinsic resolution of Ge detectors at 1 MeV.

AGATA performance under realistic conditions

The reactions used to create and investigate exotic nuclei can have very different characteristics and often rely crucially on different parameters of the detection system. They can be characterised by the following variables:

The ***multiplicity of emitted γrays*** (M_γ) and of the associated background radiation (M_x): It is highest for fusion-evaporation reactions reaching $M_\gamma = 30$ or higher. Fragmentation reactions and (low-energy) inelastic excitations typically lead to $M_\gamma = 10$ while isomeric decays and Coulomb excitation (especially at relativistic energies) are limited to M_γ = 1-5. The background radiation is highest for reactions at relativistic energies and using heavy targets, i.e. for Coulomb excitation $M_x = 10$ can be reached, while with lighter targets M_x = 1-5 is more typical. At energies around the Coulomb barrier the main background comes from neutrons and charged particles having again multiplicities below 5.

The ***velocity of the emitting source*** (v/c): It can be as high as v/c ~ 50% for reactions at relativistic energies (fragmentation and Coulomb excitation). Inelastic scattering and fusion reactions at energies around the Coulomb barrier produce velocities of v/c = 1–10%, while isomeric decays are usually observed from radiation sources at rest.

The ***reaction rates*** as determined by the (available) beam intensity, the useful target thickness and the (total) reaction cross section will be extremely diverse: Secondary fragmentation reactions, i.e. induced by radioactive beams (10^9 pps), and fusion reactions with high primary beam intensities (10^{12} pps) can produce very high source rates of 10^6–10^7 Hz; fusion reactions induced by radioactive beams (10^9pps) and Coulomb excitation of exotic nuclei (10^6 pps) will

Table 2.2: *AGATA characteristics for a few typical reaction cases : The properties of the different reaction types are described in the text. All values are given for a γ-ray energy of 1 MeV. Note that the results are obtained with today's state-of-the-art tracking codes. Due to improved algorithms and increased computer power an efficiency increase of about 25 % is expected at the time when AGATA comes online. The maximal event rate is extrapolated from the design value of 300 kHz at M=30.*

	Full energy efficiency (P/T ratio)	Maximal event rate	Energy resolution
Relativistic Coulomb excitation: M = 10, v/c ~ 20%	28 % (51 %)	0.9 MHz	~ 3.5 keV (0.6 %)
Secondary fragmentation : M = 15, v/c ~ 50%	24 % (46 %)	0.6 MHz	~ 5 keV (0.7 %)
High-spin spectroscopy : M = 30, v/c ~ 5%	22 % (45 %)	0.3 MHz	~ 2.5 keV (0.3 %)
Isomer spectroscopy : M = 5 + 5, v/c = 0	31 % (53 %)	0.9 MHz	< 2.3 keV (0.2%)

produce more moderate source rates of the order of 10^4–10^5 Hz, while decay spectroscopy will be performed at rates well below 1 Hz.

In the following sections the performance of AGATA as expected under real experimental conditions is compared to current state-of-the-art spectrometers. The RISING [Ang01] project at GSI uses 15 EUROBALL Cluster detectors and is optimised for experiments at very high velocity. The performance of EXOGAM [Sim97], i.e. 16 large-volume segmented Clover detectors used for low-energy radioactive-beam experiments at GANIL, is estimated either for the close configuration (i.e. detectors at 115 mm distance) or the wide one (at 150 mm distance) depending on the experimental situation. The energy resolution given for EXOGAM does not take into account a possible (future) improvement of measuring the emission direction by pulse-shape analysis. Some typical experiments for the investigation of exotic nuclei have been chosen. The results are also summarised in table 2.2. It should be noted that the AGATA results are obtained with today's state-of-the-art tracking procedures, which are likely to considerably improve for the final array.

Coulomb excitation of exotic nuclei at relativistic energies

High-energy fragmentation creates exotic nuclei at high velocities suitable for intermediate-energy Coulomb excitation. Secondary beam intensities of up to 10^9 pps can be achieved, but the most interesting cases will be much less abundant. Therefore, in most cases the maximum allowable reaction rate will not present a limitation. The γ-ray multiplicity is usually small ($M_\gamma \sim 2$), but the reaction is often dominated by low-energy background radiation ($M_x \sim 8$), especially if heavy targets are used to maximise the cross section. In this typical situation the efficiency of AGATA is excellent (~28%) and at v/c ~ 20% the experiments can be realised with a very good energy resolution (~5.5 keV). This combination is not achievable with any other state-of-the-art γ-ray spectrometer; the non-segmented Cluster detectors used for RISING give a rather small efficiency (~2.7%) when used at distances large enough to keep the solid angle and hence the energy resolution reasonably good (~12 keV). The EXOGAM spectrometer in its close configuration has a good efficiency (~13%) under the same conditions, but the energy resolution decreases dramatically (~50 keV), unless the same principles as in AGATA are used to determine the interaction position within a segment (see chapter 3). For both spectrometers a P/T ratio below 40% is expected compared to 51% for AGATA.

Secondary fragmentation reactions leading to highly excited nuclei

Very exotic nuclei can be created with secondary fragmentation, i.e. fragmentation induced by a high-energy secondary beam. Here the maximum available intensity is needed in order to create highly excited tertiary fragments. Violent collisions can populate high-spin states, but proceed only with very low cross sections. Consequently, the total reaction rate will be very high and determines the limit of AGATA. Intermediate γ ray and background multiplicities will be observed ($M_\gamma \sim 10$, $M_x \sim 5$) and Doppler effects are very strong due to the extreme velocity (v/c ~ 50%). Even in this situation the energy resolution of AGATA will still be comparable to values currently obtained at much smaller velocities (~6.5 keV) and very good values for efficiency (24%) and spectrum quality (P/T ~ 46%) can be obtained. For today's state-of-the-art spectrometers the same deficiencies as before are observed (concerning efficiency (RISING) and energy resolution (EXOGAM), but they are even more pronounced.

Fusion-evaporation reaction induced by intense radioactive or stable beams

Typical beam intensities range from 10^9 to 10^{12} pps, depending whether radioactive or stable beams are being used. In the latter case, the primary beam intensity probably needs to be reduced in order to limit the total reaction rate to the design value ($0.3 \cdot 10^6$ Hz at M = 30). At energies around the Coulomb barrier the fusion products have moderate velocities (up to v/c ~ 5%), but the multiplicity can be very high ($M_\gamma \sim 25$, $M_x \sim 5$). Nevertheless the efficiency is still above 20% and much larger than obtained with any current spectrometer. The P/T ratio is reduced, but still comparable to conventional escape-suppressed spectrometers. The energy resolution is practically unchanged from the intrinsic resolution of the detectors. It is indeed much better than those obtained with current spectrometers in similar circumstances.

Decay studies of a drip-line nucleus

In this case the reaction products are stopped and no Doppler effect occurs. The production rate is extremely small, often well below 1 Hz, but the total event rate can still be quite large. The γ multiplicity is usually not very large ($M_\gamma \sim 5$) and no (correlated) background is expected. In this case the best possible energy resolution is obtained with an efficiency of more than 30%. In this case the difference in performance is not as pronounced as in the higher velocity cases, but the high segmentation of the array is still very valuable in order to account for the "prompt flash" of background radiation from Bremsstrahlung ($M_x \sim 5$), especially if short-lived decays are being investigated.

2.3 World wide developments of γ-ray spectrometers

Early attempts to measure the evolution of nuclear structure with angular momentum and excitation energy via γ-ray spectroscopy were made with a few NaI(TI) scintillation detectors [Mor63]. The sensitivity of such experiments was limited both by the poor resolution of the scintillation detectors (about 90 keV at 1300 keV) as well as by the small number and size of the detectors. Nevertheless, such early experiments were able to establish the low spin ($I \leq 8$ - 10 ħ) rotational structure of nuclei [Mor63]. Scintillator arrays increased considerably in size with the construction of segmented shells of NaI(Tl) detectors arranged around the target. First examples of real 4π arrays are the 72-element Spin Spectrometer at Oak Ridge National Laboratory, USA. [Jae83] and the 162-element Crystal Ball at Max-Planck-Institute Heidelberg and GSI. These arrays made very efficient energy calorimeters and were capable

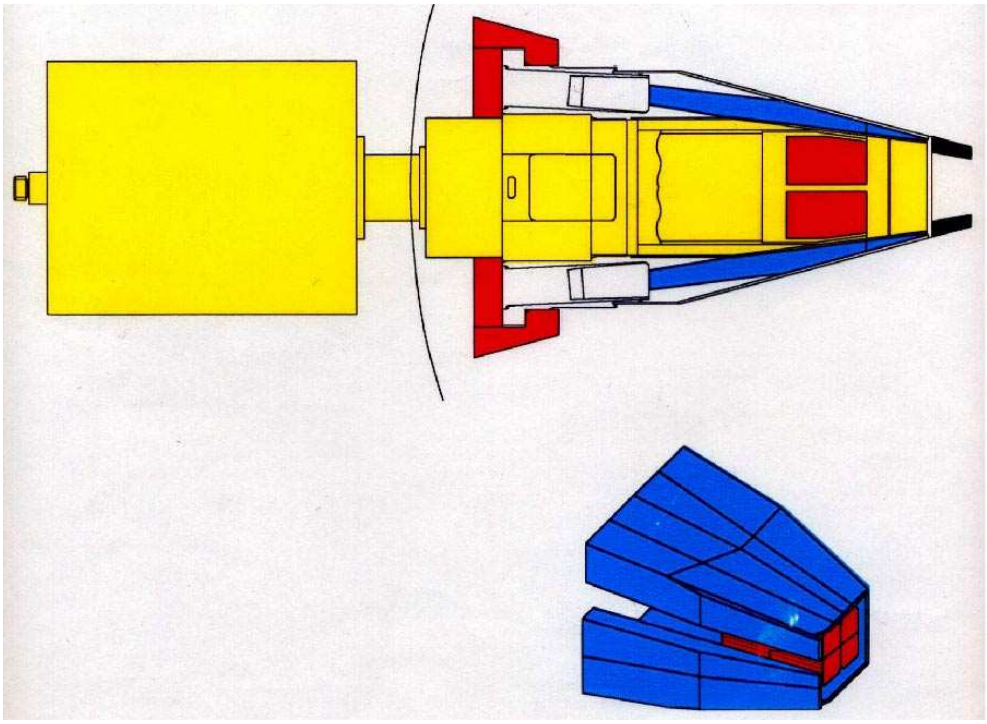

Fig. 2.1: *A schematic diagram of a modern escape suppressed spectrometer. The figure shows a Clover Ge detector of the Euroball array inside its BGO escape suppression shield comprising of 16 individual crystals.*

of detecting most of the energy emitted in the γ-ray cascade, but their application to discrete line γ-ray spectroscopy was limited by the limited energy resolution of NaI(Tl).

A major step forward came with the development of reverse biased germanium detectors in the mid 1960's. Germanium (either Ge(Li) or hyperpure-Ge) detectors have very good energy resolution, ranging from < 1 keV at 122 keV to ~ 2 keV at 1332 keV. The initial advance in the spectroscopy of high-spin states was taken at the Niels-Bohr Institute in the late 1970's when several Ge(Li) detectors were used in an array. Fast progress was indeed being made: the phenomenon of backbending (spin ~ 15ħ) was discovered by Johnson *et al.* [Joh71] using just two Ge(Li) detectors, while Riedinger *et al.* could establish the detailed quasi-particle structure of ^{160,161}Yb up to spin 30ħ [Rie80] using four such detectors.

Although these early experiments provided exceptional results, a major experimental problem remained; namely, that of a poor peak-to-background ratio caused by incomplete energy collection in the Ge detector. This problem is common to all experiments using bare Ge detectors. Even with today's large Ge detectors, a standard ^{60}Co source (with two γ-rays at 1173 and 1332 keV) typically produces a spectrum in which only ~ 20% of the counts are in the full energy (or photo-) peaks. The remaining ~ 80% of the counts form a continuous background at lower energies caused mainly by γ rays Compton scattering out of the Ge crystal. The solution is to detect this scattered radiation in a surrounding detector (an escape-suppression shield) and to reject coincident events between the Ge detector and the shield. The combination of Ge detector and shield is termed an escape-suppressed spectrometer (ESS). A schematic diagram of a modern ESS is shown in figure 2.1.

The suppression shields were initially large NaI(Tl) scintillation detectors. This scintillator material was superseded in the mid 1980's by the denser scintillator, bismuth germanate,

$Bi_4Ge_3O_{12}$ (BGO). This allowed suppression shields to be more compact and hence more ESS's could be arranged around a target. After suppression, typically 55% of the remaining counts are in the full energy photopeaks. The improvement in the spectrum quality obtained by use of an ESS is clearly demonstrated in figure 2.2. This improvement in the peak-to-total ratio (P/T) is crucial in coincidence spectroscopy. For example, in a doubles (γ-γ or γ^2) coincidence experiment the photopeak-photopeak coincidence probability is proportional to $(P/T)^2$. Therefore, for ^{60}Co, use of the suppression shield typically results in an improvement of more than a factor of 8 in the photopeak coincidences, when compared with the background, recorded in a doubles coincidence experiment. Even greater improvements are obtained when higher fold coincidence events are recorded. The improvement is typically a factor of 21 for triples (γ^3), 57 for quadruples (γ^4), and 157 for quintuples (γ^5).

The efficiency and sensitivity of escape-suppressed Ge detector arrays improved rapidly, so that by the mid 1980's arrays with ~ 20 ESS having total peak efficiencies of 0.5-1.0% were constructed. These arrays enabled the study of nuclear structure features that occur at an intensity of ~ 1% of the total intensity in the nucleus. World-wide there were about a dozen arrays [Sha88] with this level of sensitivity (for example; TESSA3 (UK) [Nol85], Chateau de Cristal (France) [Bec84], OSIRIS (Germany) [Lie84], NORDBALL (Denmark) [Her85], HERA (USA) [Dia84], 8π spectrometer (Canada) [Tar87]). One of the earliest of these arrays, the TESSA3 array, was situated at the Daresbury Laboratory in the United Kingdom. This array, which consisted of 16 ESS, had a total photopeak efficiency of 0.5%. It was used in the discovery of the classic discrete line superdeformed (SD) band in ^{152}Dy [Twi86] in the mid 1980's. Such SD structures carry around 1-2% of the individual nucleus production cross section. Using TESSA3 and other such arrays the discrete line level structure of atomic nuclei was extended to much higher spins and various exotic features of the nucleus, such as high spin band terminating states [Rag86] and superdeformation (I $\rightarrow$ 60$\hbar$) [Nol89] were studied.

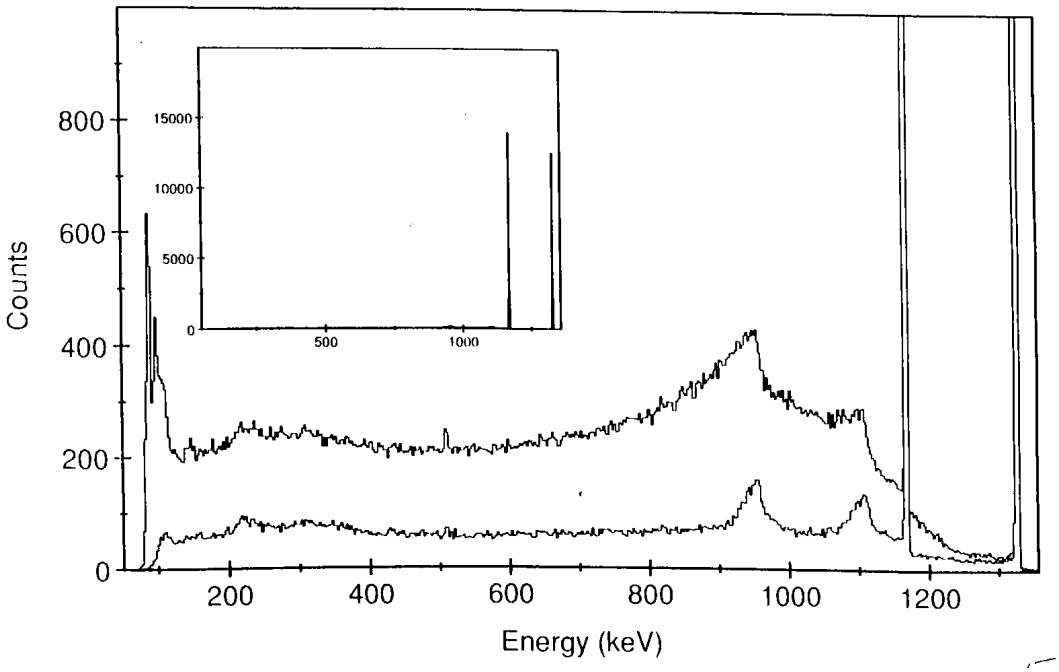

Fig. 2.2: *Unsuppressed and suppressed ^{60}Co spectra obtained with a Eurogam Phase 1 ESS. The y-axis has been scaled to show the details of the background. The insert showing the full photopeak intensity relative to the background indicates the overall quality of the spectrum.*

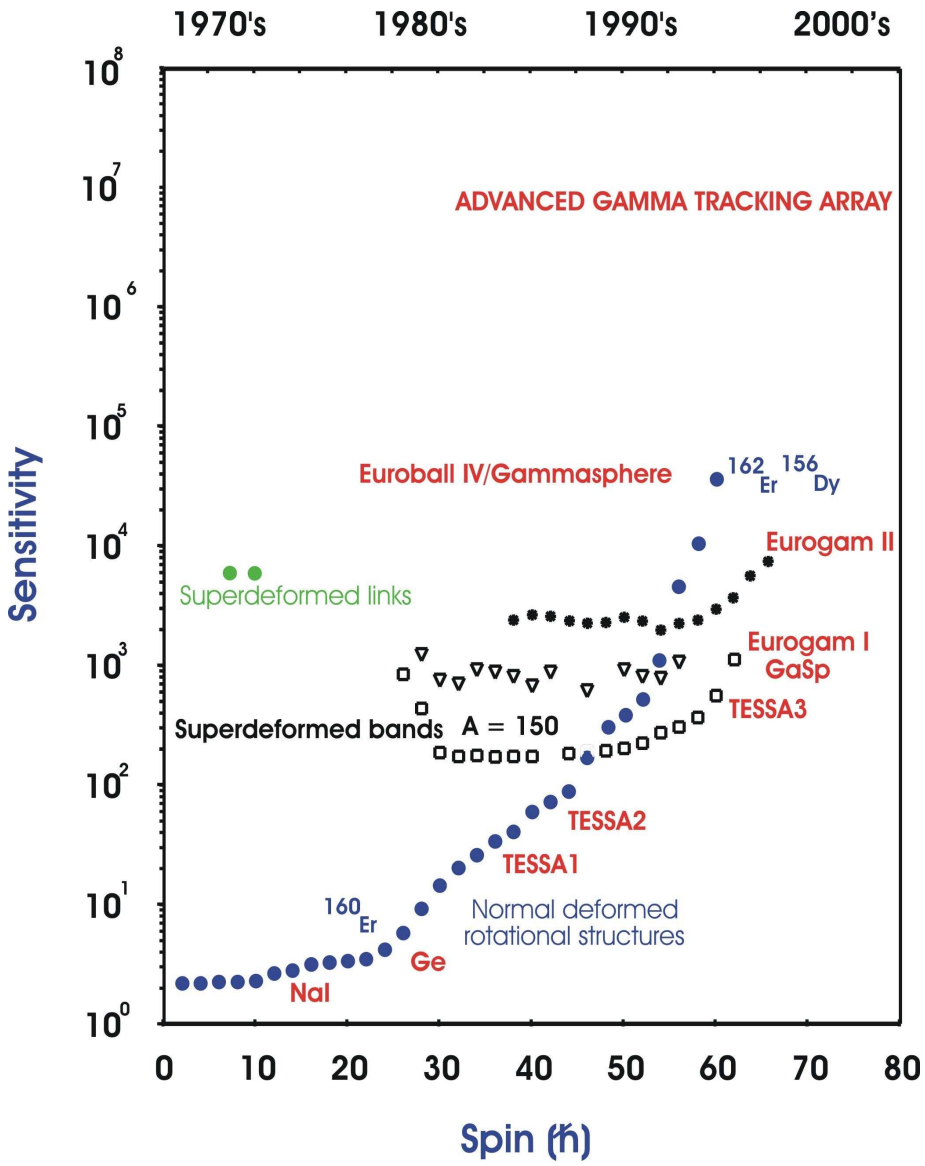

Fig. 2.3: *Plot of the spectroscopic sensitivity as a function of spin. Various arrays, including EUROBALL IV (no inner ball) and Gammasphere, are indicated at their approximate level of sensitivity in comparison with AGATA. The TESSA 1,2 and 3 arrays consisted of 4, 6 and 16 ESS respectively. The intensity distribution for selected high-spin phenomena is plotted. Normal deformed states up to spin ~ 50ħ in ^{160}Er [Sim87] and spin 60ħ in ^{156}Dy [Kon98] (●), the yrast superdeformed band in ^{152}Dy (□) [Twi86] and excited superdeformed bands in ^{151}Tb (△) [Byr90] and ^{152}Dy (+) [Dag94]. The links between the superdeformed bands and the normal deformed structures in the mass A = 190 region are also shown (*). The γ-ray energies range from 0 to ~1500 keV in this plot.*

The total efficiency continued to increase to ~5% in the 1990's with the GASP [Gas90, Ros93, Baz92], EUROGAM [Bea92, Bec92, Nol90] and the early implementation of the Gammasphere spectrometer in the USA [Gam88, Lee90]. Presently the highest efficiency and most powerful spectrometers used in stable beam nuclear structure studies are EUROBALL IV [Sim97] and the full Gammasphere. These spectrometers, with total photopeak efficiencies up to 10%, allow an unprecedented study of the properties of the atomic nucleus such that states of intensity down to or better than 10^{-6} of the production cross section can be observed. Figure 2.3 shows the fraction of the reaction channel that can be observed as a function of

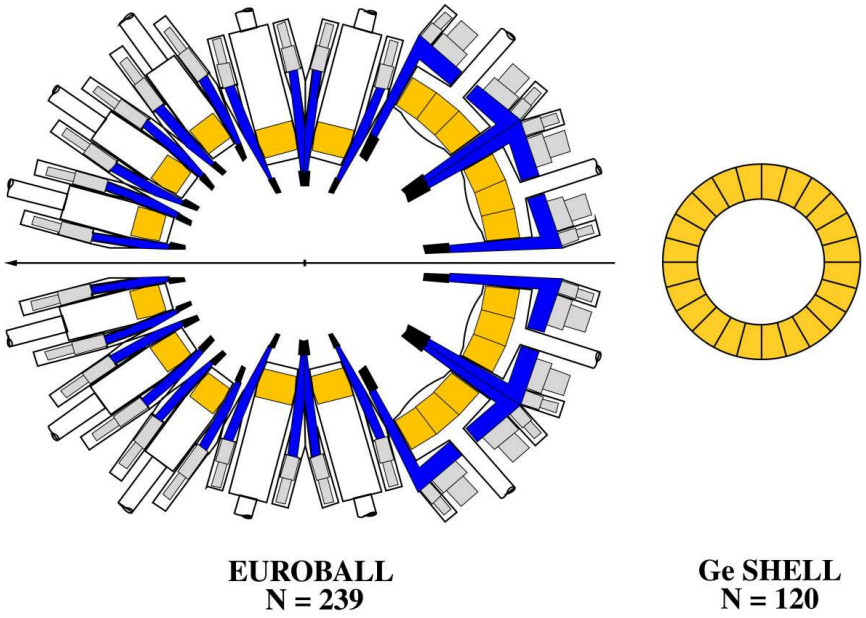

Fig. 2.4: *Section view of EUROBALL built from 239 Ge crystals and a Germanium shell built out of 120 detectors. Only the germanium part of the shell is shown. The two arrays are drawn to scale.*

spin for particular nuclear phenomena. The arrays associated with the discovery of these phenomena are indicated. This figure demonstrates the improvement in sensitivity with time as arrays developed from the TESSA spectrometers in the early to mid 1980's to EUROBALL III and Gammasphere spectrometers.

The state of the art with respect to 4π γ-detector arrays is represented by EUROBALL in Europe and Gammasphere in the USA, consisting partly of composite or (two-fold) segmented Ge detectors, respectively. Both spectrometers are optimised to study nuclear structure at high spins with heavy-ion induced fusion-evaporation reactions. The fact that, in these experiments, the nucleus is populated at maximum angular momentum results in a γ-multiplicity of an event of $M_\gamma \sim 30$ or more. In order to detect as many γ rays as possible out of the emitted 30 coincident γ rays a high total-absorption efficiency of the array and a high single-hit probability of the individual Ge detector are needed. Figure 2.4 shows a cross section of the EUROBALL spectrometer. It consists of 15 Cluster detectors (each composed of seven encapsulated Ge detectors) at backward angles, 26 Clover detectors (each composed of four detectors in one cryostat) in the central part and of 30 standard Ge detectors at forward angles. Each type of detector is surrounded by a BGO shield, which suppresses the Compton-escaped γ rays; at the same time these BGO shields act as collimators that prevent the scattering of γ rays from one Ge detectors to the others which would result in background events. Both EUROBALL and Gammasphere have enabled an impressive progress in nuclear structure physics during their so far 4 - 5 years of operation. For recent results achieved with EUROBALL we refer to the article by S. Lunardi [Lun00]. It should also be noted that composite Ge detectors, originally developed for nuclear structure, have become the standard for many applications, often outside the nuclear physics community, where large volume Ge detectors are needed.

In conclusion, most of the progress in nuclear spectroscopy within the last 30 years can be attributed to new developments in detector technology leading to an improved sensitivity as can be seen in figure 2.3. Today, the standard technology of escape-suppressed spectrometers

has reached its ultimate limit and new concepts are needed. The basis for a new generation of spectrometers has already been built through the development of composite and segmented Ge detectors as will be discussed in more detail in the following sections.

Position-sensitive Ge detectors – a new quality in γ-ray spectroscopy

The new exciting experimental perspectives at the radioactive beam facilities have triggered development programmes in Europe and the USA for γ-ray detector arrays with several orders of magnitude improvement in resolving power compared to their predecessors. However, a totally new concept is required in order to further increase the efficiency and granularity of 4π γ-detector arrays, ***a shell built purely from Ge detectors*** shown in figure 2.4 to scale besides the EUROBALL spectrometer. The Ge shell presented here is assumed to have an inner radius of 15 cm, a thickness of 9 cm and consists of 100-200 closely packed, individually encapsulated Ge detectors. In the present generation of γ-detector arrays, typically 30 % of the total solid angle is covered with germanium material, the rest being used by the BGO shields. On the contrary, the germanium coverage of the shell can be as high as 80 % so that the probability for a γ-ray to end up in the active, high-resolution part of the array is maximised.

Despite the larger solid-angle coverage, the total photopeak efficiency of this shell is a priori not better than for EUROBALL, while the peak-to-total ratio is actually 3 times smaller. The reason for such a poor performance is the large probability to detect more than one γ ray in the same detector and the scattering of γ radiation between the germanium detectors. However, if the tracks of the γ rays in the Ge shell are followed and all their individual interaction points are identified, a dramatic performance improvement will be obtained. In addition, for transitions emitted by fast moving nuclei, the Doppler-shift correction and therefore the final spectral resolution could be done in an optimal way, as the angles at which the γ rays hit the Ge detectors can be determined with high precision from the knowledge of the first interaction point.

This new concept is called γ-ray tracking. The target is surrounded by a 4π shell of 100 - 200 ***position-sensitive Ge detectors***. The position sensitivity of the detectors is achieved by a segmentation of the outer contact and by analysing the charge drift times within a segment and the mirror charges induced in the neighbouring segments. Thus, one will be able to detect the individual interaction points of a γ ray being Compton-scattered and finally absorbed in the Ge detectors. Reconstructing the γ-ray's track and comparing it with the Compton-scattering formula makes it possible to decide whether the γ ray was emitted from the target and fully absorbed in the Ge shell. From Monte-Carlo simulations one expects that a Ge tracking array will have highest efficiency (maximum coverage of the solid angle with Ge detectors), excellent performance for the correction of Doppler effects (emission angle of the γ ray determined from the first interaction point in the Ge detector) and a very good peak-to-total ratio (by distinguishing between fully and partially absorbed events).

Several Ge arrays are under construction using, for the first time, position-sensitive Ge detectors. MINIBALL [Ebe97] aims at the radioactive beam programme of REX-ISOLDE (CERN) and MAFF (Munich), EXOGAM [Sim97] is designed for use at the Spiral facility at GANIL and VEGA [Ger98] is mainly used at SIS/FRS at GSI . The physics programme at these radioactive beam facilities will concentrate on reactions with low γ-ray multiplicity, for example, Coulomb excitation and light-ion transfer reactions in inverse kinematics of exotic beams, respectively decay spectroscopy. The experiments require a high efficiency of the

arrays, because of the low expected event rates and a high effective granularity in order to improve the final resolution by Doppler correction.

All these spectrometers use Ge detectors that are segmented longitudinally, which allows the localisation of the main interaction of the γ-ray in two dimensions for Doppler correction, but they are not capable of a full γ-ray tracking, because of lacking segmentation in depth. In this sense, they are dedicated arrays for experiment with low γ-multiplicities, but they will already explore the technique of pulse-shape analysis with segmented detectors needed for future γ-ray tracking arrays.

The 4-fold segmented Clover detector for EXOGAM

The Exogam array [Sim97] will consist of 16 four-fold segmented Clover detectors [Sim00]. A schematic view of the Exogam array is shown in figure 2.5.

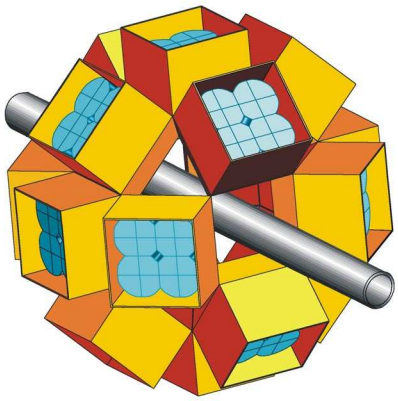

Fig. 2.5: *The EXOGAM Spectrometer.*

The Exogam Clover detector comprises four co-axial detectors mounted in the same cryostat, each being shaped from a relatively large volume Ge crystal (60 mm diameter and 90 mm length). The 20% design efficiency of the array is achieved by adding together signals from each crystal and signals caused by scattering between (two or more) adjacent crystals and/or Clovers. Each EXOGAM Clover is surrounded by a suppression shield comprising several bismuth germanate and cesium iodide scintillator detectors. The electronics developed for EXOGAM will include digital pulse processing in order to extract the radial position from the centre contact and the azimuthal position information from the mirror charges on the outer contacts. First tests have shown that pulse-shape analysis should allow to further subdivide each segment into ~16 pixels, leading to a total (effective) granularity of 4096 pixels.

The 6-fold segmented encapsulated Ge detector for Miniball

Miniball will consist of 40 six-fold segmented, encapsulated Ge detectors. The development is based on the encapsulation technology used for the Euroball-Cluster detector [Ebe96]. Encapsulation has proved to enhance the reliability of Ge detectors considerably. The failure rate of the 122 encapsulated Euroball detectors produced since 1993 is less than 4 %. After neutron damage all detectors have been annealed several times in the users lab and without any failure. From our experience we believe that this encapsulation technology is needed in order to build complex detector arrays with position-sensitive Ge detectors. Segmented Ge

detectors are more sensitive to the contamination of the passivated intrinsic surfaces, especially at the separation lines between the segments.

Encapsulation will help to preserve the properties of the detectors over many years. Even more important is the fact that, in systems using encapsulated detectors, the vacuum of the detectors is separated from the vacuum of the cryostat, which contains the cold parts of the preamplifiers. It has turned out that the position of the cold electronic components, shielding between the components and the wiring is crucial to prevent oscillation of the preamplifiers and cross talk between segments. Usually, the cryostat has to be opened several times before a perfect performance of the system is achieved. This procedure and also the repairs of the electronics can only be performed on systems with encapsulated detectors without running the risk of damaging the Ge detectors.

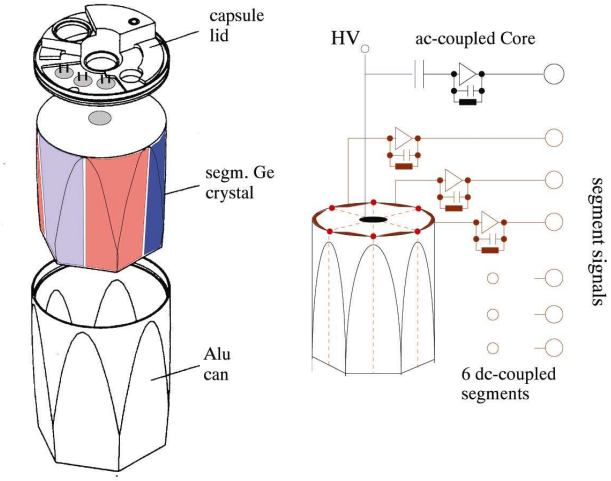

Fig. 2.6: *The encapsulated six-fold segmented MINIBALL detector.*

In figure 2.6 the 6-fold segmented Miniball detector is shown. An AC-coupled preamplifier is used to read out the total signal of the detector from the core and six DC-coupled preamplifiers to read out the segment information. All cold parts of the seven preamplifiers are mounted on top of the capsule. The energy resolution measured at the core is typical for a large Ge detector (~2.2 keV); the resolution of the segments is 200-300 eV worse due to the additional capacitance between Ge surface and the wall of the capsule.

Figure 2.7 shows a photograph of a Miniball Triple-Cluster cryostat which has been developed at the University of Cologne. Up to 28 preamplifiers are mounted on a circular mother board below the dewar. The detector end cap can be exchanged to house three or four 6-fold segmented detectors, respectively. Miniball will consist of 40 detectors clustered in eight cryostats with three detectors each and four cryostats with four detectors. These two types of cryostats are chosen to get an optimum coverage with Ge in a 4π arrangement of the detectors. The holding time for liquid nitrogen in the dewar is 12 hours.

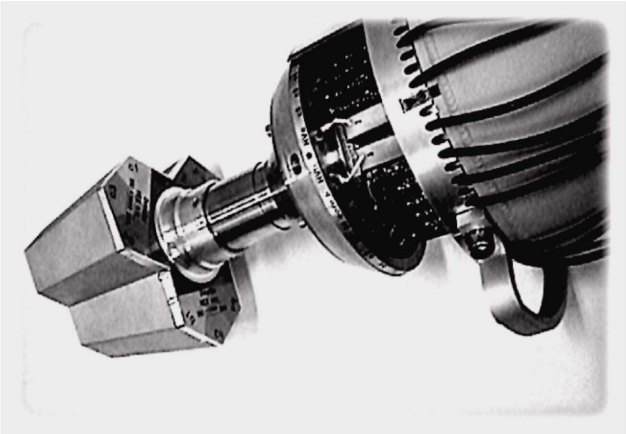

Fig. 2.7: *The MINIBALL cryostat.*

The position sensitivity of Ge detectors is based on the segmentation of the Ge crystal and the analysis of the pulse shape of the core signal for the radial position and of the mirror charges induced in the segments for the azimuthal position. This requires a large bandwidth of the preamplifiers in order to transfer the full information of the Ge detector signal. On the other hand, the need for a compact cryostat, housing up to 28 preamplifiers, places a constraint on the size of the preamplifier. Such a preamplifier has been developed by the University of Cologne and the MPI-K Heidelberg and is used today in several γ-ray spectrometer projects.

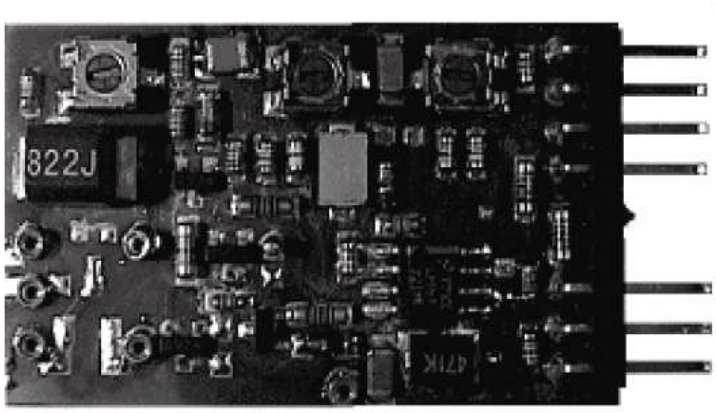

Fig. 2.8: *The SMD-Preamplifier. Gain: 175mV/MeV;*
Noise: 0.6keV + 0.15keV/pF; Rise Time: 15ns + 0.3ns/pf.

Figure 2.8 shows a photograph of the board and the most important specifications. The preamplifier has a fast rise time and an excellent noise performance; by the use of SMD components the size could be limited to 25 x 40 mm. There are adjustments for pole zero, DC offset and the drain current of the FET. For easy exchange, the preamplifiers are plugged into a motherboard mounted in the cryostat.

Latest developments for position-sensitive Ge detectors

The position resolution of current segmented detectors is limited due to missing segmentation in depth. Therefore, new developments have been started to investigate the possible improvement in position resolution by the additional segmentation in depth.

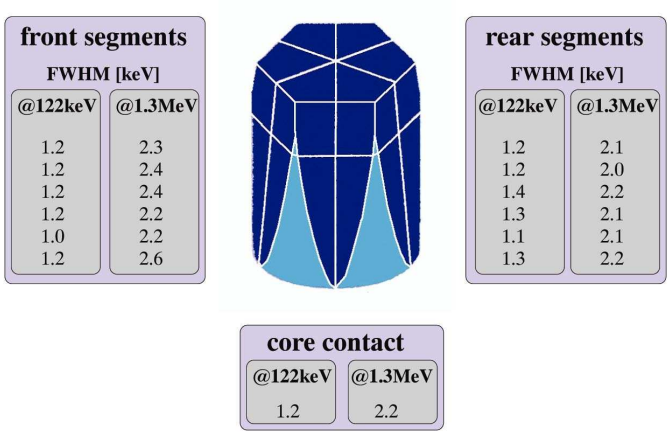

Fig. 2.9: *The 12-fold segmented, encapsulated Ge detector.*

As one example, the MINIBALL collaboration has recently received a 12-fold segmented, encapsulated detector, shown in figure 2.9 together with its specifications. It has the same geometry as the Miniball detector with the distinction that the first third of the detector is separated by segmentation from the true coaxial part. This detector uses a new technology for the segment contacts which is suited to encapsulate highly segmented detectors.

In the framework of the GRETA project [Del99] the Berkeley group has recently shown [Vet00] that a position sensitivity of less than 1mm can be achieved with a 36-fold segmented detector in a standard cryostat. In Italy, the Padova group is exploring the properties of a 25-fold segmented Ge detector in the framework of the MARS project [Kro01] in order to compare the experimental results with their extensive studies of tracking arrays by Monte-Carlo simulations.

Most of the R&D work and simulation calculations performed so far have been concentrated on coaxial Ge crystals and on the associated 4π multi-detector geometries. Recently, research programs have been launched in the USA and in Europe in order to also study the γ- tracking properties of thick, large-area planar Ge detectors. The GARBO project in the USA investigated the performance of a segmented planar Ge-strip detector. In Europe, two prototypes of position-sensitive planar detectors are being studied :

- A 5 x 5 25-fold segmented, 2 cm thick planar detector at the Univ. Stockholm, which gave a 3D-spatial resolution of 1-2 mm FWHM using a very simple pulse-shape analysis technique.

- A stack of two 2 cm thick planar crystals at IReS, Strasbourg, one segmented in 3 x 3, the other one in 4 x 4, which exhibit excellent average pixel energy resolutions of 840 eV and 1.98 keV at 122 keV and 1332 keV, respectively. In addition, the pulse shapes of the segments are very sensitive to the 3D-position of the interaction point.

The main favourable properties of planar detectors are: identical pixel size along the whole crystal, a uniform electrical field and a pronounced pixel pulse shape that should lead to an excellent 3D-spatial resolution. On the other hand, the dead layers of planar detectors which exist along the Li contact and the passivated surfaces must still be reduced. A corresponding development program is foreseen in collaboration with the company Eurisys Mesures. It should also be mentioned that all developments undertaken on preamplifiers, digital signal processing and tracking algorithms will also be exploitable for planar Ge detectors

Extensive simulation calculations have shown that a similar performance of a γ-ray tracking array can be achieved with planar detectors as compared to coaxial detectors. While the technology of segmented, encapsulated coaxial detectors has fully been developed within European TMR network projects, the development of segmented planar detectors with thin dead-layers has started only very recently. Therefore, it has been agreed to base the proposal for a European γ tracking array on segmented, encapsulated coaxial detectors, but to support and carry on the development of segmented planar detectors in order to study their possible application for future instruments in nuclear physics and in other fields, i.e. medical imaging and gamma astronomy.

Conclusions

Position-sensitive Ge detectors are the basis for a new concept in γ-ray spectroscopy, the gamma tracking array. World-wide development programs have demonstrated that a position resolution of ≤ 5 mm which is needed for γ-ray tracking can be readily achieved by pulse-shape analysis of the segment signals using digital electronics; the obtained results are indeed much better than originally expected (see chapter 3). This fact gives a very optimistic view of the feasibility of a γ tracking array as the next generation "multi-purpose" γ-ray spectrometer.

Nevertheless, a major effort is needed to construct a first γ-ray tracking array. This effort will include the development of a 36-fold segmented, encapsulated Ge detector, the construction of cryostats for composite detector systems, the miniaturisation of the front-end electronics, the implementation of pulse-shape analysis and tracking algorithms in real time as well as the realisation of a data acquisition system capable of handling the extremely high data streams. The knowledge needed to construct a γ-ray tracking array is distributed over various European laboratories which are prepared to join the common project. Therefore, excellent presuppositions exist in Europe to realise a first γ-ray tracking array and, thereby, to introduce a new quality in γ-ray spectroscopy for the application in fundamental research.

Finally, it should be noted that the development of position-sensitive Ge detectors will lead to important "spin-offs", as has been proven by previous technologies developed by the nuclear structure physics community. *Composite Ge detectors*, first developed for the EUROGAM spectrometer, have become the standard for many applications, e.g. in environmental monitoring, where very large-volume Ge detectors are needed. *Encapsulated Ge detectors* developed for the EUROBALL spectrometer are first choice when optimum reliability is demanded, for example in the INTEGRAL space mission. Combined with the latest advances in *segmentation techniques*, these developments have allowed European manufacturers to take the lead in high-end Ge detector technology in recent years. Extrapolated to the future, the γ-ray tracking techniques developed for AGATA will have a strong impact on high resolution and high sensitivity γ-imaging, being of prime importance for medical and industrial applications

3. Gamma-Ray Tracking

3.1 The principle of γ-ray tracking

A new generation of detectors is being developed to improve significantly the efficiency and resolving power of 4π arrays for high-precision γ-ray spectroscopy. They consist of high-fold segmented germanium crystals and a front-end electronics, based on digital signal processing techniques, which allows to extract energy, timing and spatial information on the interactions of a γ ray in the Ge detector by pulse-shape analysis of its signals. Utilising the information on the positions of the interaction points and the energies released at each point, the tracks of the γ rays in a Ge shell can be reconstructed in three dimensions, mainly because of the angle-energy relation provided by the Compton scattering formula.

The prerequisite for the construction of such a γ-ray tracking array is the development of γ-ray tracking detectors, consisting of:

- High-fold segmented Ge detectors
- Digital signal processing electronics
- Pulse-shape analysis algorithms for real time applications

Research and technical development on detectors for a 4π γ-detector array has been carried out by the European TMR Network Project *Development of γ-Ray Tracking Detectors for 4π γ-Ray Arrays* [Lie01] (contract number ERBFMRXCT970123) in the following areas:

- Development of segmented Ge detectors,
- Development of digital signal-processing electronics,
- Development of pulse-shape analysis methods and
- Development of tracking algorithms

In Europe, the Italian MARS [Kro00] project has strongly contributed to the progress on multi-segmented Ge detectors, while the EXOGAM [Sim97], MINIBALL [Ebe97] and VEGA [Ger98] projects are exploring the virtues of segmented detectors for the first time in real experimental conditions. Finally, a γ-ray tracking research program is being carried out in the USA by the GRETA [Del99] collaboration, which has pioneered these developments. In the following, the different components of a γ-tracking array are introduced while further details will be described in the following chapters.

High-fold segmented Ge detectors

In order to achieve a large tracking efficiency, the positions at which the γ rays interact inside the detector volume should be determined with an accuracy of 1-2 mm. This corresponds to an effective granularity of approximately 30000 voxels per Ge detector. It is impossible to achieve such granularity by a physical segmentation of the crystal. However, pulse-shape analysis methods have been developed, which can provide this position accuracy together with high-resolution energy and time information. These methods require a medium level segmentation of the outer detector contact into 20 - 40 segments.

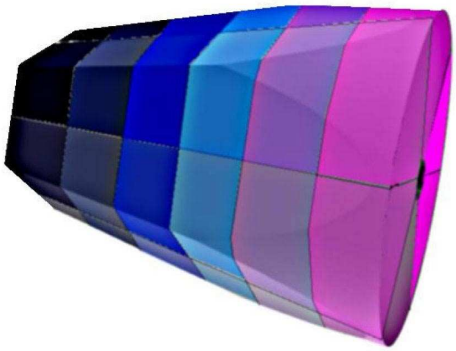

Fig. 3.1: *Schematic view of the 36-fold segmented, hexaconically tapered germanium crystal as planned for AGATA.*

A 36-fold segmented germanium detector with six-fold azimuthal and six-fold longitudinal segmentation, similar to the prototype developed by GRETA and to that planned for AGATA, is schematically shown in figure 3.1. The Ge detector has a circular shape at the rear side with a diameter of ≈ 8 cm and a hexagonal shape at the front face. The length of the detector is ≈ 10 cm. The segmentation is achieved by a separation of the outer implanted contact into six slices and six orthogonal sectors. The 36 segments together with the inner common electrode are read out via individual preamplifiers and can be considered as separate detectors.

Detector signal characteristics

The interaction points of the γ rays in the Ge detector can be localised with a much higher accuracy than defined by the geometry of the segments if the spatial information contained in the detector signals is exploited. A signal is produced when the slowing down of a photo- or Compton electron generates electrons and holes that induce image charges of opposite signs on the detector electrodes. As the charge carriers drift towards the electrodes, the amount of the image charges change causing a flow of currents into or out of the electrodes. At large distance of the charge carriers the induced charge is distributed over several electrodes in a multi-segmented detector. At closer distance to the destination electrode the induced charge

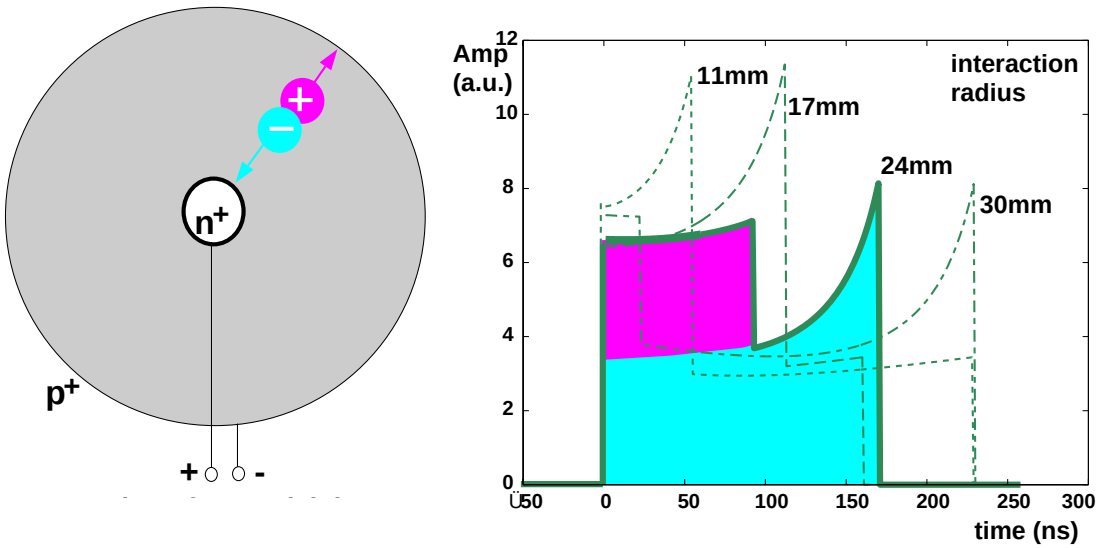

Fig. 3.2: *Transversal cut through an n-type coaxial detector showing the carrier drift (left), and induced current signals in the detector corresponding to four interaction radii (right).*

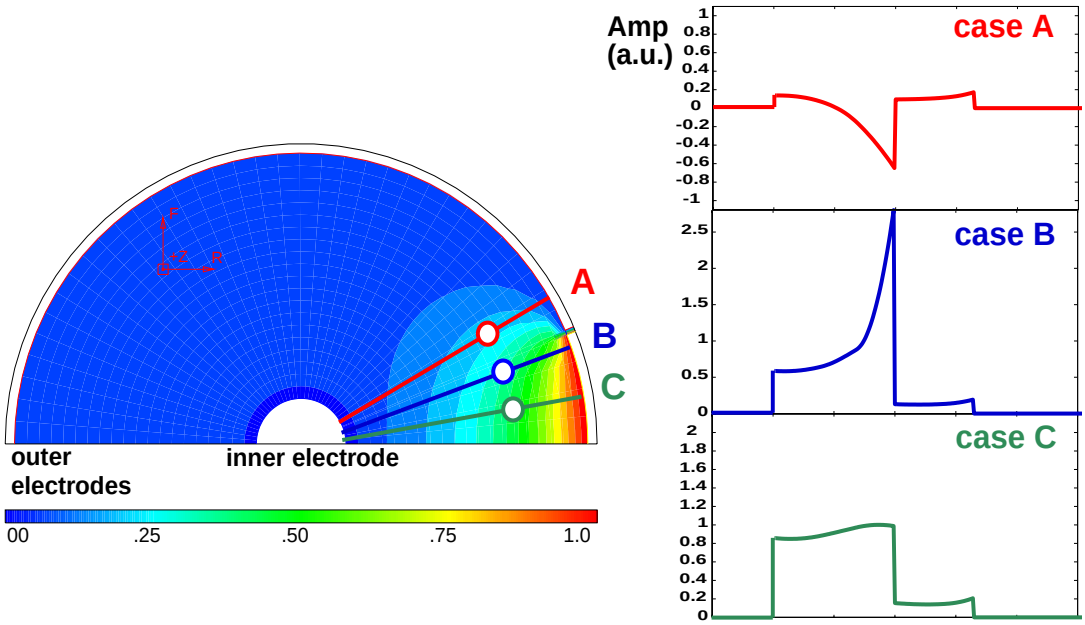

Fig. 3.3: *Weighting potential of a segment in a coaxial detector with three examples of interactions occurring at the same radius, but at different azimuthal angles (left), and the corresponding induced current signals (right).*

on this electrode increases and induced charges on the other electrodes decrease until the primary charge finally reaches its destination electrode and neutralises the image charge. The observation of a net charge on the charge-collecting electrode can be used to identify the detector sector where the interaction took place. The predominant characteristics of the transient image signals on the other electrodes (mirror charges) is that they vanish when the charge carriers are collected and that either polarity is possible, depending on the respective contribution of holes and electrons. Simply observing the polarity of the induced signal allows distinguishing between interactions at small and large radii.

Examples of calculated induced current signals in a coaxial detector are schematically shown in figure 3.2. In the left part of the figure, a transversal cut through a coaxial detector is presented together with the drift directions of the charge carriers. Depending on the radius where the charge carriers are produced, they will have different distances to the detector electrodes. Accordingly, the shapes of the induced current signals are different for different interaction radii. The right part of figure 3.2 depicts four such examples.

Calculated net and transient image charge signals are obtained by first calculating the pathway of the charge carrier for a given interaction position. The motion of the charge carriers is determined by the electrical field, which depends on the detector geometry, the applied voltage and the intrinsic space charge density and charge carrier mobility. The additional effect of the crystal lattice orientation of the detector is discussed in chapter 5. The field is calculated from the potential by solving the Poisson equation. Using Ramo's theorem for the so-called weighting field [Ram39] the signals induced in the segment electrodes can be calculated. In the left part of figure 3.3 the weighting field of a segment in a coaxial detector and three cases of interactions occurring at the same radius, but at different azimuthal angles are presented. The corresponding mirror (case **A**) and real charge signals (case **B**, **C**) induced on the segment electrode are shown on the right hand.

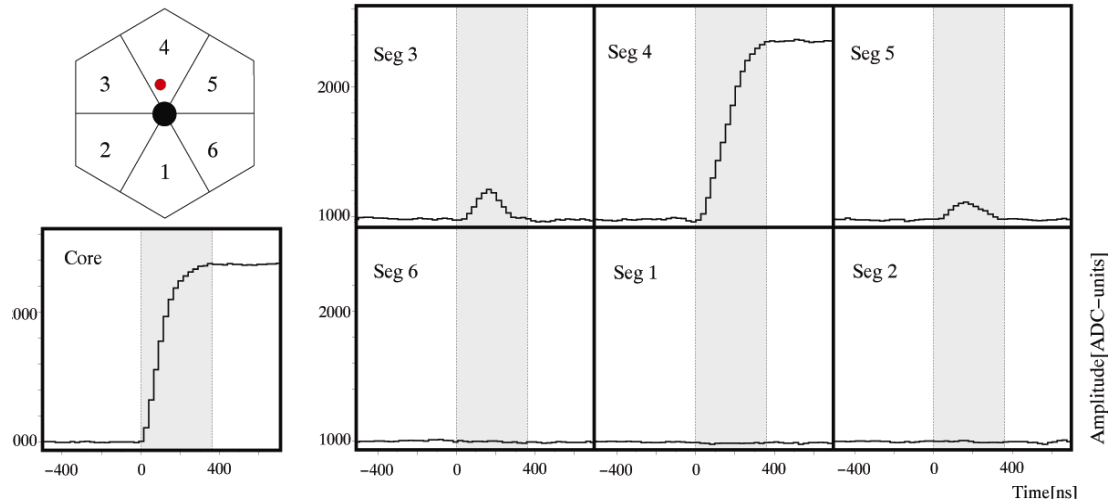

Fig. 3.4: *Signals of the core and segments for an event fully absorbed in segment 4.*

Experimentally, characteristic pulse shapes have been studied in detail with the various existing segmented Ge detectors. Figure 3.4 shows an example of pulse shapes measured at the core and at the six segments of a MINIBALL detector. The selected interaction was produced with a collimated ^{137}Cs source illuminating segment **4**. The signal of segment **4** has the same pulse height as the signal of the core, i.e. the whole energy was deposited in this segment. The neighbouring segments (**3** and **5**) show a positive mirror-charge signal, indicating that the main interaction occurred close to the core in segment 4. The pulse height of the mirror charge in segment **3** is larger than in segment **5**, showing that the interaction occurred closer to the boundary line of segment **4** with segment **3**.

Digital signal processing electronics

To make use of the spatial information of the detector signals pulse-shape analysis of the segment signals needs to be carried out. This can be achieved by digital means only. The pre-amplified detector signal must be digitised with at least 12-bit resolution and at a speed of at least 40 Ms/s (million samples per second) in order to preserve all relevant features of the signal in its digital representation. It is the task of the digital processing electronics to digitise the preamplifier signal using an analog-to-digital converter (ADC) and to provide digital signal processing hardware and software powerful enough for on-line processing of the signals. A γ-ray tracking array consisting of about 200 36-fold segmented Ge detectors will have almost 7000 digital signal processing channels producing each a primary data rate in excess of 60 Mbyte/s. This requires a compact digital signal processing electronics with high computing power for on-line data reduction. In the ideal case, the whole information should be reduced to only five values per interaction: energy deposition and its time as well as the three spatial coordinates of the interaction point.

Depending on the information that has to be extracted from the Ge detector pulses, different optimised signal processing algorithms exist or have to be developed and applied. The time invariant Moving Window Deconvolution (MWD) for instance has been proven an optimal filter, if information about the released total energy has to be extracted [Geo94]. For triggering, timing, and pulse-shape analysis only the leading edge of the signals, i.e. a small part of the data stream is relevant. Algorithms have been already developed, which allow to obtain trigger efficiencies of 100 % down to 20 keV and 80 % at 10 keV [Gas00]. More sophisticated algorithms providing timing resolution of sub sampling interval accuracy have also been developed.

Pulse-shape analysis

The shape of the current pulses produced by γ rays interacting with a Ge detector contains the information on the three-dimensional position of each individual interaction within the detector volume and the energy released at each interaction. The tracking efficiency, and hence the final performance of a complete tracking array, depends on the precision of these data.

To extract the position information from the pulse shape one must be able to compare them to the respective shapes produced by charges in each point of the detector. In principle, this can be done experimentally using tightly collimated γ-ray sources and asking for a Compton scattered γ in coincidence with an external collimated detector. It has however been shown by the GRETA collaboration [Vet00] that these are extremely lengthy measurements if the required position definition of the scattering is of 1 mm^3. The only viable way is then to calculate the pulse shapes from the electric field inside the crystal and the drift velocities of the charge carriers. Good parameterisations of the drift velocity exist for the electrons but not for the holes so that some calibration with the above mentioned method has to be done anyway. Furthermore, the fact that the conductivity in Ge crystals is anisotropic with respect to the crystallographic axis directions is expected to influence the magnitude of the drift velocities and the angle between the drift velocity and the electric-field vector. The first effect directly influences the shape of the signal, while the second one, which does not significantly affect the shape of the signal in unsegmented detectors, might be important in designing the detector segmentation [Mih00].

Various methods to determine the interaction positions of γ rays in segmented Ge detectors have been developed. They take into account the shapes of the induced "real" and "mirror" signals. Real signals are measured at the electrodes of the segment, in which an interaction takes place. Mirror signals are measured on the electrodes of the neighbouring segments, where no interaction takes place and are due to a capacitive coupling between these segments and the moving charges.

Signal deconvolution algorithms based on artificial intelligence methods have been developed using simulated real and mirror signals of e.g. a 25-fold segmented detector as input to an artificial neural network (ANN) and to a genetic algorithm (GA) in order to study their ability to distinguish between single and multiple interactions and to extract the position and energy information. A correct identification of the number of interactions was obtained for the GA algorithm at a success rate of more than 90 % with a position resolution of better than 2 mm and an energy resolution of better than 4 % for events with two interactions in the same segment. Another approach to signal deconvolution exploits a pattern recognition system based on the "wide-band" small support wavelet transform (WB4) [Mih01]. In this system, the wavelet coefficients of the signals are compared to databases with wavelet coefficients of signal shape types (pattern classes) to identify the best fit via a first nearest neighbour algorithm and a calculation of the membership function of the identified class.

It can be assumed that the interaction positions in a highly segmented Ge detector can be determined with a resolution of the order of 1 mm^3 for single events. Multiple hits may be resolved if they lie more than 2 – 3 mm apart.

Pulse shape analysis applied to a MINIBALL detector

Employing pulse shape analysis techniques in a first experiment the position sensitivity of the MINIBALL detector was studied. A collimated ^{137}Cs source was used for that purpose. The collimator was 10 cm long with a diameter of 2 mm. The detector was scanned in two dimensions in steps of 2.5 mm with the collimated γ rays hitting the detector perpendicular to its front surface. The collimation of the ^{137}Cs source reduced the count rate to 35 counts/s, so the detector had to be shielded with low-level lead, to bring the count rate from the natural background down to 5 counts/s.

The right part of figure 3.5 shows the result of a radial scan with five positions of the collimator separated by 5 mm. For each position the number of counts is plotted versus the time to the steepest slope of the current signal measured at the core.

The peaks for the five positions are clearly separated. The tails to longer charge collection times are probably due to regions of weak electric fields in the front part of the detector which is common for a semi-coaxial detector.

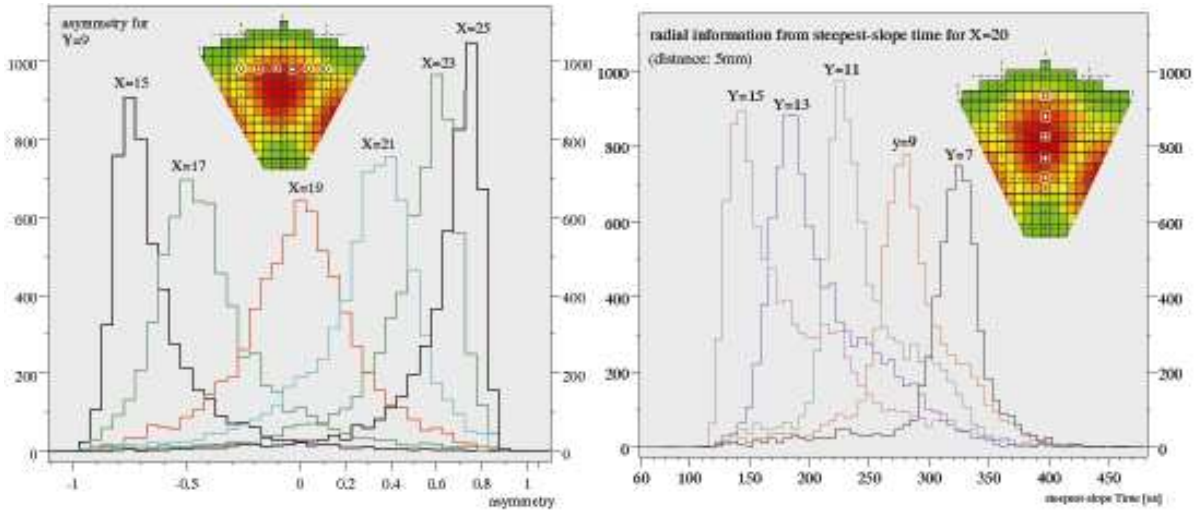

Fig. 3.5: *The Asymmetry of the mirror charges (left) and the time of the steepest slope of the current pulse (right) for various collimator positions.*

The left part of figure 3.5 gives the results of a scan perpendicular to middle radius of one segment for six points separated by 5 mm as indicated in the figure. The number of counts is plotted versus the asymmetry $A = (Q_L - Q_R)/(Q_L + Q_R)$ where Q_L and Q_R are the amplitudes of the mirror-charge signals as detected in the left and the right neighbour segment, respectively. Again the peaks for the six positions can be well distinguished.

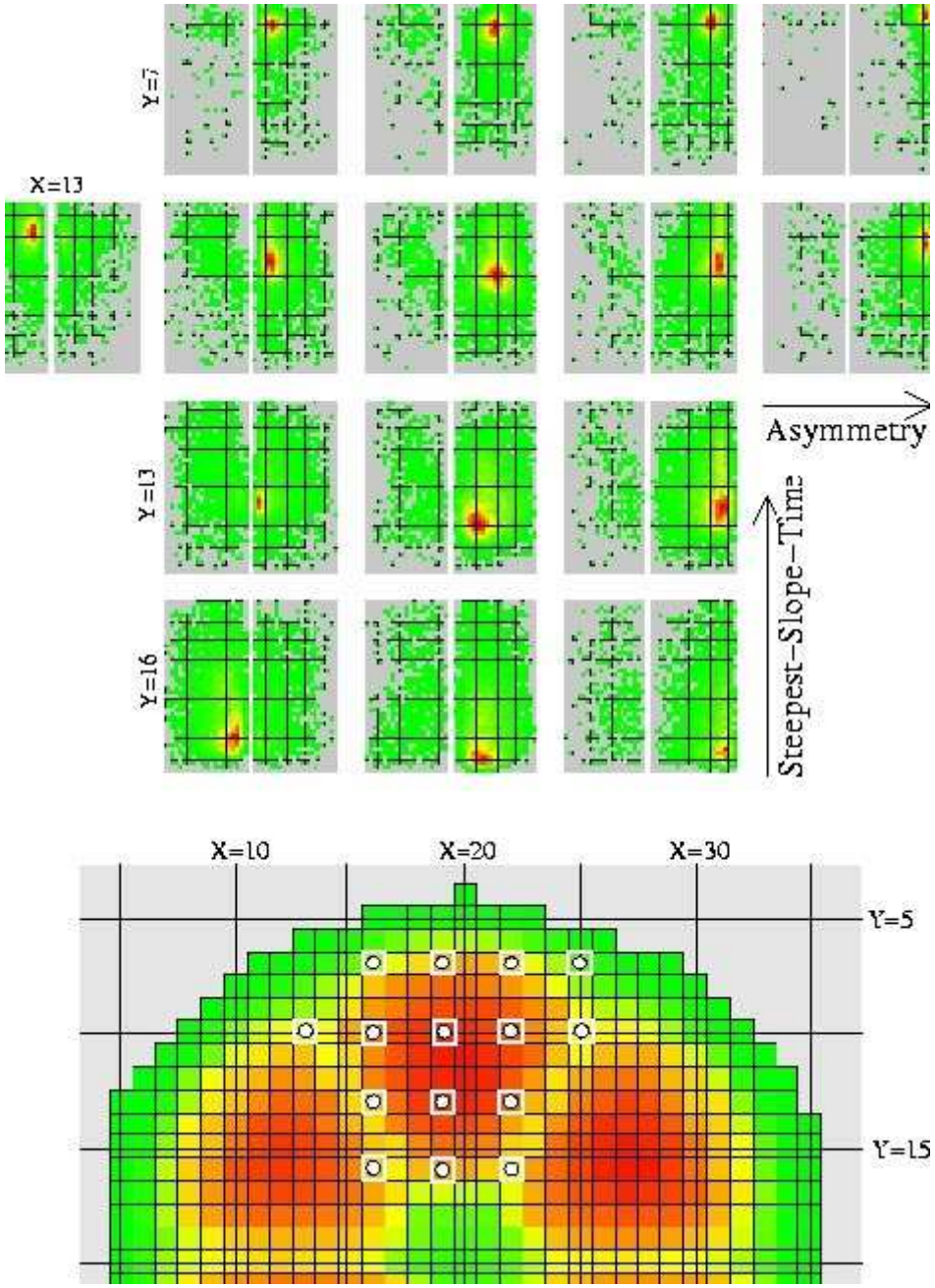

Fig. 3.6: *2-dimensional position response of segment 3 and 4. The collimator positions (separated by 7.5mm) are indicated in the right lower corner.*

Figure 3.6 summarizes the results of the 2-dimensional scan. For each of the 14 collimator positions, indicated in the figure, the time to the steepest slope of the current pulse of the core is plotted versus the asymmetry A, extracted from the mirror charges detected in the neighbouring segments. For each position the matrices of the central segment and its left neighbour are given. From a survey of all results we conclude that one can distinguish between 16 positions in one segment.

Thus, the effective granularity of one MINIBALL detector is enhanced from 6 due to segmentation to 6 x 16 ≈ 100 by the additional pulse analysis.

3.2 Gamma-ray tracking methods

In nuclear and particle physics, charged particles are tracked using their continuous ionisation in a position sensitive detector volume or indirectly via the time sequence of collected ionisation charges (e.g. time projection chamber). For γ rays, the situation is completely different since their interaction probabilities follow a statistical law and are much lower, generally resulting in a few sparsely scattered interaction points that can be separated by large distances. Therefore, the scattering path of a γ ray in the detector volume cannot be easily deduced. Gamma-ray tracking requires powerful algorithms that take into account the physical characteristics of the γ-ray interactions in the detector, i.e. Compton scattering, pair production, and photoelectric absorption. The law governing the kinematics of Compton scattering is central to such algorithms since most γ rays in the energy range of ~1 MeV, which interact with a Ge detector, will Compton scatter a few times before finally photo absorption or escape takes place. To apply the Compton-scattering law the information from the γ-ray tracking detectors on the individual interaction positions and the respective energy depositions as well as on the total integrated energy deposition must be used.

In γ-ray spectroscopy, we are interested in the detection of transitions in the energy range from tens of keV up to 10 MeV and more. The dominant interaction mechanisms are photo-electric absorption, Compton scattering and pair production: on the low-energy side photo-electric absorption dominates, the central energy range results mostly in Compton scattering, while at higher energy pair production starts taking over.

There are both practical limitations due to the detector performance and physical uncertainties in the scattering process that affect our attempts on γ-ray tracking. The former include the energy resolution of the detectors and the accuracy with which individual interaction positions can be determined. The position sensitivity is especially important for the performance of γ-ray tracking algorithms. Position sensitivity and energy resolution are limited by detector noise and by the detector geometry due to the finite range of Compton scattered and photo electrons. The physical uncertainties include effects of the momentum of the atomic electron at the instance of scattering and the occurrence of Rayleigh scattering and emission of Bremsstrahlung radiation.

Only a limited number of highly segmented Ge detector prototypes have been produced up to now so that γ-ray tracking cannot be tested experimentally in every detail. Consequently, the development of γ-ray tracking algorithms relies primarily on simulated Monte Carlo data. The main simulation tool is the program package GEANT (3.21) developed at CERN, which allows to model in details the detection of γ quanta and particles for almost arbitrary detector set ups. Actually, while discussing the general features of γ-ray tracking, the geometry of the detector is not very relevant and, as a reference, the Ideal Shell introduced in chapter 2 is used. Of course, any result obtained with this idealised detector must be checked with more realistic configurations, because dead material and the unavoidable inter-detector gaps can significantly reduce both the efficiency and the peak-to-total ratio.

The development of γ-ray tracking algorithms mainly follows two lines. In the so-called clusterisation method [Sch99] a preliminary identification of clusters of interaction points is followed by a comparison of all possible scattering angles within a cluster against the Compton-scattering formula. The second approach, called backtracking [Mar99] starts from points likely to be the last interaction and goes back, step by step, to the origin of the incident γ ray. The basic features of γ-ray interactions relevant for tracking and the two tracking methods itself are described in more detail in the following sections.

Compton scattering

Compton scattering is the most important effect in the energy range of interest and is the only mechanism that allows real tracking to be performed. Following the example of figure 3.7 let us consider a γ ray that Compton scatters at position **1**, releasing part of its energy ($\mathbf{e_1}$) to an electron; the scattered γ undergoes then photoelectric absorption at position **2**.

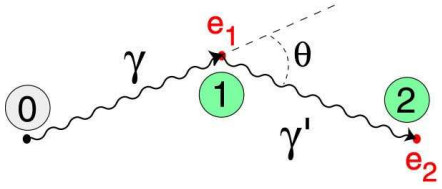

Fig. 3.7: *Quantities involved in the reconstruction of a Compton scattering interaction.*

The observable result of the Compton scattering interaction is the detection of the recoiling electron, as it releases its energy $\mathbf{e_1}$ to the Ge crystal so that $E_{\gamma'} = E_\gamma - \mathbf{e_1}$. The scattering path of electrons in the MeV range is of the order of 1 mm so that any practical detector will see it as an energy release point very close to the scattering vertex (as presented in figure 3.5) and not as a track. In the simplifying hypothesis that at the instance of scattering, the electron is unbound and at rest, the energy of the scattered γ is connected to the scattering angle by the well known Compton formula:

$$E_{\gamma'} = \frac{E_\gamma}{1 + \frac{E_\gamma}{m_0 c^2}(1 - \cos\theta)}$$

A position-sensitive detector provides both the value of the energy released at the interaction points and the 3-D coordinates of the scattering position. If the origin of the transition is known, the scattering angle can be derived from the coordinates of the three involved points:

$$\cos\theta = \frac{\overrightarrow{01} \cdot \overrightarrow{12}}{\left|\overrightarrow{01}\right| \cdot \left|\overrightarrow{12}\right|}$$

Inserting this value in the Compton formula yields an alternative measurement of the energy of the scattered γ ray ($E_{\gamma'}^{Pos}$) that can be compared with the energy release at point **2**. In an equivalent approach, we could consider the scattering angle derived from the three points and get an alternative value inserting the proper energies in the Compton scattering formula.

Keeping with the energies, the two values can be compared in a least-squares sense, e.g. using the energy of the incoming transition as an approximation for the variance of the involved quantities:

$$\chi^2 \approx \left(\frac{E_{\gamma'} - E_{\gamma'}^{Pos}}{E_\gamma} \right)^2$$

This can be viewed as a test of our model of the interaction sequence, namely that a γ ray originating from **0** has Compton scattered at **1** before being fully absorbed at **2.** A small χ^2 value would mean agreement with the model, while large values would be against the

hypothesis. Sometimes the inverse of the above-defined quantity is considered and is called then figure of merit.

A real detector does of course not provide the information that the interaction at **1** has taken place before the interaction at **2,** which means that we also have to consider the other possible scattering sequence **021**. Of the two possible sequences of two interaction points, that with the least deviation should be accepted as a model of what really happened. However, as the detector does not provide the information that the two interaction points considered here exhaust the whole energy of the impinging transition, it could also be that none of the sequences gives a sufficiently small (see later) χ^2 value.

In general, if there are N interaction points we have N-1 Compton scattering vertices and we have to seek for the minimum of the total χ^2 for each of the N! permutations of the points.

$$\chi^2 \approx \sum_{n=1}^{N-1} W_n \cdot \left(\frac{E_{\gamma'} - E_{\gamma'}^{Pos}}{E_\gamma} \right)_n^2$$

In this expression, E_γ and $E_{\gamma'}$ always refer to the energy of the scattering and scattered γ rays at the n^{th} vertex, respectively. The weighting factor W_n has been introduced to account for the probability that the γ rays involved in the n^{th} vertex have travelled for the resulting length.

Given that the defined quantity does not contain real variances, its absolute value is not very meaningful. Instead, an acceptance value is derived empirically looking at the quality of the obtained spectrum: larger acceptance values mean in general more reconstruction efficiency but also more accepted background. Figure 3.8 shows the distribution of χ^2 values obtained for a simulated case of 10^5 transitions: it is clear that at any acceptance limit some good cases are rejected while some background is always accepted. It is also evident that lower acceptance limits tend to produce better P/T ratios, at the expenses of reduced peak efficiency.

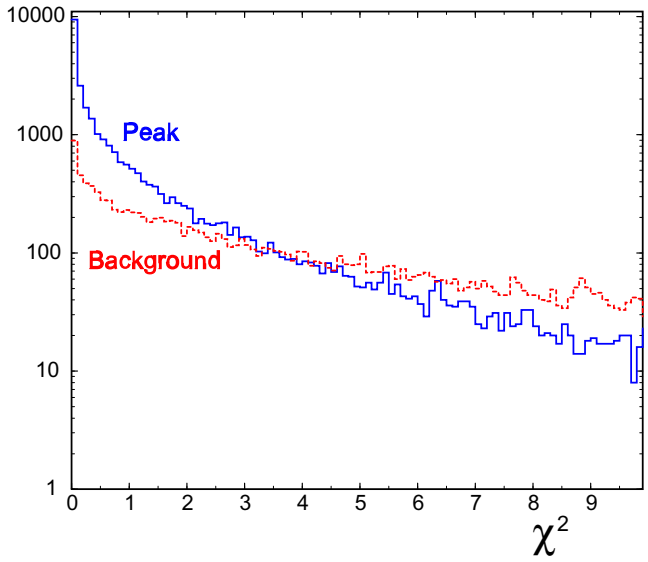

Fig. 3.8: *Distribution of χ^2 values for 10^5 transitions (at E_γ = 1.0 MeV) detected in the standard spherical shell.*

Finally, it is worthwhile to point out that in practice always more than one transition is detected in one event. This means that the acceptance test has to be used in two ways, i.e. to decide to what transition a point belongs and also to accept the transition or reject it if judged to be in the background. Given that this test is only valid in a probabilistic sense it cannot be avoided that points belonging to different transition are accepted as belonging together, giving rise to some sort of summing effects.

Photoelectric absorption

Low-energy γ rays (below ~150 keV) usually are absorbed directly by photoelectric effect and hence mostly detected as single points. There is actually no safe way to decide whether an isolated low-energy interaction point corresponds to a transition of the same energy or is the result of a Compton-scattered and partly escaped higher energy γ ray. The only criterion for reconstructing such a point is based on the probability that the γ ray reaches the interaction position in the detector. The acceptance limit can be adjusted in order to smoothly match the efficiency obtained by Compton-scattering reconstruction of higher energy γ rays. The gain in efficiency obtained in this way at low energies is however accompanied by a considerable background increase due to the weakness of the acceptance criterion. Cleaner spectra can be obtained only if the physics allows to disregard such low-energy transitions.

Pair production

Pair production becomes an important detection mechanism for γ rays above a few MeV and it overcomes Compton scattering at ~9 MeV. Real tracking is rather complicated in this case, but the interaction mechanism has such a characteristic signature that it can be easily recognised and reconstructed. Given the energy range of our interest and the energy dependence of the pair-production cross section, we need to consider in practice only the case where the pair is produced at the first interaction. The total kinetic energy of the electron-positron pair ($E_\gamma - 2m_0c^2$) is shared by the two partners in an unpredictable way. However, as both particles are in the MeV range, they are stopped in close vicinity to the pair production point. Being so close to each other they are normally seen by the detector as one individual energy release. The slowed-down positron binds to an atomic electron and forms a positronium atom that rapidly annihilates emitting, essentially always, two collinear 511 keV γ rays. These will either escape or be absorbed in some other part of the detector. Let us consider the case of full absorption: the detection pattern is that one of the experimental points has an energy corresponding to the total detected energy minus 1022 keV, while the other points stem from the two 511 keV γ rays originating from this vertex, as schematically illustrated in figure 3.7.

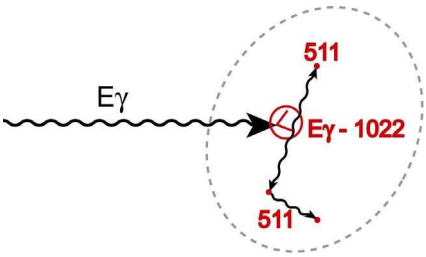

Fig. 3.9: *Pair production interaction. The electron and positron, which release their kinetic energy within a few mm of the interaction point, are seen as one point. The annihilation photons have their own absorption history and generate two γ-ray tracks originating from the interaction point.*

Actually, it turns out that it is not necessary to track the two 511 keV γ rays to the pair production vertex, because the energy distribution pattern is already such a strong signature that both the efficiency and the spectrum quality are satisfactory for transitions accepted in this way. This reconstruction method is illustrated in the following using simulated data for 4 MeV γ rays detected in the standard shell. At this γ-ray energy the total peak efficiency of the shell

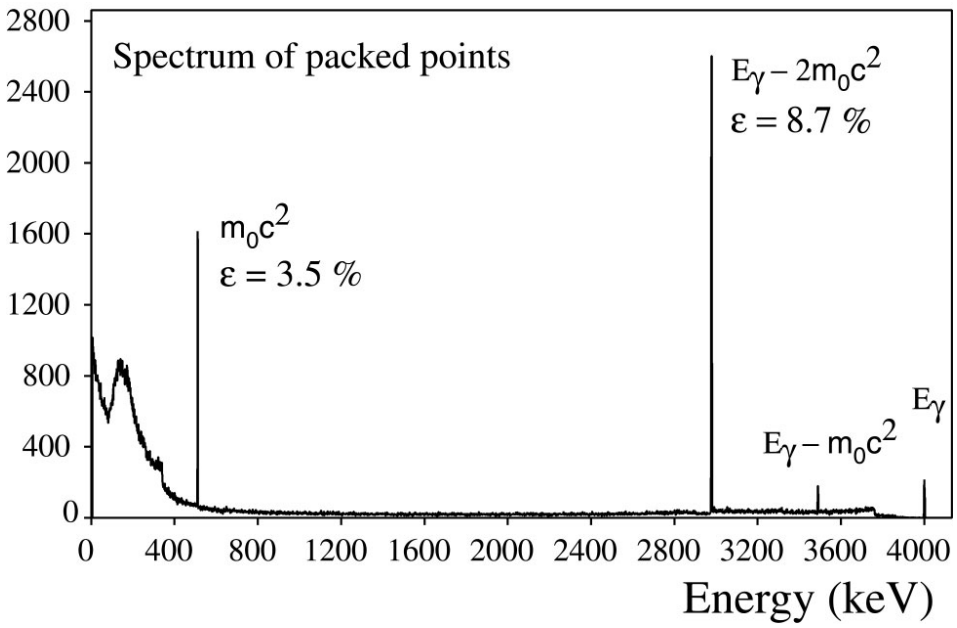

Fig. 3.10: *Energy spectrum of simulated interaction points for 10^5 4 MeV transitions detected in the standard shell. The peaks are generated by the application of a 5 mm packing procedure.*

is 49 % with a P/T ratio of 62 % while the cross section for pair production is 25% of the total interaction cross section.

This particular feature, i.e. an experimental line at an energy of E_{tot}-$2m_0c^2$, is well evidenced in figure 3.10 by the big peak at 2978 keV in the spectrum of all interaction points obtained after applying a 5 mm position smearing and packing procedure. Given that 25% of the peak counts in the total spectrum are due to pair production, 71 % of them give rise to these characteristic points. The same spectrum also shows that the packing procedure has already

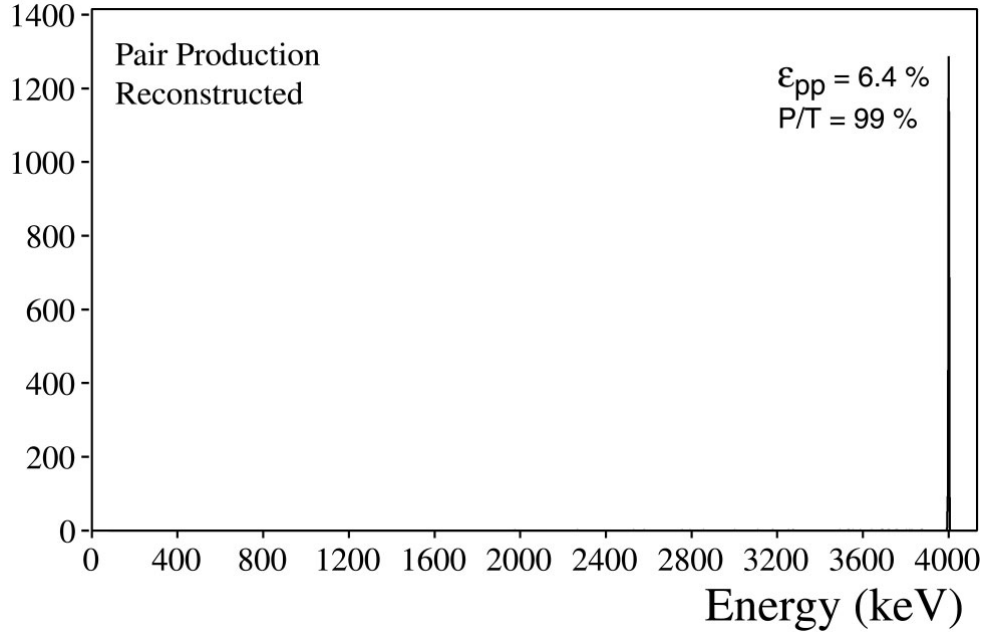

Fig. 3.11: *Fraction of simulated data reconstructed according to the described mechanism for pair prodcution. This spectrum is essentially background free.*

produced some points collecting the total energy of 4 MeV, most likely because the annihilation quanta have been detected very close to the pair production vertex. Similarly, the small peak at an energy of E_γ-m_0c^2 corresponds to single-escape events where only one 511 keV γ ray has been summed to the pair production vertex.

A simple reconstruction algorithm exploiting this characteristic signature has generated the exceptionally clean (P/T=99%) spectrum shown in figure 3.11. Owing to the fact that for individual transition there is no problem of mixing with points belonging to other γ rays, the reconstruction efficiency is as high as 74 %. Of course, the performance will be worse if other transitions are present in the analysed event.

The clusterisation method

For a γ ray scattering in a large Ge detector, the interaction points tend to confine themselves within a rather limited volume. This effect, which can also be seen as a clustering in solid-angle space, is due to the slight forward peaking of the Compton scattering cross section as given by the Klein-Nishina formula, as well as to the decreasing mean free path with decreasing energy. The clusterisation method takes advantage of this fact by first seeking to identify clusters of interaction points from individual γ rays. This can be done by means of a classification parameter corresponding to the largest allowable angular separation, with respect to the γ-ray's origin, between points within one cluster. Refinements of this scheme might consider also the spatial separation of points in the cluster. The energy of the hypothetical γ ray represented by the cluster is obviously the sum of the energies of its interaction points.

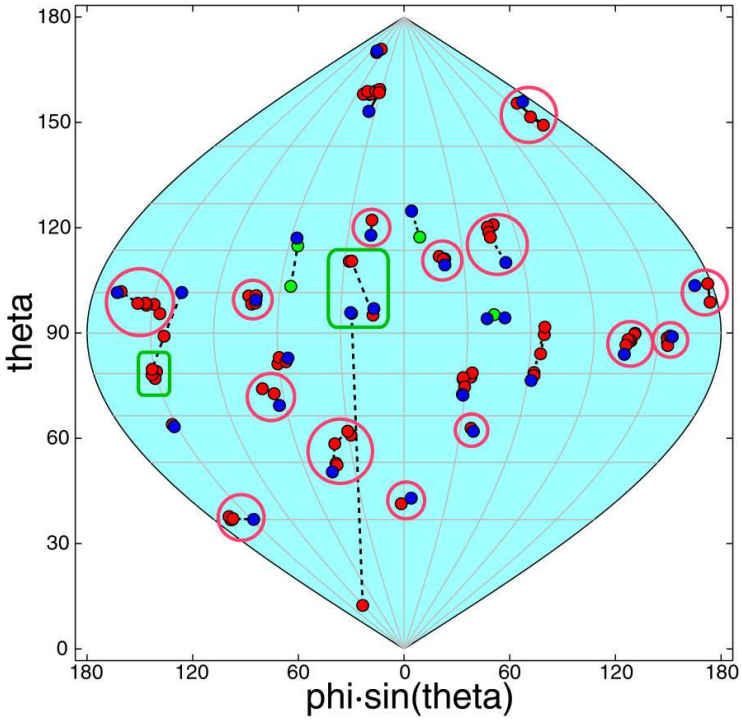

Fig. 3.12: *"World map" representation of an E_γ = 1.0 MeV, M_γ = 30 event detected in the ideal germanium shell and reconstructed with the "cluster-tracking" algorithm. Correctly reconstructed transitions are encircled and represent about two thirds of all γ rays in the event; the two rectangles represent badly reconstructed background events. About 75 % of the original transition is reconstructed correctly.*

The clusters are then evaluated based on the energy-angle relationships given by the Compton-scattering formula as explained above. Out of the clusters that have been formed, some will correspond to all the interaction points of one fully absorbed γ ray ("good" clusters) and others will not ("bad" clusters). Bad clusters can arise, for example, when two good clusters or parts of them are treated as one, or when one good cluster is misidentified as two. Reminding that the validation procedure (i.e. the χ^2) is not a perfect tool, the quality of the candidate clusters (i.e. how likely they are to contain all the points of a given γ ray and only those) is critical and various clusterisation procedures have been devised, exploiting Artificial Intelligence and Pattern Recognition methods. The optimum value for the angle parameter depends on the γ multiplicity, since the average separation of the transitions is inversely proportional to their number: for $M_\gamma = 30$ the optimum separation is about 15°. A sample high multiplicity event reconstructed in this way is shown in figure 3.12.

The backtracking method

The second γ-ray reconstruction method called backtracking is based on the observation that the energy deposition of the final photoelectric interaction after scattering usually falls into a narrow energy band as shown in figure 3.13. Here, the photo and Compton spectra of the energy depositions in all the individual interactions of the γ rays with the Ge detector are shown, considering that in most cases they interact by a few Compton scatterings before photo absorption finally takes place. It can be seen that the Compton spectra have a peak well below 100 keV whereas the photo spectra show a peak between 100 and 300 keV. The reconstruction algorithm to "backtrack" the path a Compton-scattered γ ray has followed, starts assuming a candidate point for the final interaction and then attempts to reconstruct a track onto the original emission point at the centre of the detector system. In this process, the physical characteristics of the γ-ray interactions are taken into account, e.g. the photoelectric and Compton interaction probabilities and the Compton-scattering formula. Since the reconstruction starts at the end of a path one is dealing with absolute γ-ray energies.

The maximum distance, within which the previous interaction point should be searched for, can therefore be estimated using the γ-ray energy and the Compton or photoelectric (in case of searching for the next to last point) cross sections. For each set of three interaction points a figure of merit can be deduced, gauging how well the measured positions and interaction energies match the Compton-scattering formula. The total figure of merit is also accumulated along the track. In each step, a trial is always made to track the γ ray back towards the known source position. If the figure of merit for finalising the track in this way is above a certain predefined value the track is considered "good". The algorithm works iteratively, similarly to the clustering method, and tracks receiving poor figures of merit may be broken up or added to accommodate more favourable combinations of interaction points. This method allows, in principle, to disentangle the interaction points of two γ rays entering the detector very close to one another. Furthermore, long-range scattering such as backscattering across the target region may also be recovered. It should be noted that the backtracking method in principle does not require prior information on the source position. This method is therefore advantageous for applications involving imaging of unknown source distributions, e.g. in nuclear medicine, environmental monitoring and γ-ray astronomy.

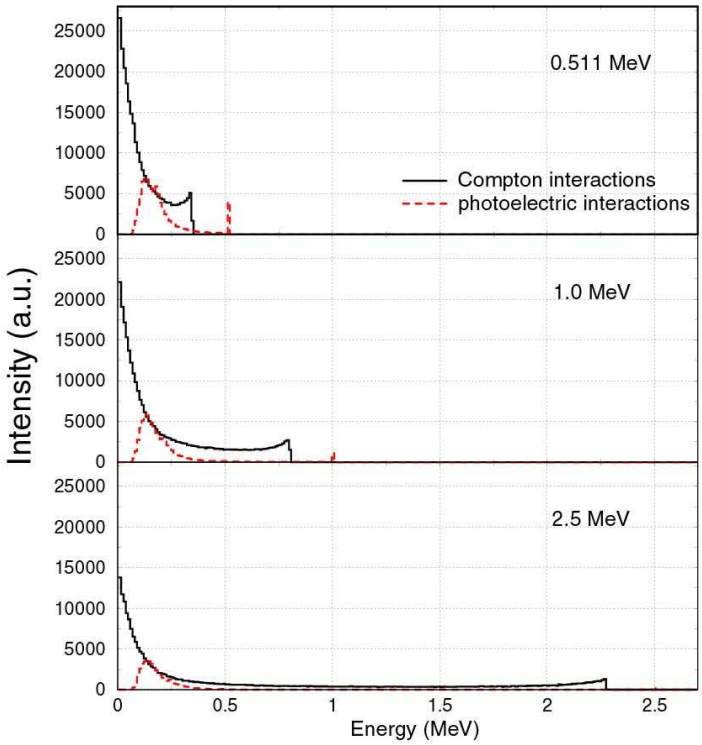

Fig. 3.13: *Photo and Compton spectra of the energy depositions in the individual interactions of the γrays with the Ge detector for γ-ray energies of 0.511, 1.0 and 2.5 MeV.*

3.3 Gamma-ray tracking results

The two main γ-ray tracking algorithms have been briefly described. The optimal tracking algorithm may be a combination of cluster recognition and backtracking both including features such as pair production and active neutron rejection. Neutrons tend to generate interaction patterns that differ so much from γ rays that they are naturally rejected by the tracking algorithms. However, also neutron interactions involving both elastic and inelastic scattering can be actively rejected using their special interaction characteristics. In heavy-ion fusion experiments neutrons may be rejected by means of the accumulated time of flight along the scattering path.

There are, however, some basic limitations to the applicability of the Compton scattering vertex test. On one side, we have to consider the limited energy and position resolution of the detectors, while on the other side the assumption that the electron upon which the scattering takes place is unbound and at rest is certainly not valid.

Let us consider first the effect of the limited detector resolution. The Monte-Carlo codes contain physical models of the interaction processes, but have no knowledge of the real detector performance. Therefore, the simulated data is usually too precise and, to be made realistic, the provided energies and positions must first be passed through a random "smearing" process. The *energy resolution* can be taken into account by a random folding of

the value provided by the simulation with a Gaussian distribution in order to produce a resolution of 2.3 keV FWHM at 1.33 MeV typical for germanium detectors.

For the *position resolution* the situation is more complicated as the achievable experimental precision is likely to be different in different parts of the detector, to depend on the energy deposited at the interaction point and on the number of interactions per segment and their relative energies. It is realistic to assume that for isolated interaction points the spatial resolution will be a few millimetres or better. In this work, the experimental resolution is modelled with an independent Gaussian distribution on each of the three Cartesian coordinates of the point. To be more realistic with respect to electronic noise, the FWHM of these distributions is inversely proportional to the energy of the interaction point. As a further feature, points that are closer to each other than the position resolution are packed together to an energy weighted average position. Figure 3.14 shows the overall obtained detector efficiency as a function of the position resolution for cascades of 1.33 MeV transitions detected in the standard shell.

The behaviour for individual transitions seems rather peculiar, but it is simply the result of packing points close to each other. Even if the absorption takes place in successive Compton scattering events, the packing tends to reduce everything to an individual point that is accepted by the reconstruction algorithms as a photoelectric interaction. Obviously, with just one γ ray in the event this mechanism can only produce good data.

The position resolution becomes an important factor already at multiplicity 2, because the packed points can now belong to different transitions. If accepted by the reconstruction algorithms, such points end-up in the background. The probability to mix points belonging to different transitions becomes larger at higher multiplicity and, therefore, the losses are bigger if the position resolution is worse. With respect to an "ideal" 1 mm position resolution, the "safe" assumption of 5 mm resolution yields a loss of 6%, 9%, 10%, 13%, and 15% for multiplicity 2, 5, 10, 20, and 30, respectively.

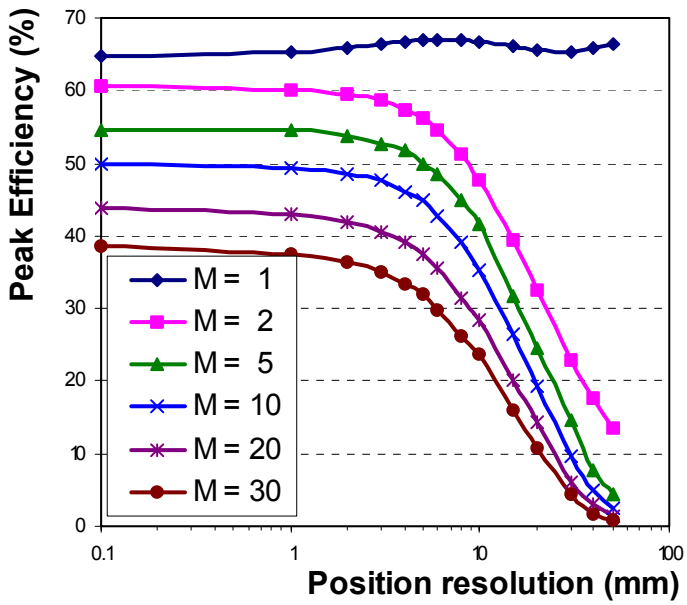

Fig. 3.14: *The total peak efficiency of "cluster-tracking" reconstructed data is shown as a function of assumed position resolution and γ-ray multiplicity.*

Tracking results for the standard shell

Many features and results of γ-ray tracking are conveniently illustrated making use of the simple-to-treat ideal detector consisting of a spherical 4π germanium shell. As already stated, our "standard" ideal shell has an inner radius of 15 cm, a thickness of 9 cm leading to a weight of 233 kg of germanium and thus corresponding roughly to the amount of germanium as used for EUROBALL.

For a simulated test case (a cascade of 30 γ rays in the standard spherical shell) both tracking algorithms discussed above achieve already today a reconstruction efficiency of up to 60 %, depending on the assumed accuracy of the interaction positions in the detector system. By further optimisation this value is likely to improve over the next few years. In the following calculations an energy resolution of 2.3 keV FWHM is used and a conservative estimate for the position resolution of 5 mm FWHM is assumed if not otherwise mentioned. The full energy detection efficiency obtained in this way for γ rays between 80 keV and 2.7 MeV is shown in figure 3.15 for different multiplicities of the cascade between 1 and 30.

The efficiency loss from the total response to $M_\gamma = 1$ is due to the experimental (simulated) errors that lead to a wrong reconstruction by the algorithms for a fraction of good data. The next big loss takes place already at $M_\gamma = 2$ and is due to assigning interaction points to the wrong transition. This effect becomes more important as the multiplicity of the cascade increases, resulting in the displayed gradual loss of performance.

A typical spectrum for a cascade of 30 equally spaced transitions of equal intensity having energies from 100 keV to 3 MeV is shown in figure 3.16. The structure of the background shows some evidence of sum-peaks corresponding to the acceptance of all points of two

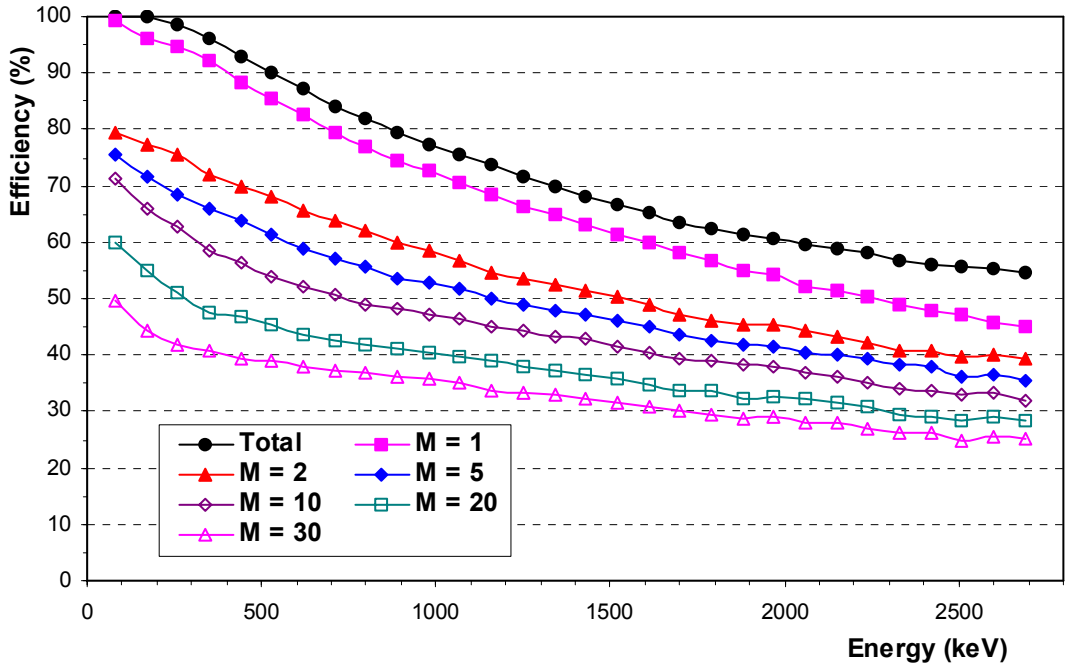

Fig. 3.15: *Efficiency of an ideal shell as a function of transition energy and multiplicity.*

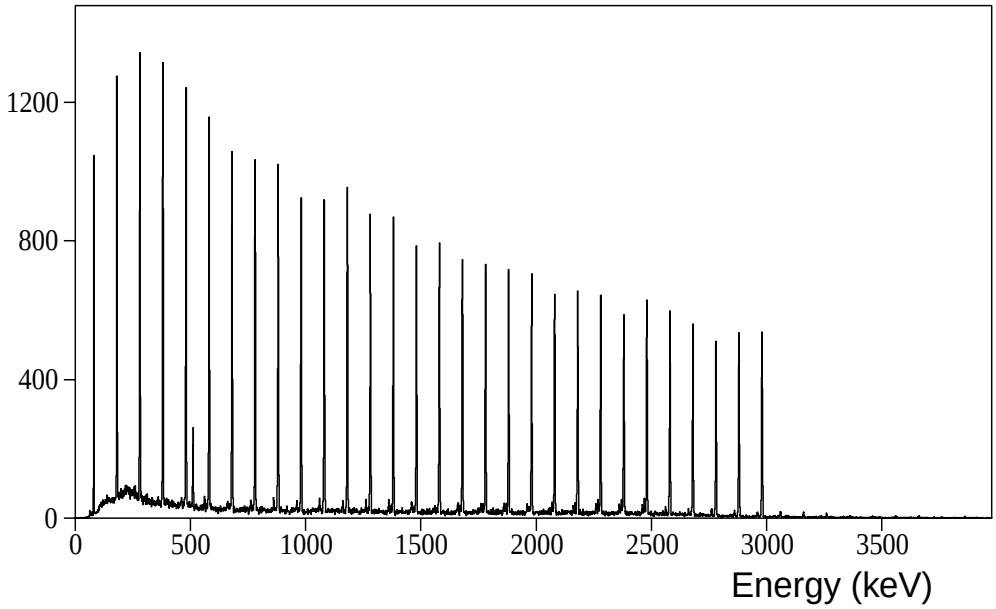

Fig. 3.16: *Reconstructed spectrum of a cascade of 30 equally spaced transitions detected in the standard shell.*

γ rays as one transition. The amount of summing can be reduced using smaller angle parameters, but this tends to produce spectra with a reduced P/T. The rather strong 511 keV peak corresponds to annihilation radiation that has been incorrectly tracked to the source position at the centre of the shell. The full energy detection efficiency and the P/T ratio, both averaged over the cascade, are 72.6 % and 80.1 %, respectively. The reconstructed data has ε_{ph} = 34 % and P/T = 50.8 %, corresponding to an average reconstruction efficiency of 47 %.

Doppler broadening correction capabilities

A very important result provided by the tracking algorithm is the ordering of the interaction points in the scattering history. Once the position of the first interaction point is known it is possible to determine the emission angle of the detected transition, if the position of the source is known. If the velocity vector of the source is also known, the Doppler shift correction can be performed in a simple manner. In a classical detection system the emission direction cannot be determined to better than the detector's opening angle. For tracked data, the limit is certainly much smaller and corresponds to the achieved position resolution for the first interaction point. Therefore, a tracking array should provide the "best" possible Doppler correction keeping the energy resolution close to the intrinsic value also for large recoil velocities. This feature is shown in figure 3.15 for 1.33 MeV transitions detected in the standard ideal shell.

Here, only the contribution to the Doppler broadening from the emission direction is considered, as velocity and recoil direction of the emitting source are supposed to be exactly known. It is clear that, as we are dealing with a simulated case, the figure reflects the assumed position resolution, which is a conservative 5 mm FWHM with a Gaussian distribution in the three spatial coordinates. At v/c = 50 % the energy resolution is ~5 keV, a value similar to that obtained with classical arrays at 10 times lower recoil velocity.

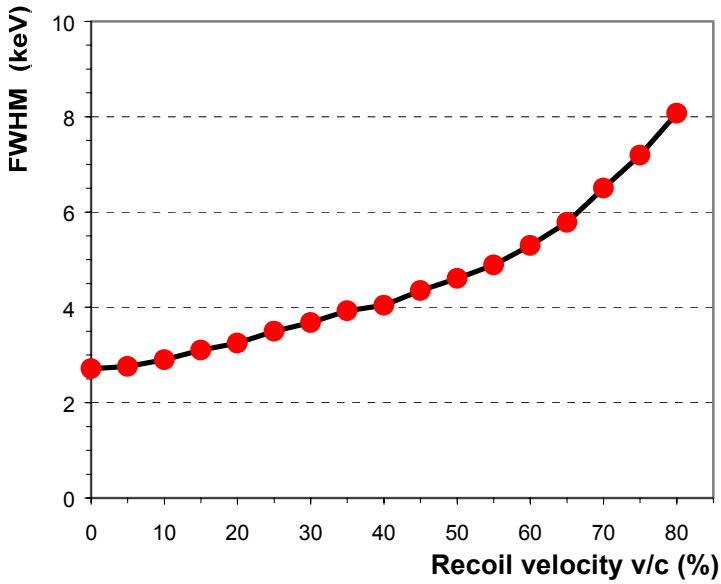

Fig. 3.17: *Energy resolution of reconstructed and Doppler corrected 1.33 MeV transitions as a function of the velocity of the emitting source. Direction and velocity of the source are supposed to be perfectly known.*

Performance of some realistic configurations

This section compares the performance of a few "realistic" configurations for arrays built out of large-volume closed-end coaxial germanium detectors. Because of inter-detector spacing, dead layers, and dead materials, which are unavoidable when dealing with real detectors, the optimal performance obtained with the ideal shell cannot be realised in practice.

In view of its symmetry, the first considered geometry is a spherical shell of tapered detectors. As will be shown in more detail in chapter 4, there are only a few "magic" numbers of hexagonal shapes that, together with 12 regular pentagons, cover (tile) a spherical surface. We will consider here only the geometry built from 110 hexagons, which is the underlying structure of existing arrays like GASP and GAMMASPHERE and is proposed in the USA for the tracking array GRETA. The regular spherical shell discussed here is built out of 110 equal, regular hexagonal plus 10 pentagonal crystals, all being tapered and individually canned. This is at variance with the final version of AGATA (as being discussed in the next chapter) and with GRETA, where irregular hexagonal shapes are used in order to obtain the optimal solid-angle coverage. The Ge crystals are 10 cm long and have a diameter at the back of 8 cm. The inner radius R_i = 10 cm of this configuration is rather small for a general-purpose array, which will be used with stable well-focused beams, but also with radioactive beams from relativistic fragmentation facilities.

Next, we will try to cover the solid angle around the target with a smaller number of all equal cylindrical or hexagonal crystals of the largest available size (14 cm long, 8 cm diameter). This results in "barrel-type" configurations with 36 or 54 crystals, providing very good solid angle coverage; unfortunately, they also turn out to have a rather limited inner space. Other packing schemes, e.g. cube-like arrangements, of these detectors have not yet been calculated in detail, but they will also suffer from the limited inner space, if the number of detectors is to be kept small.

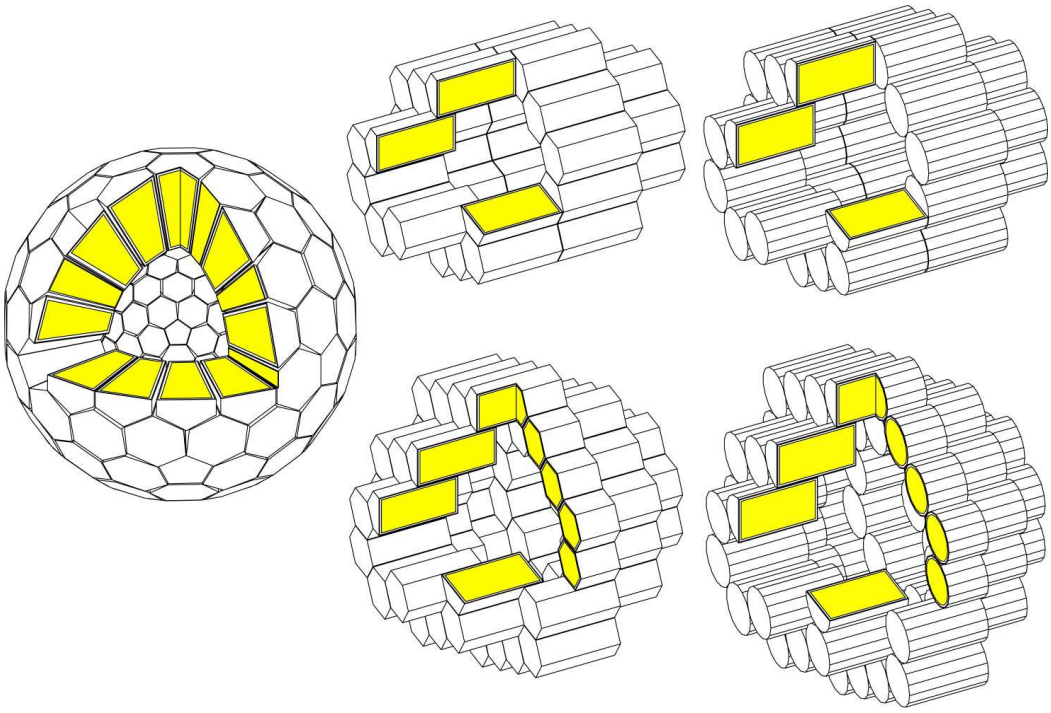

Fig. 3.18: *4π arrays built out of all equal, individually canned, regular Ge crystals.*

The considered configurations are shown schematically in figure 3.18 and a summary of their performance is reported in table 3.1; here the peak efficiency and the P/T ratio are compared for $E_\gamma = 1.33$ MeV and at $M_\gamma = 1$ and $M_\gamma = 30$.

For the barrel-like configurations, the performance is roughly the same independent of the fact whether they are built out of hexagonally shaped or directly from cylindrical crystals. The better packing achieved with hexagons seems not to be sufficient to compensate for the ~20 % smaller amount of germanium lost by cutting the original cylindrical crystal.

Table 3.1: *Performance at $E_\gamma = 1.33$ MeV for various 4π arrays built out of all-equal regular crystals. EUROBALL has 239 Ge crystals packed into 71 cryostats.*

	Number of Detectors	Germanium (kg)	ε_{ph} [P/T] % M_γ=1	ε_{ph} [P/T] % M_γ=30
Standard shell		233	65 [85]	36 [60]
Ball	120	140	30 [56]	18 [50]
Barrel hexagons	36	90	25 [52]	12 [44]
Cylinders		112	26 [56]	14 [50]
Barrel hexagons	54	135	30 [55]	15 [46]
Cylinders		169	29 [58]	16 [48]
EUROBALL	71(239)	210	9 [56]	6 [37]

Conclusions

The principal feature allowing to perform γ-ray tracking with AGATA is the possibility to obtain precise position information for all γ-ray interactions in the detector array by pulse-shape analysis. The position resolution obtained in this way is much higher than the (intrinsic) granularity of the system obtained by segmenting the Ge detectors. The results obtained so far are better than originally anticipated and do indeed already allow for γ-ray tracking. The final limits will only be determined by intrinsic limitations of the underlying physical processes.

Tracking algorithms based on realistic estimates for the position resolution achieve already today a reconstruction efficiency of up to 60 %. Further improvements are expected over the next few years by combining the different tracking approaches. Therefore we can be very confident to achieve the basic requirements for AGATA (as discussed in chapter 2).

The R&D programme performed within the European TMR project has laid the basis for a γ-ray tracking array and allows us to establish the properties of AGATA. This will be done in the following chapters, dealing with the design of individual detectors and the whole array (chapter 4), a detailed evaluation of the different pulse-shape analysis tasks (chapter 5) as well as a description of the necessary hardware for electronics and data acquisition (chapter 6).

4. Design

In order to define the geometry of the array and the shape of its detectors several aspects have be considered:

- Performance, i.e. full energy efficiency and spectral response
- Symmetry
- Modularity
- Available inner space
- Amount of germanium used (cost)

As the array will be used in very different experimental conditions characterized by a limited reaction zone, it seems obvious that a spherical configuration of Ge crystals around this zone provides the best solution. This arrangement also provides the most symmetric configuration, which is important for many methods used in gamma-ray spectroscopy, such as angular distribution or correlation measurements as well as the application of Doppler-shift methods.

4.1 Array configuration

A simple and elegant method for tiling the spherical surface into almost regular hexagons and a few pentagons has been extensively used by the architect Buckminster Fuller in the design of his famous geodesic domes. In full generality, the idea is to tile the spherical surface with the projection of the same simple pattern drawn on each of the faces of an enclosed regular polyhedron. The maximum symmetry of the spherical tiling is obtained using the icosahedron, which, with its 20 regular triangles, is the platonic polyhedron with the largest number of faces. As our goal is to cover the sphere with the best approximation of circular figures the pattern on the faces of the icosahedron should have the shape of regular hexagons. It is easy to show that a regular triangle can be tiled by n+1/2 regular hexagons, with $n=[i^2+3j^2-4]/8$, i+j even, 2n, i and j integers. The first values of n are 0, 1, 1.5, 3, 4, 5.5, 6, 7.5, 9, 10, 12. The projection of the 20 regular triangles onto a sphere produces $N_H=20\cdot n$ hexagons and $N_P=20\cdot 3/5=12$ pentagons. Probably, the best known object that can be built with this procedure is the standard soccer ball with its 20 hexagons (n=1) and 12 pentagons. This is also the only configuration where the hexagons are regular. In general the hexagons are slightly irregular and of a few different shapes. For symmetry reasons, the pentagons are always regular.

Of prime importance for the array is its detection efficiency. For a spherical shell the efficiency is mainly determined by the solid angle coverage and the thickness of the detector elements. To obtain a good coverage several crystals need to be grouped into clusters in one cryostat with as small gaps as possible between clusters. Up to 10 cm thickness the efficiency in the γ-energy region until about 2 MeV (i.e. the basic domain of nuclear spectroscopy) rises strongly with thickness. Larger values mainly increases the efficiency at higher γ energies, e.g. caused by strong Doppler effects associated with relativistic beam energies. However, above 10 cm the amount of Ge required increases prohibitively. Therefore a value of 8 - 10 cm is suggested. The minimal inner shell radius is given by the maximal size of any given

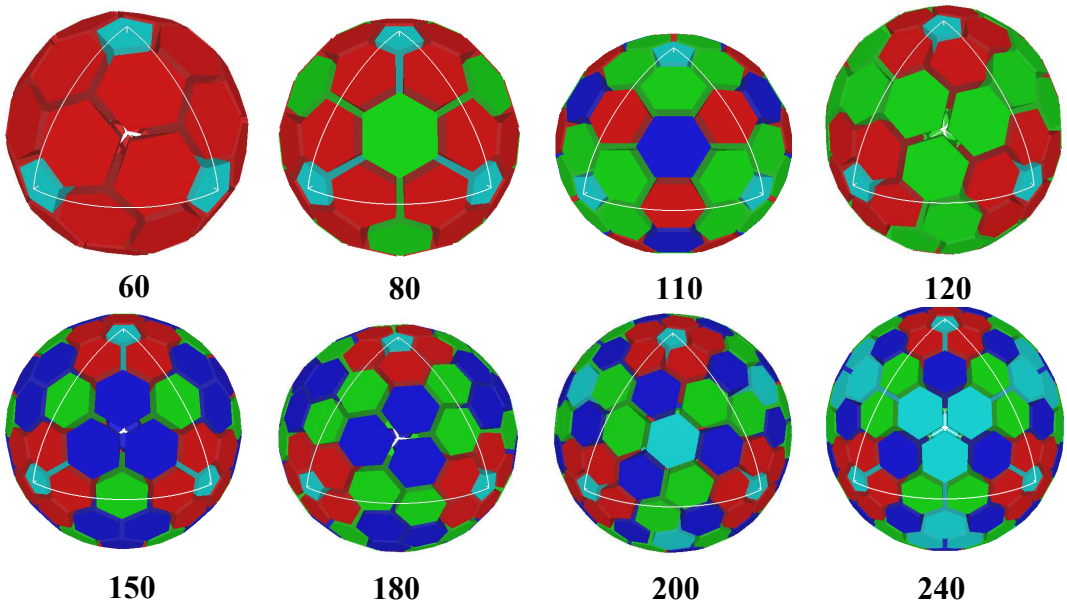

Fig 4.1: *The investigated configurations. The light blue triangle reflects the underlying icosahedral structure that defines the 20-fold symmetry of the construction. The figures are not to scale.*

beam (respectively reaction zone) and the space requirements of ancillary detectors. Experience suggests an inner shell radius ranging from at least 10 cm to about 18 cm. Therefore the outer radius of the shell could be 18 – 28 cm. Using germanium crystals of the maximal available radius of 3.5 – 4 cm and assuming for simplicity a mean gap of 4 mm between crystals we need ≈ 65 – 262 detectors to cover this surface. This means that we should study the geodesic configurations with 60, 80, 110, 120, 150, 180, 200 and 240 hexagons. These configurations together with the next smaller one are shown in figure 4.1, where the different hexagonal shapes are coded by different colours and the spherical triangle represents the projection of one of the faces of the underlying icosahedron.

Additional information about the studied configurations is given in table 4.1, assuming a crystal length of 9 cm and a maximum crystal diameter at the back of 8 cm. For the sake of comparison of the different possibilities, the germanium crystals are individually canned; the thickness of the aluminium can is 1.5 mm and the vacuum spacing is 2.5 mm; the 12 pentagonal crystals are also included.

The intrinsic efficiency of the array depends on the total solid angle coverage, which is almost identical in all the cases. The next important criteria to compare the different configurations are the opening angle of an individual detector/segment (determining the rate limit and the single-hit probability and thus again the efficiency), the angular resolution obtained for a given position resolution (also determining the final energy resolution) and the inner free space. Finally, modularity, i.e. if the array can be built out of (identical) clusters of a few different hexagonal shapes, is an important criterion. Pros and cons of the different configurations are discussed in the following.

Inner space reasons as well as the very large tapering of the crystals (inefficient use of the Ge crystal material) clearly dismiss the configuration with 60 and 80 hexagons, although it is the most modular one as it needs only one hexagonal shape. The configuration with 110 hexagons has been originally proposed for GRETA, but there appears to be no simple way of grouping the detectors into modular clusters and the inner radius is too small.

Tab 4.1: *Details of the geometrical configurations investigated for AGATA. The last column shows the number of crystals that can be packed into all-equal clusters.*

Number of hexagons	Number of hexagonal shapes	Shell inner radius (cm)	Solid angle (%)	Amount of Ge (kg)	Cluster types
60	1 (60)	7.2	78.8	66	3
80	2 (20,60)	8.7	78.2	81	
110	3 (20,30,60)	11.4	78.5	116	
120	2 (60, 60)	12.8	78.1	139	2, 4, 6
150	3 (30,60,60)	15.1	78.6	171	
180	3 (60,60,60)	17.1	78.1	215	3, 9
200	4 (20,60,60,60)	18.0	78.3	232	10
240	4 (60,60,60,60)	20.9	78.7	295	

The two largest configurations with 200 and 240 hexagons are appealing due to their large inner space, but they already need four different hexagonal shapes and they cannot be easily grouped into (small) modular clusters. In addition, the amount of germanium needed is huge, especially if losses due to tapering are taken into account.

The configuration with 120 hexagons is more interesting as there are only two different hexagonal shapes that can be arranged into 60 double clusters, into 30 quadruple clusters or into 20 6-fold clusters. The inner space is barely sufficient for additional detectors and the rather large beam tube required at a fragmentation facility cannot be accommodated without removing a relatively large number of crystals. The final angular resolution and the rate capabilities with this configuration will also be less than required.

The remaining configurations with 150 and 180 hexagons use three different hexagonal shapes and provide sufficient inner space. However, there is no easy way to arrange the detectors of the 150-configuration into modular clusters while for the 180 one they can be grouped into 60 all-equal triple-clusters or into 20 all-equal 9-fold clusters.

In view of its modularity and symmetry as well as for its rather large inner space, the selected configuration for AGATA is that with 180 hexagons. For practical reasons only triple-clusters have been considered, as the construction of 9-fold clusters is likely to be too complicated. With the three different hexagonal crystals packed into triple clusters the final figures for AGATA turn out to be: inner radius 16.8 cm; solid angle 77.2 %; total amount of germanium 206 kg. A few more specific details are reported in table 4.2. In figure 4.2 the corresponding AGATA design is shown including crystal encapsulation and side walls of the cluster cryostats.

It is worthwhile noting that the weight of the original cylindrical germanium crystals, from which these tapered polygonal shapes are machined, is about 400 kg. Such a yield of ~50% is typical with these constructions; in the detailed final design this figure will improve resorting to "hexaconical" shapes (obtained by a partial detector tapering as done for the Euroball Cluster detectors).

Tab 4.2: *Details of the configuration with 180 hexagonal crystals selected for AGATA.*

Crystal type	Ge diameter front (cm)	Ge diameter back (cm)	Crystal volume (cm^3)	Corresponding solid angle (%)
12 pent.	2.84	5.09	86.4	2.1
60 hex.	4.24	7.06	180.7	21.9
60 hex.	4.70	7.65	211.2	25.0
60 hex.	4.95	8.00	236.3	28.2

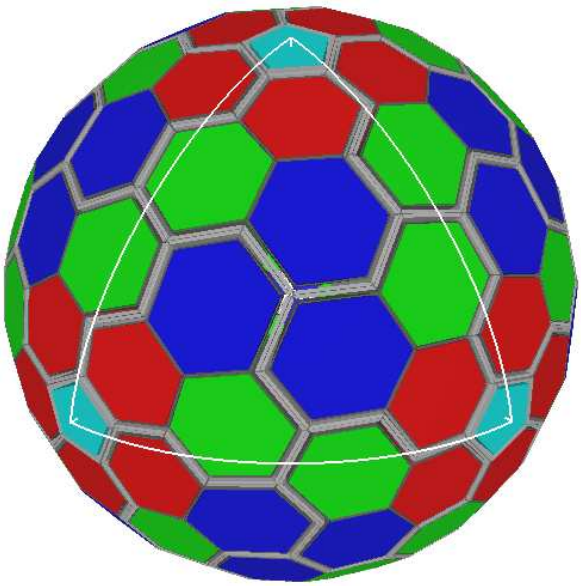

Fig 4.2: *The final AGATA configuration with encapsulated crystals grouped into 60 equal triple clusters.*

4.2 Performance of AGATA

The performance of AGATA, as designed in the previous paragraph, has been evaluated for crystals with a maximum diameter at the back of 8 cm tapered over the full length of 9 cm. For the final array these numbers are expected to improve, i.e. an efficiency around 50 % should be achieved for 1 MeV γ rays, since partially tapered crystals of 10 cm length are planned in order to increase the high energy efficiency and to reduce the loss of Ge material. The performance has been calculated in the two different fields of application, namely the low recoil-velocity and high recoil-velocity regime.

The maximum achievable efficiency is of course obtained by summing all interaction points produced from the Monte-Carlo simulation for M_γ=1 transitions, i.e. using the whole AGATA array as one individual detector. The results are shown in figure 4.3.

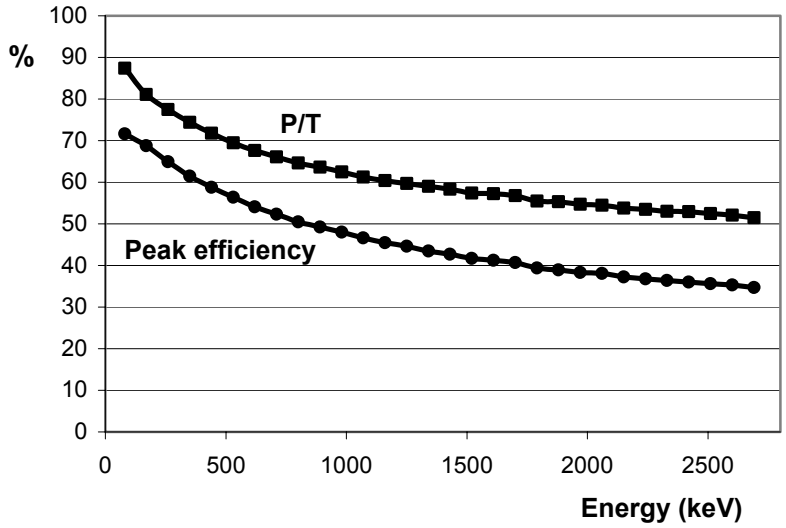

Fig. 4.3: *Response of AGATA as a function of γ-ray energy. Result obtained by summing all interaction points. As no tracking is applied this is valid only for M_γ=1.*

The real performance obtained when the tracking algorithms are applied to this data depends on the position resolution and therefore it is worthwhile to repeat here the assumptions made in the following calculations. Before using them for the reconstruction, the position of the interaction points given by the simulation is modified in a random way along the three coordinate axes according to a Gaussian distribution with a FWHM that depends on the energy of the point. Typically the FWHM is 0.5 cm at 100 keV and scales inversely proportional to the square root of the energy. Points that are closer than 0.5 cm are then packed together into an energy-weighted average position. The energy is perturbed in a similar way yielding a FWHM of 2.1 keV at 1333 keV.

Performance at low recoil velocity

For the case of zero recoil velocity, the response of AGATA to cascades of 1 MeV γ-rays is shown in fig. 4.4 as a function of multiplicity. It can be seen that with the present status of development of the reconstruction algorithms the achieved peak efficiency at 1 MeV is ~22 % for M_γ = 30. This is a factor of 5 better than EUROBALL and is likely to improve, as the tracking algorithms will be further developed.

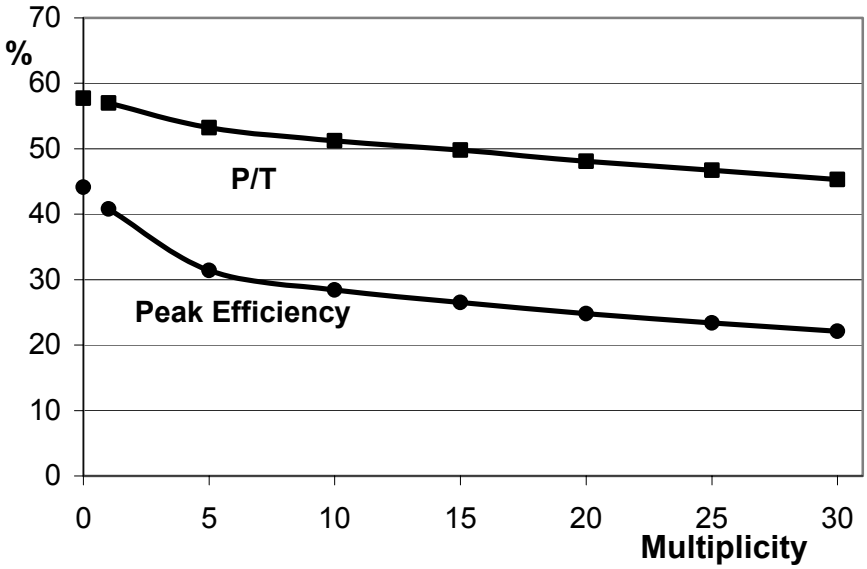

Fig. 4.4: *Efficiency and P/T of AGATA as a function of multiplicity for cascades of 1 MeV transitions. The values at M= 0 are the response of the array, obtained summing all interaction points. The other, tracking, results depend on the assumed position resolution and will improve following the development of the reconstruction algorithms.*

As long as the multiplicity is not too high (≤10) it is possible to increase slightly the detection efficiency moving the target off centre along the beam axis as shown in figure 4.5. This effect is due to the radial symmetry of the constructions, which implies that radiation starting from the geometrical centre has the largest chance to escape through the inter-detector gaps.

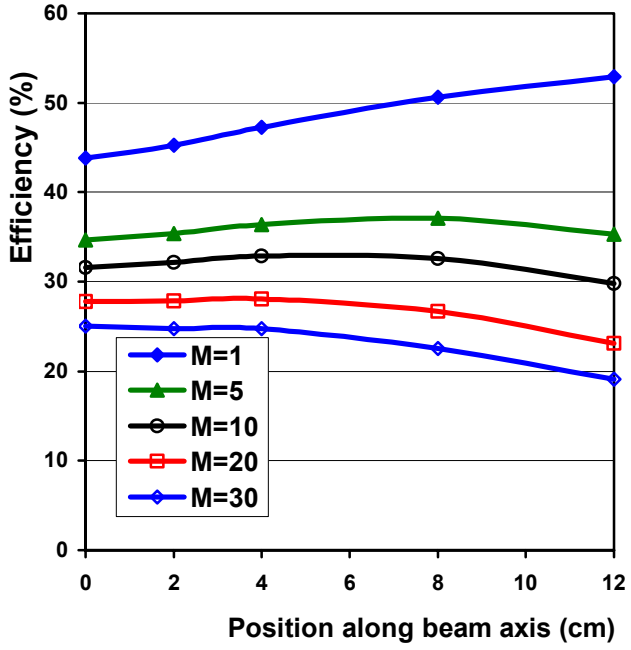

Fig. 4.5: *Efficiency of tracked data as a function of position of the γ-ray source along the beam axis. The calculation has been done for E_γ= 1 MeV.*

A set-up for high recoil velocity

At very high recoil velocity the effective multiplicity of the emitted radiation is focused in the forward part of the array. Therefore, one can envisage a first 1π set-up of AGATA prior to completion of the full array with 15 of the 60 clusters covering the forward quadrant as shown in figure 4.6. The performance of this array is shown in figure 4.7. It is worthwhile noting that, due to the superior performance of tracking detectors, the efficiency of this configuration at low recoil velocity is roughly equivalent to that of Euroball; at high recoil velocity the performance is about five times bigger.

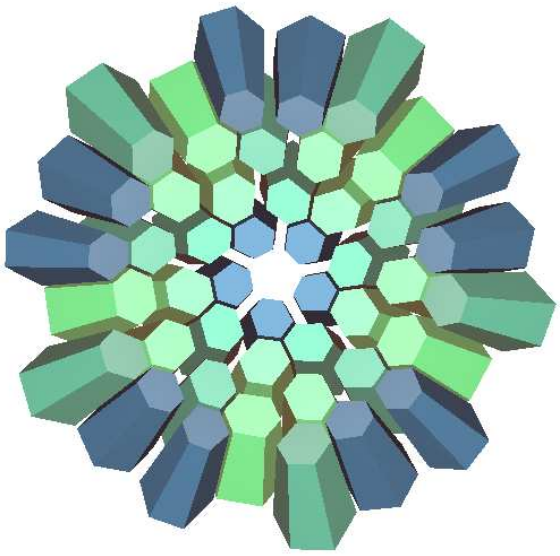

Fig. 4.6: *1π set-up for relativistic beam energies. The forward quadrant is covered by 15 triple clusters.*

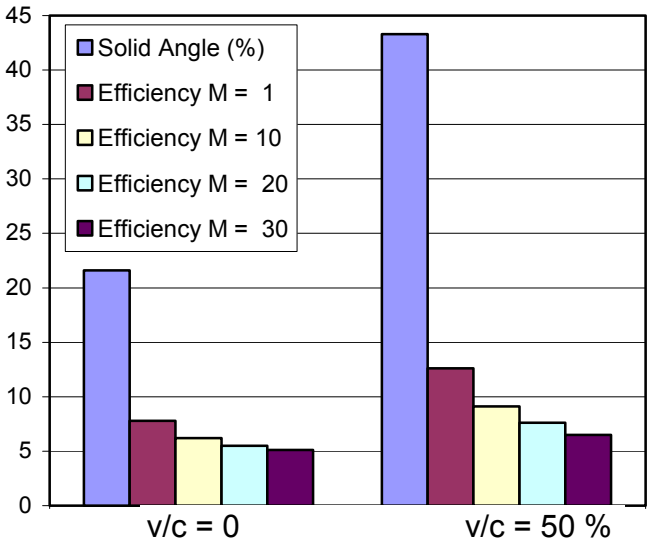

Fig. 4.7: *Efficiency of the 1π set-up for stopped and relativistic beams. Due to the kinematic focusing, the effective solid angle of the array increases by about a factor of two at v/c = 50%.*

4.3 Detector unit

In order to achieve optimum coverage of the shell (see section4.1), the design of γ-ray tracking modules needs to be based on the concept of composite detectors. Only encapsulated, segmented detectors provide high reliability for such systems and allow access to the cold part of the electronics of the many high-resolution channels to fix problems like noise, cross-talk or burned FETs. Three encapsulated detectors are merged together in a common cryostat as a compromise between packing a high amount of germanium and the cooling power needed for both the crystals and the FETs. Figure 4.8 shows the tracking detector module which has been designed on basis of extensive experimental and theoretical studies performed within the framework of an European TMR network.

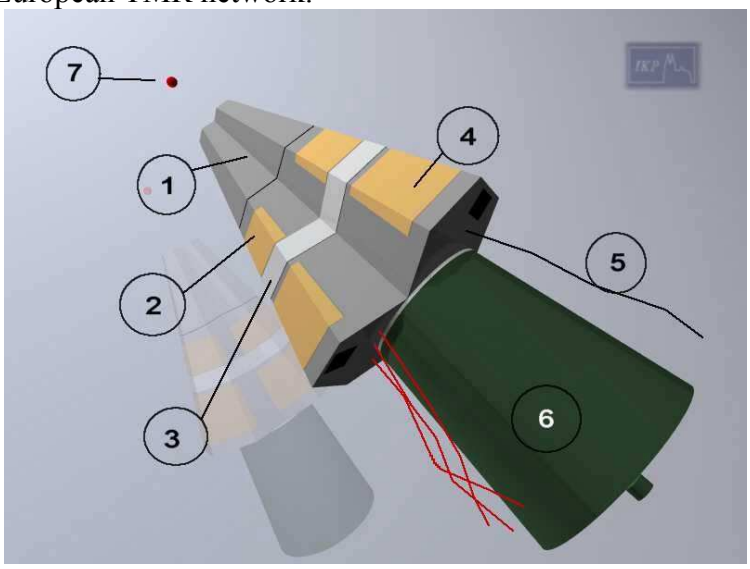

Fig. 4.8: *The γ-ray tracking module: ① Cryostat end cap containing the 36-fold segmented Ge detectors, ② preamplifier section, ③ support frame, ④ digital front-end electronics, ⑤ fibre-optic channel readout, ⑥ LN2 dewar, ⑦ radiation source.*

Each cryostat contains three 36-fold segmented Ge detectors of hexagonal, tapered shape (8 cm diameter, 10 cm length). The individual Ge crystals are encapsulated in a very thin Aluminium can – a new technology, developed in the framework of the Euroball and Miniball projects, which strongly improves the reliability of the detectors (see figure 4.9).

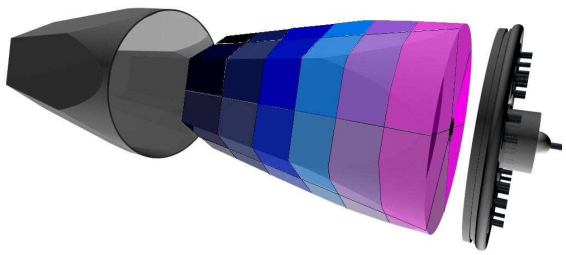

Fig. 4.9: *The 36-fold segmented, encapsulated Ge detector*

The 111 preamplifiers consist of a cold part including the FET´s mounted inside the cryostat and a warm part behind the Ge detectors. Highly integrated digital pulse processing electronics is mounted in a second layer behind the preamplifiers. The data is transferred via a fibre-optic channel for further analysis. A central support frame is situated between the preamplifier and the pulse-processing section. The Ge detectors are cooled with liquid nitrogen contained in conical dewars. The geometry of the tracking module is chosen to form part of a spherical array. A full tracking sphere will consists of 60 of these modules and 12 additional detectors of pentagonal shape. Figure 4.10 gives an artist's view of an AGATA sub-unit consisting of seven three-way cluster detectors.

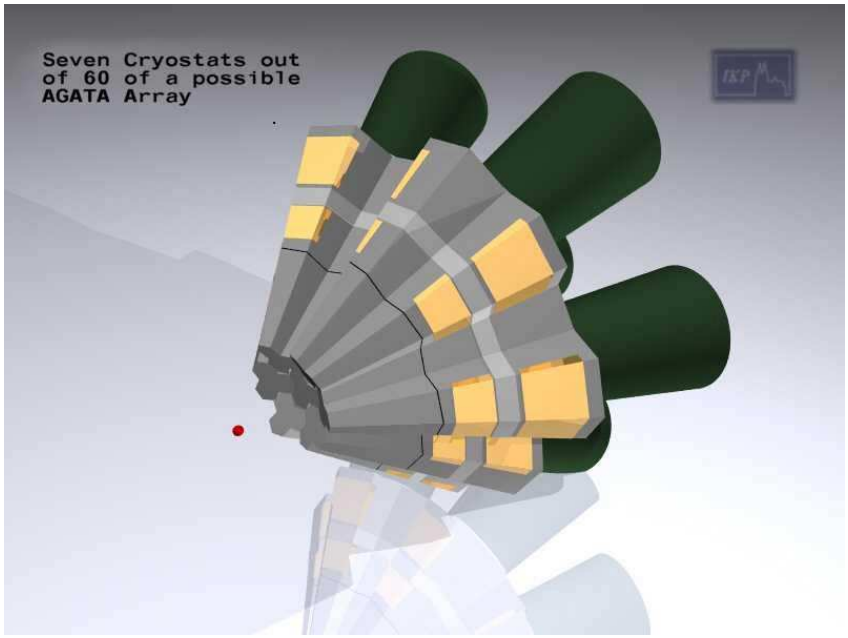

Fig. 4.10: *A sub-unit of the AGATA array showing seven of the 60 cluster cryostats.*

4.4 AGATA mechanics

A highly stable mechanical structure is required to support the 180 hexagons and 12 regular pentagons in the spherical array configuration. This structure will be required to support a total weight in excess of 1.5 Tonnes, and must accurately position each detecting element such that it will maintain a focus at the target point to within a sphere of confusion of 0.5mm. This is a considerable design task, which will require the use of the very latest CAD (computer aided design) and FEA (finite element analysis) software.

It will also be necessary to access the target point in order to change target chambers and load target specimens. In order to do this the whole spherical array must be easily split in the direction perpendicular to the beamline. This requirement places a considerable demand on the mechanical structure, and will necessitate the provision of a highly precise mechanism and control system to safely and accurately drive the 1.5 Tonnes of detecting elements back and forth around the target point.

A further requirement of the mechanical design is to provide a structure in which the detectors in the hexagons and pentagons can be easily removed. This will require an automatic mounting facility on the structure itself, and also a versatile robotic type manipulator that is possibly computer controlled in order to accurately remove and replace all detectors around the full spherical configuration.

The final major requirement of the mechanical support structure is that it should be easily removed to different experimental areas. Again, this imposes a considerable demand on the mechanics, possibly requiring the design of a fully integrated platform to support the array, auto-fill, data acquisition, and power supplies.

The proposal also includes provision for several target chambers. These will vary in cost and complexity ranging from a simple target beam pipe design with single target holder to a space optimised multi-functional chamber with automated multiple target loading mechanism. Specific target chambers will also be required to accommodate specific ancillary detectors.

5 Pulse Shape Analysis

5.1 Introduction

Besides high efficiency and energy resolution, the most important new feature of the tracking array AGATA is that it will provide good position sensitivity. Usually position sensitivity for semiconductor detectors is obtained by segmenting the electrode in geometrical areas forming pixels or stripes. The signals of each of these electrode segments are read-out separately, such as when an interaction occurs, its position can be assigned to the detection volume underlying the segment, which gives a signal. Since large volume, coaxial Ge detectors are used for AGATA to optimise efficiency, segmentation in depth is needed in addition. The size of the resulting volume elements, or voxels, represents the attainable 3D position resolution in such a scheme. As it was pointed out before, this 3D position resolution has to be better than 2 mm for an efficient γ-ray tracking. This would correspond to a number of about 30000 voxels into which each AGATA detector has to be segmented. Such high-fold segmentation is technically impossible for reasons of complexity, number of read-out channels, and inclusion of large amounts of insensitive materials in the detection body, which would destroy all the positive features of Ge detectors.

However, due to the fact that, depending on the interaction position within the segment, different signal shapes will be induced, a position resolution much superior to the dimension of the segment can be obtained by analysing the shapes of the signals taken from the segments. The reason for the shape variations is the different path length of the charge carriers (electrons and holes), which, after being created following an interaction, drift towards the detector electrodes. Since signals are induced only if there are moving charge carriers inside the detector, different signal shapes will result for interactions occurring at different distances from the electrodes, or for different distances from the segment borders. Following this approach AGATA will use pulse shape analysis methods to reduce the segmentation scheme to a technically feasible level while maintaining the position resolution needed for tracking. In fact, for an efficient tracking especially in case of multiple interactions not only the accurate positions of the interactions, but also their number, and the partial energies released at each interaction, have to be determined. Pulse shape analysis can provide this information, however with a finite accuracy, which depends on various parameters. Detector geometry, segmentation level, impurity concentration, preamplifier bandwidth, signal-to-noise ratio, and sampling frequency are some of them. In this respect pulse shape analysis plays a key role for the AGATA detector and electronics design and for γ-ray tracking in general.

The complex analysis of detector pulse shapes, which is needed to provide precise tracking data, can only be carried out using state-of-the-art digital signal processing techniques. Digital signal processing electronics for high-resolution spectroscopy with semiconductor detectors has been introduced almost ten years ago [Geo93, Geo94], but only recently research in the completely new field of digital pulse shape analysis for γ-ray tracking started. Various prototype algorithms for digital triggering and to extract energy, time, and position information from sampled detector signals have been developed and tested already, mainly in the framework of the TMR network project *Development of Gamma-Ray Tracking Detectors for 4pi Gamma-Ray Arrays* and the GRETA project. They will be used as basis for the determination of the AGATA design parameters and for further developments dedicated to the project.

5.2 Pulse shape analysis methods

Theory and simulations

The tracking array AGATA will consist of 190 individual, large volume Ge detectors. Each of these detectors will exhibit individual properties regarding electric field geometry and strength, crystal orientation, impurity concentration, bias voltage, contact quality, neutron damage, detector temperature, and preamplifier characteristics. All these properties determine the specific pulse shape generated by an interaction at a specific position. To reach a position resolution of about 1 mm by pulse shape analysis, i.e. an effective granularity of 30000 voxels per detector, the corresponding 30000 position specific pulse shapes for each of the 190 detectors have in principle to be known.

An experimental determination of these pulse shapes is ruled out by the fact, that such measurements are extremely difficult and time consuming. The event rate of the required precision Compton coincidence set-up amounts to values significantly below 1 Hz, as it was demonstrated by the experimental studies with the GRETA prototype Ge detector [Vet00].

Therefore, such measurements have to be substituted by reliable pulse shape simulations. A theoretical model for each detector of the AGATA array has to be established providing a concise and realistic representation of its characteristic features, and how they influence the position dependent pulse shapes. Optimal symmetries regarding crystal orientation and detector geometry will be chosen to keep the parameterisation as simple as possible. In this context, it is important to have a good control on the charge carrier collection process, which involves a reliable representation of the carrier drift velocity and the electric field inside the detector.

The physics underlying the charge collection process, i.e. the carrier drift in Ge detectors at high electric fields and low temperature has been theoretically studied in the framework of the TMR network project. Suitable model descriptions, which take into account the crystal orientation dependent anisotropy of the drift velocities and the angular shift of the drift direction have been worked out and tested against experiment [Mih00].

On the basis of these models simulations of the induced signal shapes of both, the real charges as well as the mirror charges have to be performed, in order to investigate the characteristic features relevant for tracking. The inclusion of both types of signals into the pulse shape analysis is an important new concept specific to segmented detectors. Real charge signals are measured at the electrodes of the segment, in which the interaction takes place, i.e. where real charge carriers are generated and collected on the electrodes. Their net charge, that is, the total charge integrated over the charge collection time, is therefore non-zero. Mirror charge signals are measured on the electrodes of the neighbouring segments, where no interaction takes places. They represent influenced charges, induced by the movement of the real charges in the neighbour segment, the electric field of which extends over the segment borders. The mirror charge signals are calculated using the Weighting Field approach and their net charge is zero (cf. figure 3.3). The analysis of the real and mirror charge signals allows a localisation of the interaction positions with a much higher precision than that provided by the segmentation pattern only. Since the amplitude of the mirror charge signals depends on the segment size, the optimal segment size relates to the required minimum signal-to-noise ratio of the mirror charge signals.

Pulse shapes are simulated by calculating the electrical field in the Ge detector and taking into account the charge carrier transport. The calculations can be performed analytically only for some simple detector configurations. More complicated detector geometries can be calculated in detail using codes based, e.g., on Finite Elements Analysis. To exemplify the position dependence of the pulse shapes, a set of signals is shown in figure 5.1 for a 24-fold segmented closed-ended Ge detector [Kro01]. The segment where the interaction takes place is assumed to be in the coaxial part of the detector. The real charge pulses are shown in the left lower panel of figure 5.1 while the transient mirror charge signals are shown in the right lower panel.

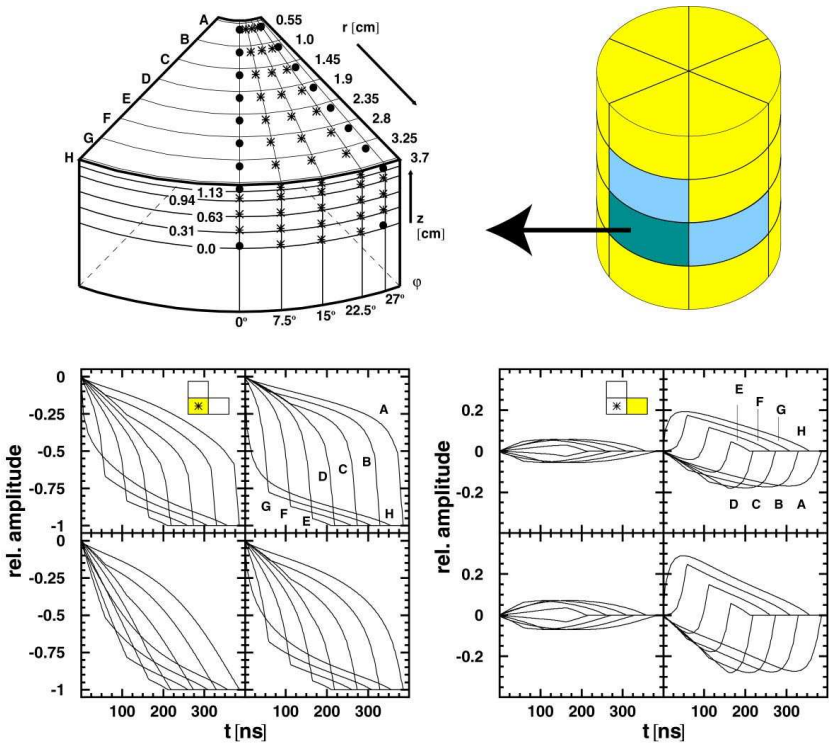

Fig. 5.1: *Calculated pulse shapes for the coaxial part of a closed-end Ge detector. The real charge pulses shown in the four graphs of the lower left panel are due to interactions at different radii, azimuthal angles, and longitudinal positions in the upper right quarter of the selected segment (indicated by dots). The corresponding transient mirror charge pulses in the neighbouring horizontal segment are shown in the left panel.*

This basic description of the pulse shapes has to be extended to a realistic modelling of each of the AGATA detectors, which takes into account their individual properties. To simplify this task all properties, which can be controlled, like detector geometry, segmentation pattern, crystal orientation, and preamplifier type will be chosen to be as identical as possible. For the remaining parameters, efficient strategies have to be developed to determine them experimentally by measuring a minimal number of reference values. These values should be significant enough to allow an easy and reliable extrapolation to the characteristics of the whole detector.

The two most important parameters affecting the signal shapes at the output of the preamplifier, which remain, are the actual electric field distribution inside the detector and electronic effects. The electronic effects include detector and preamplifier noise, preamplifier impulse response, and signal corruptions due to capacitive coupling between the segments, or electronic cross talk. However, they can be measured relatively easy, and various analytical

and numerical methods for a description of these effects have been developed, which can be used in the detector model.

In contrast to that it is much more difficult to get experimental access to the electric field distribution inside the detector, since it cannot be measured directly. Actually, it can be determined only indirectly via the object under study itself, namely the pulse shapes. Detailed reference studies of pulse shapes for a selected number of AGATA detectors under different operating conditions have to be performed to determine the most significant reference values. In addition, a close collaboration with the detector manufacturers will yield valuable information about actual impurity concentration profiles and other detector and contact properties affecting the electric field distribution.

Algorithms and implementations

Based on realistic models for the AGATA detectors describing their pulse shapes, existing algorithms to extract the relevant information will be adapted to the AGATA specific conditions, or novel algorithms will be developed. The design goal concerning the AGATA signal processing and pulse shape analysis is to extract from the detector signals, on-line and in real time, trigger and timing information, as well as the number of interactions and their individual energy deposits and positions inside the detector.

Although the AGATA data acquisition is designed to be triggerless, the determination of the event occurrence is essential for all time variant algorithms of the subsequent digital signal processing and for the generation of a time stamp. Conventional triggering and timing methods in nuclear spectroscopy are based on the analogue Constant Fraction Discrimination (CFD) concept. Since the AGATA electronics is designed to exclusively employ digital signal processing techniques, digital counterparts for the conventional analogue trigger and timing discriminators are to be developed. The digital environment provides an additional advantage in the sense that the algorithms can be made recursive, since virtually any part of the input signal can be made available for analysis at any time.

The main requirements for the triggering system of a segmented tracking detector are to provide a low threshold level, a reasonable time resolution and support of high event rates. A low threshold is required, since besides incident γ rays also scattered γ rays of low energy have to be detected, which, if not observed, would spoil the tracking and increase the background in the final γ-ray spectra. The timing accuracy should be sufficient to control the subsequent, time variant processing and to define the coincidence conditions. The Slope Condition Counting (SCC) algorithm, developed in the framework of the TMR network project, will be used as starting point for that purpose. It employs an unconventional statistical method to detect the onset of a pulse. The basic idea is, that in a given data set with statistical fluctuations the probability of a data point value to be larger than its precessor increases, when the data set exhibits a rising slope.

While the timing accuracy offered by the digital trigger is limited, mainly because the generated trigger signal is synchronized to the sampling frequency, a much more precise timing with sub-sampling interval resolution is needed for lifetime measurements and for the pulse shape analysis. This is because all pulse shape information is contained in the development of the pulse amplitude as function of the carrier drift time, i.e. the accuracy of any pulse shape information is directly correlated to the accuracy of the time reference. A novel, digital timing method, the Normalized Step Response (NSR) algorithm, has been developed, that provides this accuracy. The main idea behind this algorithm is, that for small time intervals (approx. 50 ns) the main limitation in bandwidth is given by the preamplifier

transfer function. Therefore, for an accurate determination of the occurrence of sharp variations in the detector signal, corresponding to the onset of an event, the preamplifier impulse response function has to be deconvolved from the measured signal. A very sensitive issue for deconvolution problems is the noise amplification. To put a limit on the noise amplification, regularization methods are applied, making use of information known a priori about the signal, which has to be reconstructed. In the case of a Ge detector, it is reasonable to assume that the beginning of the detector current signal is a step function.

The time invariant Moving Window Deconvolution (MWD) technique [Geo94] will be used, to extract precise energy information from the sampled detector signal. It is a well-established digital algorithm providing a trapezoidal filtering, which is insensitive to ballistic deficit effects, and which allows to achieve resolution and throughput performances for large volume Ge detectors, which approach the theoretical limits.

All of the algorithms presented above are ready for an on-line implementation in hardware on Programmable Logic Devices (PLD) or as software modules on the Digital Signal Processors (DSP) of the AGATA electronics. Test results are presented in the following section.

However, the main aim of the pulse shape analysis is to obtain relevant information, which can subsequently be used by the tracking algorithms to reconstruct the sequence of interactions of a γ ray in the detector. Ideally, the full 3D position and energy deposition of each of the γ-ray interactions give the relevant information. The pulse shapes of the segment signals are the only source, which can provide this information if accuracy better than the segment size is desired.

Since analytical methods to analyse the pulse shapes are hardly feasible, due to the complexity of the pulse shapes, induced especially by the complexity of the weighting fields, an involvement of pattern recognition concepts is one of the approaches presently under development. It implies that a database has to be constructed, which has to cover the various expected classes, and the recognition system has to identify to which class the experimental data pertain. A class corresponds to a set of particular interaction positions characterized by a specific pulse shape. In case of AGATA simulations based upon realistic detector models will allow to obtain these data.

However, since the signals exhibit a strong non-stationary character, and since the concept of tracking implies that one deals with a sequence of scatterings, i.e. multiple interactions, the problem is even more demanding. This is because now the aim is not only to identify a single class within the experimental data, but a superposition of different classes with different weights. In order to be able to decompose different components of a noisy experimental signal, an adequate pre-processing becomes important, which emphasizes the differences between signal components corresponding to different classes. A new representation of the signals, featuring an increase of the distance between classes with increasing distance between physical interaction positions, represents the optimal choice, since the ideal case of complete orthogonality between classes is not possible here.

In the present approach a wavelet transformation is chosen for the pre-processing producing this new representation, because of the strong non-stationary character of the detector signals, with relatively small variations during the drift time of the carriers and steep slopes at the moment the charge carriers reach the electrodes. The portions with low and high frequency components are the features, which characterize the signal and hence should be extracted. The wavelet transformation is ideally suited for that, because it gives good time resolution for the

high frequency components of the signal, and good frequency resolution for the low frequency components, where good time resolution is not so important.

Because the amplitude of the induced signals is significant not only in the irradiated segment, but also in its first neighbours, the performance of the final identification system can be further improved by correlating the information obtained from the irradiated segment with that obtained from its neighbours. This correlation system has also to decompose the different components found in case of multiple interactions. During the development of this combined Wavelet transformation - Pattern recognition - Correlation analysis (WPC) identification system special attention was paid to simple and compact algorithms, which allow on-line processing in real time.

Another development, representing an example for an off-line approach, is the application of Artificial Neural Networks (ANN) or Genetic Algorithms (GA) to quantify the number of interactions per segment and to determine the position and the energy deposit for each interaction. Neural networks and genetic algorithms have the ability to extract the features themselves by learning, with the additional advantage, that no analytical or numerical description of the features needs to be found, or even to exist. Therefore they provide an important, model independent measure of the information content of the signal in general.

5.3 Pulse shape analysis results

The results of the research on pulse shape analysis carried out so far not only demonstrated, that position sensitivity for large volume Ge detectors can be achieved, which is sufficient to make a tracking array a realistic concept, they also helped to define various parameters in the design of the AGATA detector and the AGATA signal processing electronics.

Anisotropic charge carrier mobility in Ge detectors

The physics underlying the charge collection process, i.e., the carrier drift in Ge detectors at high electric fields and low temperature has been theoretically studied and tested against experiment. To extract the position information from the pulse shape it is essential to know the drift velocities of the charge carriers at each point in the detector. The fact that the conductivity in Ge detectors is anisotropic with respect to the crystallographic directions [See85] is expected to have important effects, (i) on the magnitude of the drift velocities and (ii) on the angle between the drift velocities and the electric field vectors.

The dependence of the experimental drift velocity in a Ge detector on the applied electric field for the <100> and <111> directions [Ott75] together with the calculated drift velocities for the <110> direction [Mih00] are shown in fig. 5.2 for a temperature of T = 80 K. The differences between the drift velocities are largest for electric fields in the region of ~500 to ~6000 V/cm, indicated in fig. 5.2 in yellow.

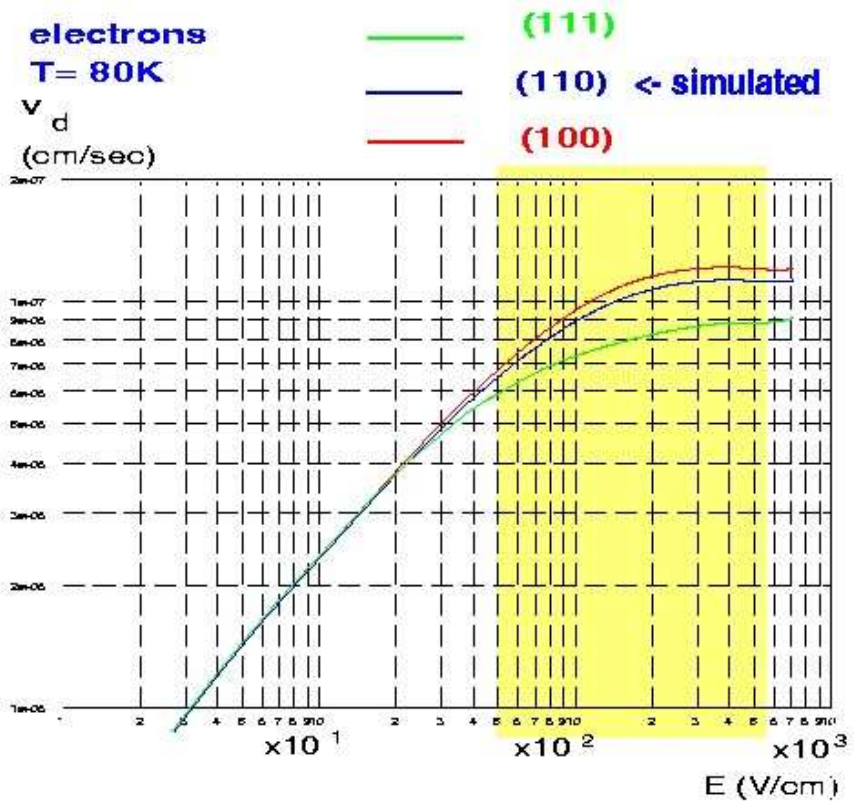

Fig. 5.2: *The experimental drift velocities of electrons in a Ge crystal along the <111> and <100> directions at a temperature of T = 80 K and the simulated drift velocity for a field oriented along the <110> direction.*

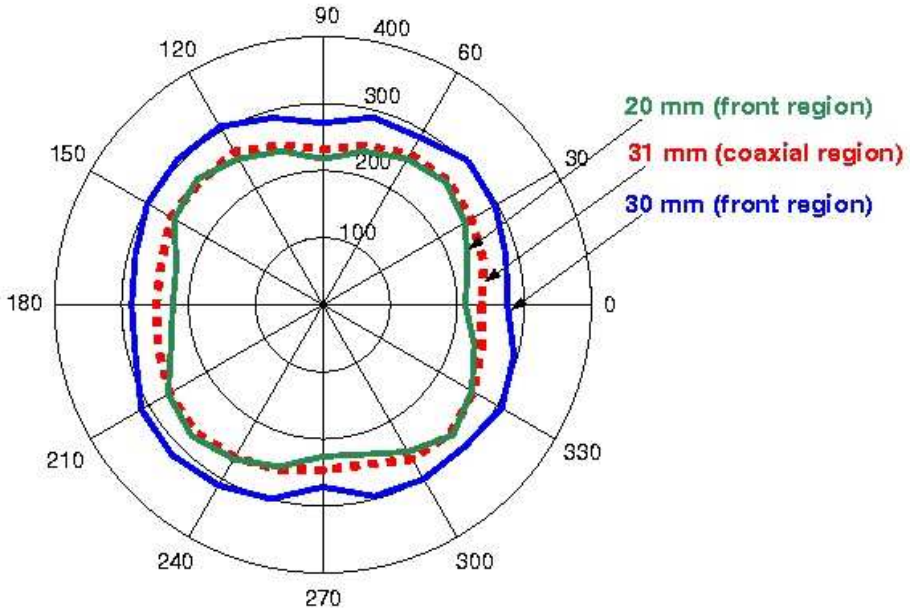

Fig. 5.3: *Polar plot of the time-to-maximum (in ns) for pulses from 60 keV γ rays emitted from a ^{241}Am source measured with a Ge detector. The angles 0° and 90° correspond to the <100> and <010> crystallographic directions, respectively.*

Experimental investigations [Mih00] of the influence of the anisotropic drift velocity on the pulse shapes have been carried out by scanning a semi-hexagonal Ge detector of the EUROBALL project with collimated ^{22}Na and ^{241}Am sources. The orientation of the Ge crystal was determined by means of neutron scattering. As result the time between the beginning of the pulse and when it reaches its maximum (time-to-maximum) is plotted in figure 5.3 in a polar diagram for radial and longitudinal positions as function of angle. It was found, that the charge collection time depends on the azimuthal angle showing a 90º symmetry with a maximum at the <110> direction and a minimum at the <100> direction of the face-centred cubic (FCC) Ge crystal.

The variation of the charge collection time as function of angle is especially large in the front part of the Ge detector. Differences of up to 18% have been obtained for different drift directions relative to the crystal orientation. In the rear coaxial part of the Ge detector, the differences are only of the order of 6%. In addition, the pulses are in the rear coaxial section about 20% shorter than in the front section for a given angle. The reason for these differences is the following. In the front part the charge carriers travel, because of the field distortions in the closed-end Ge detector, to a large extent along the <111> direction, in which the drift velocity is lowest. However, in the rear coaxial part the electric field is cylinder symmetric and the charge carriers travel along the <100> or <110> directions, in which the drift velocities are higher. The results are in good agreement with simulations and the charge collection process is considered to be well understood now [Mih00].

Experimental evidence for the dependence of pulse shapes in closed end coaxial Ge detectors on the anisotropy of the electron drift velocity, and hence on the crystallographic orientation, has been established by this research for the first time. In the case of segmented detectors, the anisotropy will affect not only the pulse shape of the real charge signals induced in the segments, in which charge actually is collected, but also those of the induced mirror charge signals in the neighbouring segments. The principal conclusion is that the anisotropy of the drift velocity has to be taken into account, when modelling the AGATA detectors and when analysing measured pulse shapes. To simplify this, the crystallographic axes and the hexagonal geometry of the AGATA detectors will have a fixed orientation relative to each other.

Segmentation pattern

The accurate determination of the full three-dimensional position of the interaction will involve the correlation of the induced pulse shapes of the irradiated segment with the pulse shapes of the neighbouring segments in the azimuthally as well as longitudinal directions. This implies that the amplitude of the induced mirror charge signals in both directions should be maximized and made comparable. This requirement correlates the segmentation geometry in one direction to that in the other direction, a certain width of the segments in one direction determining that of the other direction. Since the calculated weighting fields appear to decrease faster in longitudinal direction, the height of the segments, i.e. the dimension in the longitudinal z-direction (detector axis), should be smaller than the width, at least if the accuracy in determining the z-coordinate is as important as that of the other directions. The azimuthal segmentation of the AGATA detectors is predefined to be six-fold due to their hexagonal geometry. Given the diameter and length of the crystals, the adequate segmentation in longitudinal direction turns out to be six-fold, too. Hence, the AGATA detectors are chosen to be in total 36-fold segmented.

Trigger

To define a trigger is the first digital processing task of the AGATA signal processing electronics and the full data stream of samples at the output of the sampling ADC has to be analysed. A possible solution for that is the Slope Condition Counting (SCC) algorithm, which comprises a time invariant digital moving window filter, the output of which is fed via a moving window averager to a maximum detector with a built-in threshold comparator. For each new sample entering the window, the digital moving window filter produces a new value representing the probability of having a rising slope inside the window. Maxima of this discrete probability function occur, when the window actually covers the leading edge of a pulse. They are detected by the maximum detector, which generates a trigger signal, when a predefined threshold is exceeded. As main components, the digital moving window filter and the maximum detector each employ approximately N comparators and N(N-1) registers, where N is the number of samples in the window. The SCC algorithm can easily be implemented on the Programmable Logic Devices (PLD) of the AGATA digital front-end electronics. Performance tests of the algorithm were carried out employing a 40 MSPS PPADC module with 12-bit resolution. In figure 5.4 the resulting low energy efficiency (red line), i.e. the low threshold performance, measured using a large volume Ge detector irradiated by a combination of a ^{60}Co and a ^{241}Am source, is compared to those of an analogue Constant Fraction Discriminator (Canberra model 1326A) with two different parameter settings, optimised for low threshold (black line) and good timing (blue line), respectively. The observed efficiency is 80 % at 10 keV and 100 % down to 20 keV.

The trigger algorithm detected 99% of all events within a time range of 195 ns and 90% within a range of 103 ns. This accuracy, and the observed Full Width Half Maximum (FWHM) of 50 ns, which approaches the theoretical minimum of two sampling intervals, is sufficient for the control of the subsequent time variant processing tasks, and for coincidence timing and time-stamp generation. For improved trigger time resolution the sampling rate of the digitising ADC could be increased.

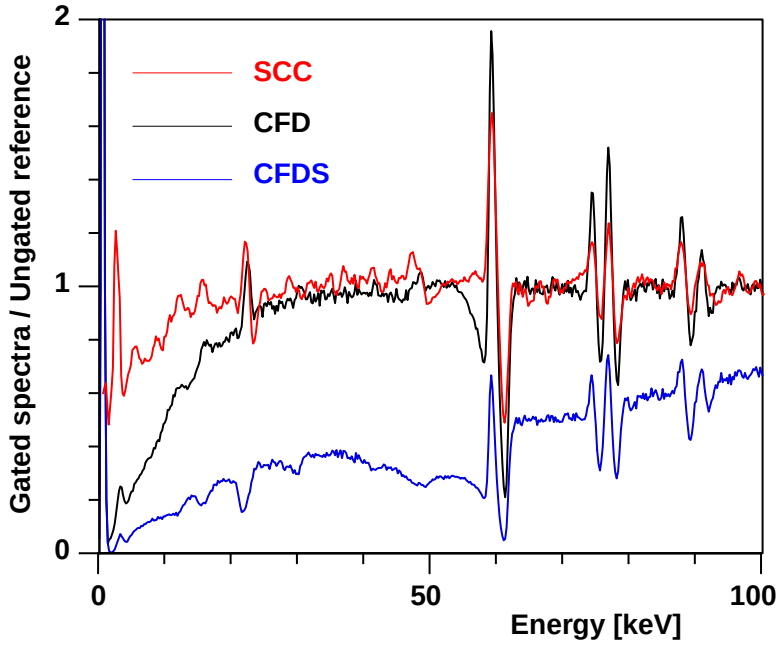

Fig. 5.4: *Measured efficiency of the SCC discriminator (red line) compared to that of an analogue Constant Fraction Discriminator (Canberra model 1326A) for two different parameter settings optimised for low threshold (black line) and good timing (blue line), respectively.*

Energy

The Moving Window Deconvolution (MWD) for precise energy determination represents a time invariant digital filter, too. Therefore, it also has to be applied to the full data stream in order to obtain optimal performance with respect to resolution and throughput. However, the event data samples can be diminished, since details of the pulse shape are not relevant. The reduction can be implemented on the PLD, where the trigger algorithm resides. The basic MWD algorithm is very simple and comprises just a multiplication and accumulation. However, the complexity increases rapidly, as soon as advanced features, like gated baseline restoration, adaptive shaping, adaptive ballistic deficit correction, etc., are included. This favours an implementation on the DSP of the AGATA signal processing electronics. Various DSP implementations, also on commercial modules, exist, which may be adopted for AGATA. Since it was the first digital algorithm introduced in high-resolution spectroscopy [Geo93, Geo94], the MWD represents a well-established technique, and all details about its features and performance can be found in the literature.

Time

The Normalized Step Response (NSR) algorithm has been tested for high resolution time information. This algorithm for digital time discrimination with sub-sampling interval resolution is a recursive, time variant filter, dealing only with the samples from the leading edge of the signals. Although very simple, too, it involves the comparison of normalized samples, i.e. subtraction and division operations. Hence, preferably a DSP, as in the case of its test installation on the PPADC prototype hardware, has to be chosen for its implementation in the AGATA signal processing electronics. In table 1, the measured performance of the NSR discriminator with respect to time resolution and efficiency is compared to a conventional approach, the Extrapolated Baseline Crossing with linear (EBC1) and quadratic extrapolation (EBC2), respectively. Digital algorithms for the latter have been implemented on the PPADC hardware, too. They use a 1^{st} order polynomial to fit the baseline and a 1^{st} order (EBC1) or a 2^{nd} order (EBC2) polynomial, fitted to the first few samples of the leading edge, to extrapolate the baseline crossing, respectively.

Table 5.1: *Performance of the NSR digital timing discriminator (see text).*

Algorithm	Full dynamic range		Dynamic range 1.0-1.4 MeV	
	FWHM [ns]	Efficiency [%]	FWHM [ns]	Efficiency [%]
NSR	8.5	68.5	6.5	80.2
EBC2	9.0	63.4	7.0	79.9
EBC1	14.0	63.1	11.5	76.8

The time spectra were measured with a ^{60}Co source using the leading edge discriminated signal of a fast scintillator as time reference. In fig. 5.5 the time spectrum of the NSR discriminator, obtained for the full dynamic range of 10 keV to 2 MeV is shown as an example.

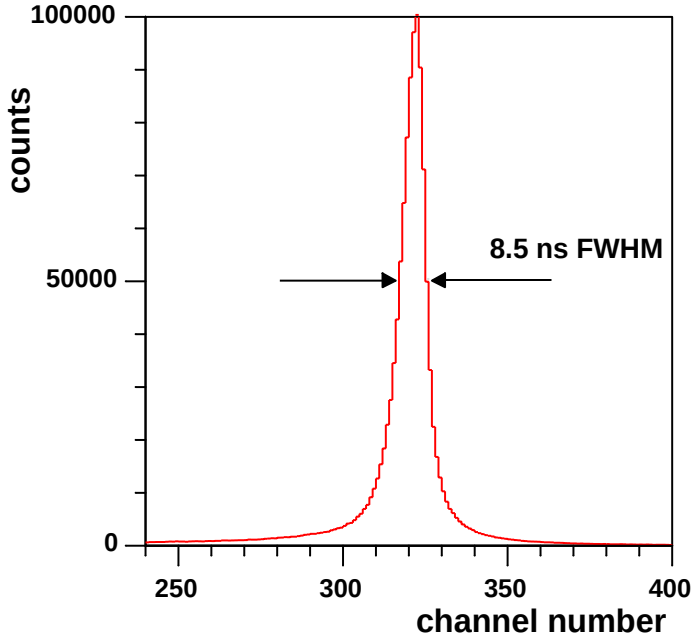

Fig. 5.5: *Experimentally measured sub sampling interval timing accuracy of the digital NSR discriminator running at 40 MSPS sampling speed.*

Position

Simulated signal shapes of a segmented, cylindrical Ge detector were used to test the combined Wavelet transformation - Pattern recognition - Correlation analysis (WPC) identification system. For the pre-processing stage, a custom wide-band wavelet transformation (WB4) was designed. It allows emphasizing localized temporary information on fast varying features of the signal via the determination of low scale coefficients, whereas from the higher scale coefficients the more global features are obtained. This method allows noisy signals to be correctly identified by the subsequent pattern recognition system, simply by weighting more on large-scale coefficients. The database of the pattern recognition system was created by storing the wavelet transform coefficients of pulses, simulated for positions on a grid with a distance between grid points of 1 mm. The identification stage, i.e. the pattern recognition and correlation analysis, comprises in principle three steps. First, the irradiated segments are identified. Second, the pattern classes of those segments are found, defining mainly the radius of the interactions and the segments in which mirror charge signals are expected due to these interactions. Finally, the decomposed relative amplitudes of the mirror charge wavelet coefficients of the mirror charge segments are analysed and correlated to the real charge wavelet coefficients of the corresponding irradiated segments.

Results of a two-dimensional wavelet analysis of a 8-fold segmented true-coaxial detector are shown in figure 5.6**.** The simulated interaction points are marked by dots while positions derived by the wavelet analysis are indicated by open squares The segments 1, 2 and 5 show real signals while all other segments, except 7, show mirror signals. In segments 1 and 2, the real signals are superimposed by mirror signals. The agreement of the results of the WPC analysis with the original simulated interaction positions is excellent. It should be pointed out that two interactions were assumed in segment 1 and that both interactions have been identified with high precision. Hence, it is possible to decompose pulse shapes resulting from the superposition of several signals, here two real and one mirror signal.

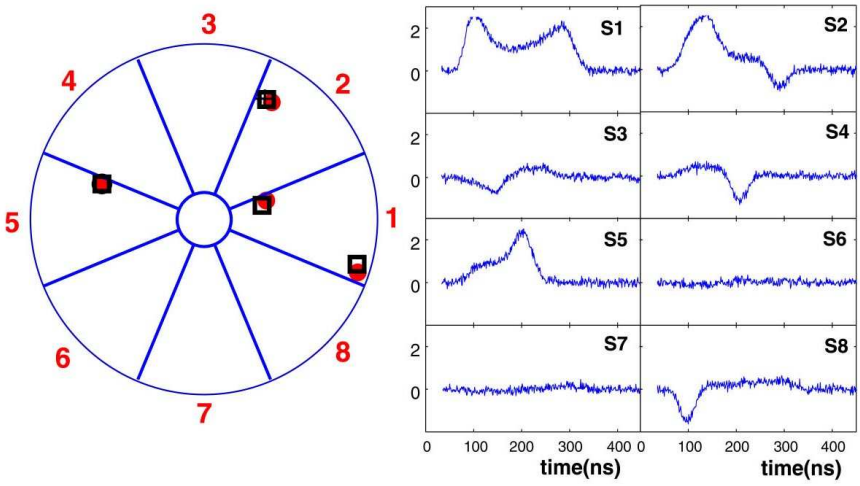

Fig. 5.6: *Cross section of a 8-fold segmented coaxial Ge detector with simulated interaction points (dots) and derived positions (open squares). The interaction points are at different depths in the detector. The left panel shows the simulated current pulse shapes, with added noise, as seen in the eight segments.*

The WPC analysis has also been applied to a determination of the interaction coordinates in three dimensions, considering that the Ge detector is also segmented in longitudinal direction. A Ge detector with an eight-fold azimuthal and a four-fold longitudinal segmentation has been assumed. In fig. 5.7 the resulting position resolution of the WPC analysis is given for three different noise levels. A similar precision for the localization of the interaction points in three dimensions as for the two-dimensional case has been obtained. It was found, that the interaction positions in a Ge detector can be determined with a resolution of the order of 1 mm^3 for single events. Multiple hits may be resolved if they lie more than 2 – 3 mm apart. The position resolution depends on the noise. The limit of the position resolution is finally given by the dimension of the charge carrier cloud produced in an interaction, being approximately 1 mm.

The Artificial Neural Network (ANN) and the Genetic Algorithm (GA) approaches were tested using samples of simulated signals for real and mirror charges of the 25-fold segmented MARS prototype Ge detector and experimental data measured with the 36-fold segmented prototype Ge detector of the GRETA project. First, signals originating from single interactions were analysed using a base system of simulated pulse shapes calculated on a 1.5 mm grid. The use of simulated pulse shapes for the base system was justified by a comparison between simulated and measured pulse shapes of both detectors, which showed that they agree well. The positions of the interactions were reproduced within 2.0 mm, when individual signals were analysed, and within 1.6 mm, when signals averaged for each position were used. Constructing artificial double interactions within one segment from these average signals, the positions of the interactions could be determined within 4.6 mm.

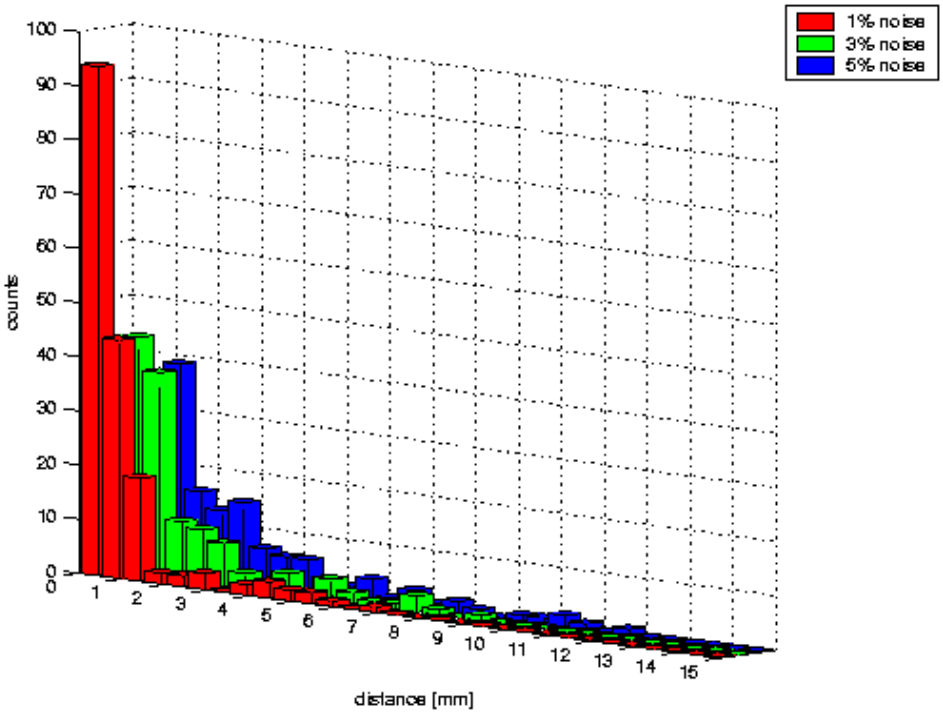

Fig. 5.7: *Position resolution of the WPC identification system in three dimensions for three different noise levels.*

The approach using artificial neural networks (ANN) for decomposition was also examined concerning its robustness against noise. The simplified problem having only one or two interactions within one segment was studied. Trained with noise-free signals, the success rate to recognise the correct number of interactions drops from 95% down to 58%, if the noise level increases from 0% to 10%. Success rates from 87% to 72% are achieved, if the training is done with signals having noise levels randomly chosen between 0% and 10%. The error in reproducing the position of single interactions increases with the noise level from 0.4 mm to 17 mm (training without noise) and from 0.8 mm to 4 mm (training with noise), respectively.

Conclusions

The worldwide efforts on the development of pulse shape analysis of detector signals for γ-ray tracking already now results in viable solutions for the on-line determination of the 3D position of the γ-interaction points, the deposited energies and the time. From algorithms tested, it can be concluded that a position resolution of about 2 mm can be achieved, i.e. interaction points as close as 2-3 mm apart can be separated. The energy resolution equals that of the best analogue electronics solutions and the time resolution even with moderate digitising sample rates of 40 MSPS is similar to state of the art CFD timing. The AGATA design parameters are thus based on these results. Future development will concentrate on the hardware implementation of optimised algorithms to minimize the computational effort and to maximize the throughput.

6. AGATA Electronics and Data Acquisition

6.1 Introduction

AGATA electronics will work on the principle of sampling the preamplifier outputs with fast ADCs to preserve the full signal information. Digital processing will be used to extract energy, timing and interaction position from the sampled data. Data will be time-stamped and software triggering will be implemented in the data acquisition system. Software triggering is very flexible, for instance it collects infrequent events efficiently and will allow the construction of delayed coincidences without dead time problems. It is planned to house the processing electronics as close to the detectors as possible in cooled, electrically shielded enclosures at the end of each cryostat. Data will be transferred by high bandwidth fibre links from the experimental area to the data acquisition equipment.

In the AGATA Data Acquisition system an Event Builder will receive data packets in parallel from the front end detector electronics. It will perform the necessary functions of time-ordering, data-merging and gain-matching in order to fully reconstruct the gamma-ray interaction sequence using tracking algorithms. User-defined data selection criteria will be applied to reduce the data volume by eliminating unwanted background data. Finally, formatted events will be written to the data recording medium with a data rate of up to 100 Mbytes/s. The processing power required to accomplish all these stages will be substantial, and will involve several stages of pipelining and parallelism.

6.2 System design

The AGATA system will digitise the detector's preamplifier outputs by sampling them using a fast Flash Analogue to Digital Converter (FADC). Using the data samples, the electronics will derive energy, time and position of each gamma ray interaction using digital data processing techniques. These data will be associated with an unique timestamp and an unique positional label which will be used by the data acquisition processors to associate data produced by the same physics phenomenon. Typical criteria used for associating data will be, for example, prompt or delayed coincidence windows and spatial correlations.

Each detector segment will have its own FADC producing data which need to be processed to extract energy, time and a 3D position from the data samples. Timing will be obtained by extrapolation after reconstructing the input pulse rise time using curve fitting. The start time will be recorded relative to the nearest timestamp or to an external time reference (or both).

Energy will be calculated by deconvolving the preamplifier's pulse response from the preamplifier output pulse, leaving the charge pulse from the detector which will then be filtered digitally to give the energy. Techniques for both timing and energy determination exist and have been implemented already commercially and in research projects. The position determination, however is a novel technique for which there are several algorithms under development. All involve analysing the shape of the current pulses resulting from the gamma ray interactions in the detector, not just in the segment collecting the charge, but also the

induced charge in the neighbouring segments. Using the segmentation geometry together with pulse shape analysis, a 3D position of the interaction within the detector can be derived. At present no algorithm for position determination in a closed end coaxial detector where multiple interactions occur under each segment has been implemented on processing hardware. The closest is an algorithm which works on true coaxial detectors [Gat01] and processing power estimates are made using this algorithm as a guideline (one (1) Field programmable Gate Array (FPGA) and one (1) DSP per segment).

Several arrangements of the processing electronics are possible ranging from a highly integrated scheme, option **A**, which packs all the digital processing in the detector and uses fibre optics for data transmission, through to a conventional modular solution, option **C**, where preamplifiers are connected to racks of external electronics using coaxial cables. Between these two extremes, other options are possible too, one of which is shown as **B** in the following diagram. The possibility of incorporating FADCs at the preamplifier and transmitting the full digital data stream over fibres to an external processing system was considered. It was rejected because of the high data rate (almost 50 Gbits/s) which necessitates multiple fibres from each detector .

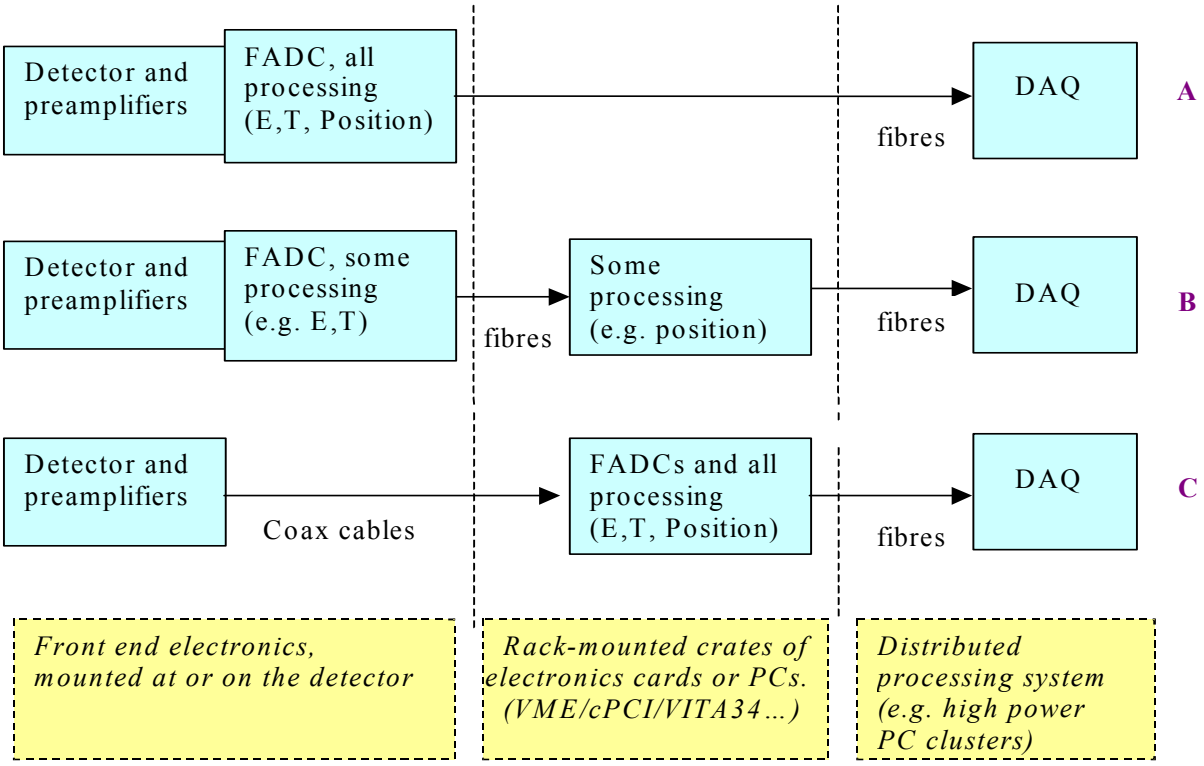

Fig. 6.1: *Various options for distribution of processing.*

The E, t and position parameters will be packed together with data from the other segments, a detector and segment identifier and a header word into a data block for transmission via a fibre network to the data acquisition system. As a diagnostic aid for low rate setups, or for single detectors at higher rates, the raw data samples (or a subset) may be sent as data too. This is not the normal mode of operation because the data volume for raw data transmission

from all active channels would be very high and so would lead to un-necessary expenditure on additional data transfer bandwidth.

The data acquisition will receive the data from all the detectors and process them in three stages. Firstly several parallel processes will merge the data and order it according to timestamps. The ordered data will be sent to the second part of the processing which reconstructs the gamma ray tracks around the whole detector shell using a large farm of processors. The third stage of the data acquisition processing will be to merge the data from the tracking farm, format it and transmit it to the tape drives for storage.

Data transmission from front end electronics to the data acquisition and within the data acquisition will use fibre optic connections. Several options have been considered, and the current candidates are Gigabit-Ethernet and 10 Gbit-Ethernet. Bandwidth considerations (including internal bandwidth) are discussed later in the data acquisition section.

The system will be controlled from a Graphical User Interface (GUI) from which the user can load experiment configuration files which control all the processing described so far, either by fine-tuning parameters or by reloading a whole processing section with new code. A separate control network path will be used, with IEEE1394 (Firewire) interfaces into the front end electronics for control, setup and monitoring. As well as reading/writing all registers, the Firewire interface provides a route by which the processors can be reprogrammed by downloading new processing algorithms. Signals in the electronics will be monitored using FADCs to digitise and display analogue input signals and a logic analyser function, together with JTAG access, to display digital signals. JTAG will also be used for DSP debugging. Monitored data will be timed using the same global timestamp as the event data (to permit comparisons of data from many sources) and made available via the control network for display in the GUI.

AGATA's global timestamp will use a distributed common timing clock sent to all the electronics down paths of equal length, each with a fine vernier delay adjustment. Certain edges of the clock will be selected at predetermined times to set up and maintain synchronisation. Using the common clock, data will be timestamped when they are generated and packed into events in software based on software triggering conditions such as coincidence and delayed coincidence windows.

6.3 Electronics design

This section describes options A to C, noting advantages and drawbacks of each. The choice between the options will be made at the time when the detailed design specification is produced. The factors to be taken into account include:

- the progress of development of highly integrated low power electronics for other instrumentation projects (using ASIC and other miniaturisation techniques) which could possibly be exploited in AGATA
- whether the progress of commercial electronics towards lower power and higher performance matches the assumptions made in this document

- the maturity of the position determination algorithm and the processing power required
- the amount and competence of the manpower available for the project.
- whether the cooling and Electromagnetic Compatibility (EMC) issues for options A and B are expected to be overcome by a reasonable investment of manpower and funds.

Electronics description

All three options carry out essentially the same function, as described in section 6.2. What differs is the level of integration and the consequences for the system design (cabling, cooling etc.)

Option A

The full processing electronics for each detector is integrated into a single shielded metal box and becomes an integral part of the detector, mounted either in a compartment within the detector module or in a separate enclosure behind the dewar. The electronics will be in three stages, each comprising one or two PCBs depending on the overall dimensions. The first stage is the input which will contain 36 analogue pre-filters, 36 fast flash ADCs and 36 Field programmable Gate Arrays (FPGAs) for time stamping, data buffering and some data processing (energy and time).

Secondly we have the processing stage containing an input switching matrix to connect the active segments to the 20 processing elements for the position determination, each comprising a DSP and an FPGA. This stage also contains the high bandwidth fibre optic data output with data packing.

The third section is the control and power supply stage containing the HV module to bias the detector, the analogue and digital supplies for the other two stages. All these will be derived from a single input voltage. The IEEE 1394 (Firewire) control/monitoring/reload interface is in this section too. Inspection points for key internal signals will be multiplexed in the control stage to both feed-through connectors and the internal oscilloscope and logic analyser which will transit data frames over the Firewire interface.

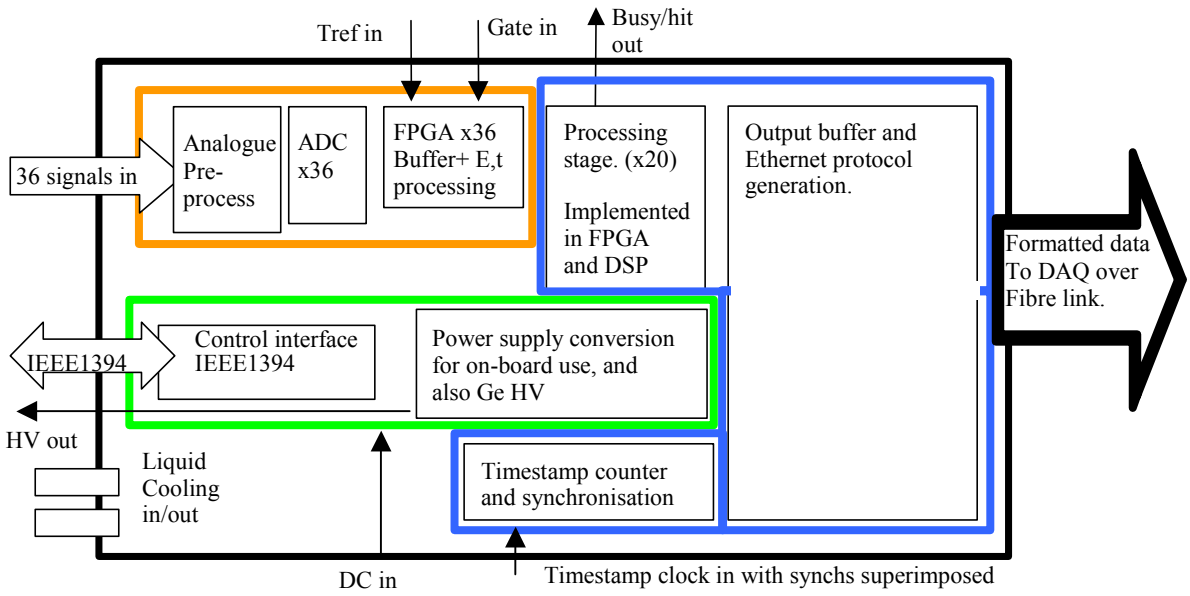

Fig. 6.2: *Option A electronics*

The main advantages of option A are that

- It drastically reduces cabling compared to a conventional approach.
- Detector, electronics and HV become one integrated unit which can be tested and moved as a complete entity.
- It offers a fully modular approach to systems design: each additional detector brings its own electronics and HV.
- Use of fibres to reduce grounding problems is another significant advantage.
- Digitising at the detector also improves noise immunity during data transmission.
- Use of programmable devices (FPGAs) and DSPs means that enhancements to algorithms can be made without changes to the hardware. FPGA changes will require the intervention of engineers. The use of DSPs with a software communications harness allows users to download their own compiled C code if they want to modify the processing algorithm.

The drawbacks are that it assumes certain inherent difficulties can be overcome.

- The integrated electronics is estimated to dissipate 180 watts, even after allowing for advances in IC technology over the next few years, so a dedicated cooling system is required.

- Temperature stability is key to good data stability, so a very well controlled thermal environment is vital.

- A potential problem is that of injecting electronic noise at the detector: the fast digital electronics must be very well isolated from the sensitive low level analogue signals coming from the Ge crystal.

- Another assumption is that the algorithm for position determination in a segmented closed-end coaxial detector will be known before the processing stage is designed (this document presupposes that the extra processing power required compared to the true-coaxial algorithm will be provided by the advances in DSP and FPGA technology over the intervening few years.)

Option B

Option B is similar to A except that some of the processing (shown in blue) is removed from the integrated electronics and moved to a new stage. The position determination is implemented in external processors, for example a PC farm such as a Beowulf cluster. Another possibility is to use rack-mounted processing in VME cards using either DSPs or other processors. The front end integrated part of the electronics will be mounted at the detector as described in option A. It will contain the input stage with flash ADCs and the processing for energy and timing. Part of option A's processing stage must be retained in the front end electronics at the detector in order to be able to transmit the data to the external processing farm. So the output buffer, data formatting and fibre driver remain at the detector along with the control, monitoring and power supply stage which is the same as option A.

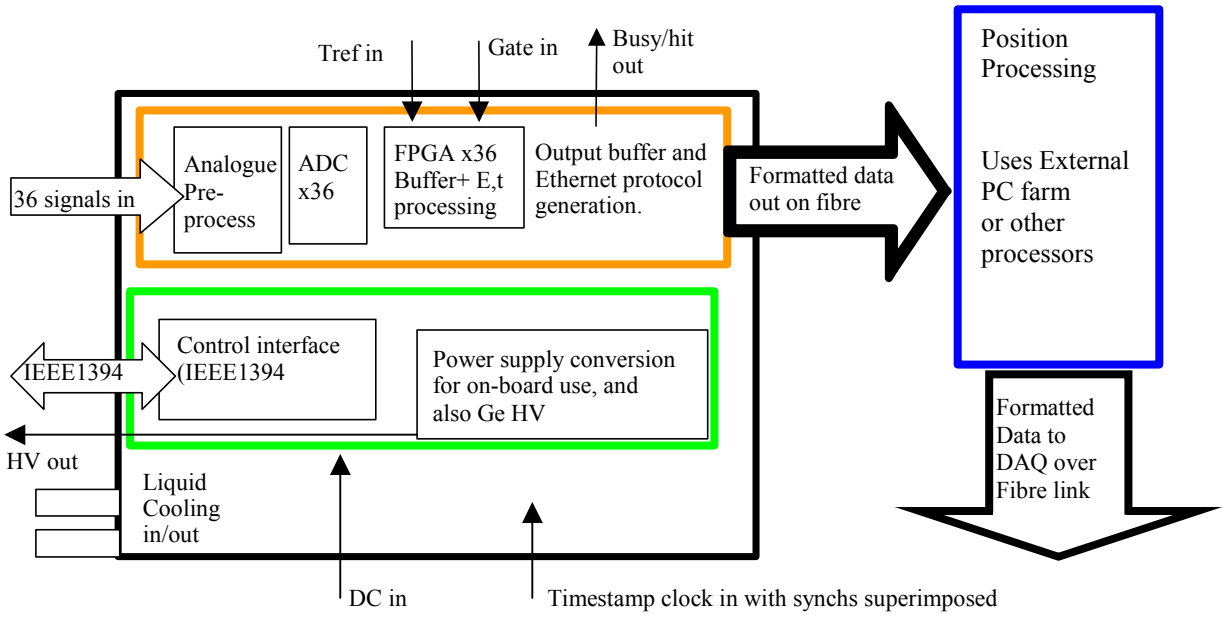

Fig. 6.3: *Option B electronics*

The main advantages of option B are similar to A:

- It reduces cabling compared to conventional approach (but not as much as option A)

- Detector, front-end electronics and HV become one integrated unit which can be tested and moved as a complete entity. It offers a somewhat modular approach to systems design: each additional detector brings most of its own electronics and HV.

- Use of fibres to reduce grounding problems is another significant advantage.

- Digitising at the detector also improves noise immunity during data transmission.

- Use of programmable devices (FPGAs) means that enhancements to algorithms can be made without changes to the hardware. FPGA changes will require the intervention of engineers.

- The use of external processors means that additional processing power can be added for the position determination algorithm if a better algorithm is found. This is constrained only by financial resources.

- A PC based processor farm can be purchased on a just-in-time basis to get the best possible value for money. The estimated cost of the 20 DSP+FPGA processing elements in option A equates to 4 nodes in a high speed PC processor farm, shared by 36 segments. If DSP cards are used then a communications harness would be required, as proposed for option A, to provide an environment in which users can run their own C code generated using an optimising C compiler targeting the DSP family.

The drawbacks of option B are also similar to those of A and it is assumed certain inherent difficulties can be overcome.

- Firstly the integrated electronics is estimated to dissipate 110 watts, even removing the position processing, so a dedicated cooling system is still required.

- Temperature stability is key to good data stability, so a very well controlled thermal environment is vital.

- A potential problem is that of injecting electronic noise at the detector: the fast digital electronics must be very well isolated from the sensitive low level analogue signals coming from the Ge crystal.

- The extra processing between the detector electronics and the DAQ adds more connections and makes testing a detector and its electronics in isolation dependent on a powerful PC.

Option C

The third option offers the most conventional backup solution in which no electronics are housed at the detector apart from a conventional fast preamp. The digital pulse processing electronics would be implemented electronics in a card/rack system such as is used in existing arrays. The cards would contain either the new electronics described in this document or else repackaged/enhanced versions of electronics which is available or under development from Milan, Juelich, Daresbury, or CSNSM Orsay. The card/rack system would be a commercial bus format (VME, Compact PCI, CAMAC or VITA34 if it becomes available on the right timescale). Typical density would be 16 channels/card. To illustrate the scale, using VME crates this means 424 modules in 21 crates, housed in 7 water cooled 19 inch racks. The inputs would come via almost 7000 coaxial cables from the AGATA detector's preamps.

The advantages of option C are:

- The smallest amount of manpower and development work is required if the system is based on enhancements of existing designs.
- No risks with electronic noise injected into the detector from the digital electronics.
- Flexibility, limited only by finance, for the hardware with which to implement the position algorithm is provided by this solution as it is in option B.

The disadvantages are:

- The risk of noise in the system unless the cable management, and grounding are implemented perfectly.
- Power dissipation in the racks is a problem, so water cooling will be required in the electronics racks rather than at the detector.
- A separate HV system must be purchased and cabled in. A test lab HV system will be required for detector testing.
- The need for 7000 coax cables and 190 HV cables around the AGATA array.

A note about costing

Costs would be broadly similar in all three options because essentially the same electronics and processing must be implemented. Costs have been estimated assuming that all electronics is designed and built within the collaboration or by sub-contractors. Where commercial units are used (as processors in options B and C and possibly as front end electronics in C) the price would be increased because the commercial companies need to make a profit, pay overheads and recover development costs. However, the development manpower reduction within AGATA would partially compensate for the higher price of any commercial units used.

Triggering

The AGATA system will be designed to be triggerless, using timestamps to correlate data in software by applying prompt or delayed coincidence conditions. However, in a few of the proposed configurations the counting rates will be very high and would overrun the data acquisition. The choice must be made between spending even more on the data acquisition (often subject to the law of diminishing returns near the performance limit) or to use some sort of hardware rate reduction. AGATA will use an optional rate reduction system whereby each channel has a gate input which can either be permanently enabled (free running) or active only when an input pulse is present. Externally a hardware multiplicity can be calculated by counting the coincident busy/hit pulses and the resulting threshold discrimination output pulse applied to the gate inputs. The busy/hit pulses will be produced by digital discriminators in the front end electronics, using a logic OR of all 36 segments. The gate input to a channel will be used in a delayed coincidence test with the discriminator's firing time and only if a coincidence is found will the data be passed on to the processing stage. In addition to the timestamps, the front end electronics will have a time reference (T*ref*) input to permit the γ arrival time to be measured against an external global time reference (beam RF, for example) as well as against the global timestamp.

Power Management

The electronics described here in options A and B is expected to dissipate 180 and 110 watts respectively, even allowing for lower voltages and improvements in efficiency over the next few years. Clearly the management of the heat will be a key part of this project. The electronics enclosure must be sealed against electromagnetic interference so that the detector resolution is not compromised by the fast digital processing. So the heat must be extracted by some sort of conduction system.

The heat extraction can be achieved using a liquid cooling system flowing through channels machined into the metal box housing the electronics. 190 flow/return systems would be required between the heat exchanger and the electronics so that all electronics gets coolant at the same temperature. A system without water pipe connections would be easier to manage when moving detectors and electronics, so alternative systems will be investigated as part of the project. For example a system which transfers heat through metal-metal conduction from the electronics box to an external closed loop fluid cooled system could be envisaged and is expected to be feasible if materials with the right thermal transfer characteristics are selected.

Inside the electronics box, thermal management will be a vital topic too, and care must be taken with component placement to accommodate the mechanical constraints brought in by the need to extract the heat.

It is recognised that thermal management is an important part of AGATA and that the electronics and DAQ will require mechanical engineering effort as well as electronics effort.

6.4 Data Acquisition

The AGATA array of detectors will provide a significant challenge in designing the necessary computing components required prior to writing event data to a recording medium.

The aim of this section is to try and show what may be available in about five years time, and attempt to estimate the computing power required for the AGATA Event Builder.

Where specific products are mentioned, they are only to be taken as examples and not as final choices for the project, since radical changes and improvements in technology may be expected on that timescale.

Detector Rate Contributions

There are three types of physics experiment presented as typical for the AGATA array.

- The first type involves collecting heavy ion and γ data, with perhaps ancillary detectors. The heavy ion rate could be as high as 10^7/s together with 10^5 γ events/s with multiplicity up to 30.
- The second type is similar to the first with the exception that the interesting γ events would be delayed, but with a prompt γ background. The rates of interest would be much lower.
- The third type involves no heavy ion detectors, collecting γ data, with perhaps ancillary detectors. The γ event rate could be as high as 10^6/s with multiplicity up to 40.

The various event rates quoted above imply a very high data rate to be read out over the network into the Event Builder. The data volume output from each detector needs to be reduced by simple coding in the front end electronics, so that the Event Builder is capable of receiving it.

All the following calculations assume that the data words from a detector are packaged into buffers prior to transmission over the network. Each buffer is assumed to have a 48-bit absolute timestamp and detector address in the header, and contain the data from many hits. Each hit would have a well defined sub-format for efficiency including a relative timestamp. It is expected that such packing will reduce the transmitted data rate by about a factor of three.

Of the three types of experiments presented, the two that include heavy ion detectors have a lower overall data rate. The Ge detector total event rate is assumed to be $3 \cdot 10^5$/s with an average incident multiplicity of 5. This results in 1.5 M γ-quanta /s and about 8k/s/detector. The total transmitted data rate would be of the order of 60 MB/s. The heavy ion detector total event rate is expected to be 3 10^5 and contribute around 16 MB/s data rate. The data rate contribution of any ancillary detectors will depend on detector type. Data rate estimates can vary from 40 MB/s to 200 MB/s.

The third type of experiment under consideration involves a stable beam and no heavy ion detectors, and will involve a higher data rate. The Ge detector total event rate is assumed to be $3 \cdot 10^5$ /s with an average incident multiplicity of 30. This results in 9 M γ-quanta/s and about 50 k/s/detector. The total transmitted data rate would be of the order of 360 MB/s. The data rate contribution of any ancillary detectors will again depend on detector type. Data rate estimates can vary from 400 MB/s to 2 GB/s.

Tracking analysis

Investigations of tracking algorithms suggest the computing power required for a full calculation is enormous. Typically, one can decode one detector at 1k events/s on a 200 MHz PC. Even accounting for improvements in efficiency to 2.5k events/s, then scaling up to future PC performance levels will give about 250k /s. This implies 90 cpus. For a total calculation including the whole array, increase this by, say, an order of magnitude, and we require 900 cpu equivalent power. It is conceivable that this processing could be achieved in a Beowulf cluster of probably dual-processor machines.

Network transmission

Ignoring ancillary detectors for now, since they can be treated separately in a similar way, and looking at the higher rate case of experiments, results in a data rate of about 360 MB/s.

It may not be sensible to cope with that rate using standard IP protocols. Specific optimised network interfaces using, for example, buffer lists and bus-mastering DMA would probably be necessary. Developments in virtual interface architecture are being made that dramatically reduce the processor overhead involved in network access. These developments are currently proprietary. It would be possible to use different network architectures for array to event builder transfers, as for event builder to tape server and data spy.

The standard PCI bus, even at 64bits and 66 MHz, would saturate at around maybe half maximum, allowing 250 MB/s to be transferred. Bearing in mind that this would be a sensible maximum for input and output combined. We would have to hope for a new higher capacity interconnect bus, or spread the processing load out.

As to product feasibility, there is a series of network solutions which satisfy the System Area Network and clustering market. These are all proprietary solutions, including, for example, Myrinet-2000 with PCI and PMC adaptors and open software. The hardware runs at 2 Gb/s per node, and has the advantages of low cpu utilisation and zero-copy delivery into DMA-able memory.

There are various products available now that could be used. Hence, it is not foreseen as a major problem in the future,

Control and Online monitoring

Control and setup of the data acquisition system will be via LAN connections to each detector electronics. One or more standard workstations are sufficient for this task. All necessary set-up and control will be automated via user-friendly GUIs.

Data monitoring is an important feature of all data acquisition systems. The data transfer from the Event Builder system to storage on a recording medium will be via a private high-speed LAN. One or more workstations can spy on this data stream in passing to analyse data quality, and perform initial analysis. A system provided program should be available to provide standard information. It is anticipated that a standard interface be provided to allow user written programs to be executed.

Data Storage

When considering tape drive parameters, the uncompressed data rate should be taken as the more correct figure, since it is necessary that the event data format be reasonably efficient to ease data transfer problems.

The currently available tape drive of choice would probably be the DLT8000 at 6 MB/s uncompressed data rate and 40 GBytes capacity. There is also the LTO drive which is currently available at 15 MB/s and 100 Gbytes capacity.

However, it is known that tape drives of higher data rate and capacity are being proposed. For example, the Super DLT range has a roadmap indicating drives of 80 MB/s uncompressed data rate, and capacities of 1 Tbyte at some future date. High data rates and capacities are available now, but are very expensive for drive and media.

The rates described above would imply post-tracking formatted Ge events of 10-20 MB/s ignoring heavy ion and ancillary detector contributions.

Hence, it looks feasible to write data at many 10's of MB/s in the timescale of this project, but probably at a higher cost compared with, say, a DLT8000 currently.

Data Analysis

Although not included in the costings for data acquisition, offline analysis of the experimental data must be considered.

The project will need to investigate new technologies such as GRID which is being promoted for LHC analysis by CERN. This would involve regional data centres connected by high speed network links where data would be stored and analysed. This would require very large disk arrays and sufficient processing power.

It is expected that the project will also need local infrastructure at the host laboratory to support the experimental program. It should be noted as an order of magnitude example, that a five day experiment running at 100 MB/s will produce around 43 TBytes of data.

Cpu performance

Various cpu manufacturers have announced performance improvement estimations up to around 2011. At this time it is hoped that 10 GHz cpus will be available with around 100 times current performance. However, this is too far into the future for us. In around five years time it is stated that cpus running at speeds in the region of 4 GHz with 10 times current performance are the aim.

Whatever the exact numbers, this information shows that the cpu chip manufacturers still expect Moores Law to apply over the next decade. This is essentially that performance doubles every 18 months.

So, to make estimations of the computing power requirements, in the rest of this document units of a "standard" cpu power are used that might be available in five years time. Assuming that todays standard is an Intel/AMD chip of around 1 GHz, it is proposed to work with 8 to 10 times that performance for a single microprocessor.

Design

This section does not propose a definite system design, as this could change with revised data rates and available technology, but merely an example of a scenario that would work.

Taking the third case Ge detector data rate of up to 360 MB/s, with present technology (PCI bus) one would need to limit the input data rate for one computing element to around 125 MB/s. Let us assume that this would require six separate PCI busses.

The array data could be transferred to one of six computing systems for localised data processing. These are represented as Partial Merges in fig. 6.4. The heavy ion data could be processed separately, and the relevant information broadcast to these systems. Each system would need sufficient memory to hold the data until the processed heavy ion data arrived. Then the data would be split into sections of timestamp and transmitted to tracking processors.

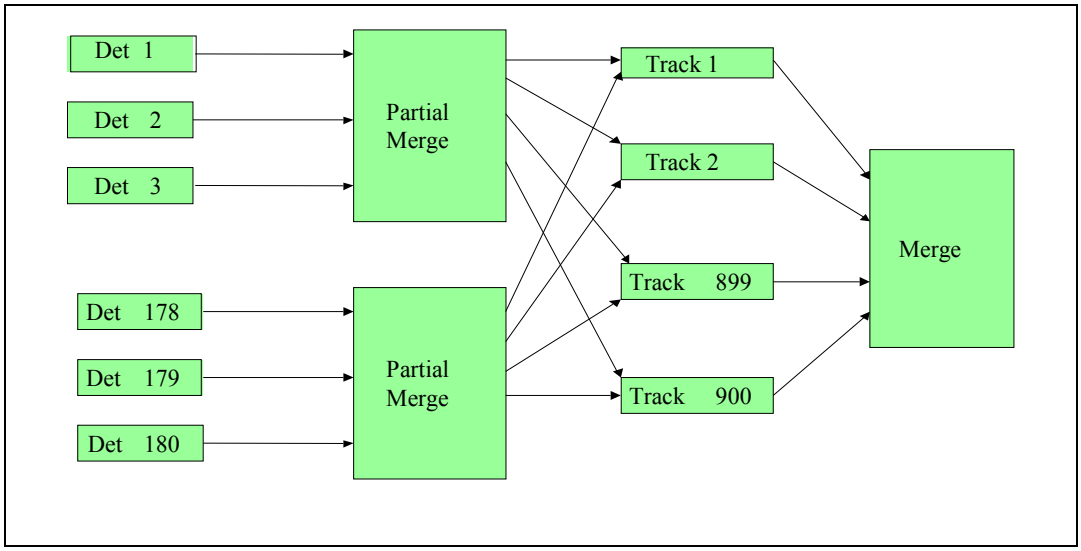

Fig. 6.4: *Merging of data.*

Each tracking processor in turn would receive an agreed range of timestamps. Problems at this stage involve synchronisation and coping with boundary effects. For example, how to cope if a section of data did not arrive for a particular processor.

The data for one particular tracking processor would be available at the full data rate, and hence, may take longer to transmit than receive from the front end detector systems. Hence, overlapped transmission for several adjacent tracking processors would be necessary.

The tracking processors would merge the received partial events and then apply a multiplicity filter if necessary, before processing the events through the required tracking algorithm.

Then, a much smaller data set would be output to a further computing system for data merging and formatting. Ancillary data could be merged at this point also, after any necessary or possible data reduction steps. The resultant total data stream would then be transferred to recording medium and spy workstations. The maximum output data rate would be of the order of 80 to 100 MB/s.

It must be noted that there is a single system at this merge point. This will limit the total date rate to tape. It would be possible to write to tapes in parallel by merging partial events into more than one system at this point.

7. Quality Assurance

This project is on a different scale of size to any previous γ-ray array worldwide. Current arrays have typically a few hundred-detector channels (e.g. GAMMASPHERE 110, EUROBALL 239, MINIBALL 280), whereas AGATA will have almost 7000 channels! Moreover, unlike conventional arrays where the failure of a few percent of the channels reduces the overall efficiency only linearly, in a tracking array the tracking capability is also diminished which compounds the reduction in efficiency. Therefore the **reliability** of the whole system is of utmost importance.

Disentangling the interactions of many γ-rays is an inherently complex process, which is very sensitive to any kind of disturbances like thermal drifts or data flaws. The volume of data is such that raw data can't always be stored, so errors in the online processing are very hard or even impossible to repair later offline. To make such a system manageable and maintainable all detector, electronics and software components must be stable and controlled. Interfaces and operating procedures must be well defined and observed. Thus, a high **quality** of the components, the system and its operating modes is mandatory.

The AGATA project will have to deal with limited funds and particularly limited expert manpower together with an ambitious time plan. Therefore, to deliver the system as demanded and in time R&D, production and commissioning must be performed in an **effective** manner.

To make AGATA a reliable high quality array realized in an effective way requires sophisticated project management methods new to nuclear spectroscopy projects.

7.1 Quality and project management

There are several implications of working on a project as large as this: the most important is that the high level of funding and manpower utilised means that good project management practice is essential to control the work and the expenditure. This starts with realistic planning and continues through detailed specification to a design phase where not only timescale and cost, but also quality must be monitored. Thorough testing of prototypes and a small-scale system will prove that the design objectives are met before committing resources to the production phase.

Quality goals must be defined during the specification phase, for example temperature stability and thermal drift will affect the stability of peak positions in spectra. Electronics noise levels will affect peak width. Reliability of detectors, electronics, software and mechanics will define the mean time between failures (MTBF) for the complete system. Maintainability (time to exchange/repair faulty units or to fix software bugs) is another important design criterion. These points are in addition to the normal specifications of efficiency, resolution, data rate and functionality. It must be recognised that Quality, Time and Cost (including manpower) are inter-related, so any reduction in funding or manpower

results in a longer timescale or lower quality or both. Similarly a shorter timescale leads to either higher cost or a lower quality (less stable) system.

AGATA is developed and built in a European collaboration of groups and individuals with diverse knowledge, expertise and skills in all fields required for the project. Good project management will ensure that the necessary communication takes place between people with different background, different working styles and working in different geographical locations.

7.2 Project management method

Project management standards

A consistent approach to the execution of the project is necessary. Formal methods for project management including documentation and communication systems have been defined by some of the AGATA partner organisations (CLRC and IN2P3 for example) and will be applied to the AGATA project. Quality systems are defined, for instance, in the ISO9000 series of standards based on eight quality management principles including motivation and communication by both good leadership and involvement of people, effective use of resources by analysis of design processes and systems, making informed decisions based on facts. Appropriate features of quality management methodology will be used in AGATA.

Roles and responsibilities

The AGATA collaboration will establish representatives responsible for program and resources. It is assumed that the project as a whole will have a project manager who will oversee several sub-projects and interface with the representatives. Sub-project managers are required who will ensure that there is a project specification defining the scope of the project (what is and what is not included), the design goals, the initial estimates of cost and timescale, the key deliverables and what are the criteria for accepting that these deliverables work correctly. The specification should also define when reviews would take place during the project. The sub-project managers should then produce a project management plan including detailed scheduling, planning and costing, description of the methods to be used for monitoring and control of progress and resource usage, plans for achieving quality for identifying and managing risk and for change control. Tools, standards and procedures exist for all these things and should be used where possible.The sub-project managers report to the project manager. Team members are responsible to the sub-project manager. Their duties include: ensuring that their tasks, work packages or parts of the sub-project, are completed to the agreed specification, time and budget; reporting to the sub-project manager on the progress and performance of their task; escalating issues that are outside their authority to the sub-project manager.

Project management processes

There are several project management processes present in the conception, feasibility and implementation project life cycle phases. In the conception phase it is ensured that all ideas for the project are properly considered. An important part of it is the writing of an appraisal report, which in fact is this proposal. The feasibility phase starts when the project is approved.

Now a more detailed look on the scientific, technical and planning issues is taken, a formal project specification is written and approved at a preliminary review by the collaboration representatives. Planning is not a defined project phase but is a key process that will start during the feasibility phase and will continue into the implementation phase. It leads to a comprehensive project management plan. The project strategy has to be defined including: identification of the project's objectives, organisational structures, technical feasibility, logistics, risks, control policies, quality, communications and PR. Planning is necessary for time, cost and resource management, procurement, quality, progress control and documentation. The implementation phase consists of doing the work, namely designing, prototyping, testing, producing etc. The project management task in this phase is to monitor the project, to forecast the project performance and to correct deviations by appropriate actions. It is important to monitor and control progress, performance, changes, schedules, costs and quality during implementation and good project management provides the tools to do this.

7.3 Documentation

All documents are subject to changes whenever necessary. Any change to timescale, specification, quality, cost or manpower has to follow well-defined formal change control procedures and needs to be approved by the AGATA representatives.

The project specification describes the context, purpose and scope of the project, the deliverables, critical success factors, estimates of costs, effort and timescales and the agreed program of project and technical reviews.

The technical specifications describe for the sub-projects the technical details of the deliverables, like features, geometrical layouts, electronics schemes etc.

The project management plan includes plans for time, cost and resource management, procurement, risk management, reviews, progress reporting and control, documentation control, quality and safety.

The technical documentation includes the technical specifications of the final system, operating procedures and maintenance instructions.

8. Resources and time scale

A rough estimate of the cost of AGATA as described in the previous chapters yields about 40 M€ without tax. This includes development of prototypes, and the complete hardware including spares.

About 140 person-years of scientist's, engineer's and technician's effort is anticipated to realize AGATA. This assumes the detectors and the electronics (Option A) to be developed tested and installed by the collaboration as well as all the tracking and processing software.

The AGATA array is optimally realized in phases depending on progress in technology and the availability of funds. For the development, test and commissioning of the triple detector module, parts of the electronics and the tracking algorithms an EU IHP proposal has been submitted. After development of prototypes of the detectors and electronics a sub-array shall be produced to test the pulse shape and tracking algorithms. One quadrant of the final array will be built as next phase. Both, the rather complex data handling and the tracking procedure can be tested and optimized with this sub-array. During the manufacturing of the remaining hardware the quadrant can already be employed in nuclear physics experiments providing the capability of the EUROBALL array combined with the position resolution of MINIBALL and EXOGAM. The full AGATA array will be ready for operation within eight years.

References

[Ang01] RISING Letter of Intent '*Gamma-Spectroscopy with RISING at the FRS*, ed. G. de Angelis *et al*., June 2001, GSI.

[Baz92] D. Bazzacco, Proc Workshop on Large γ-ray Detector Arrays, Chalk River, Canada, (1992), AECL-10613, 376.

[Bea92] C.W. Beausang *et al.,* Nucl. Instr. Meth. A313 (1992) 37.

[Bec84] F.A. Beck, Proc. Conf. on Instrumentation for Heavy Ion Nuclear Research, ed. D. Shapira:Vol. 7 in the Nucl. Sci. Research Conf. Series (Harwood, New York) 1984,129.

[Bec92] F.A. Beck *et al.,* Prog. Part. Nucl. Phys. 28 (1992) 443.

[Byr90] Th. Byrski *et al.,* Phys. Rev. Lett. 64 (1990) 1650.

[Dag94] P.J. Dagnall *et al.,* Phys. Lett. B335 (1994) 313.

[Del99] M.A. Deleplanque *et al*., Nucl. Instr. Meth. A430 (1999) 292.

[Dia84] R.M. Diamond and F.S. Stephens, Proc. Conf. on Instrumentation for Heavy Ion Nuclear Research, ed. D. Shapira: Vol. 7 in the Nucl. Sci. Research Conf. Series(Harwood, New York) 1984, 259.

[Ebe96] J. Eberth *et al., Nucl. Instr. Meth.* A 369 (1996) 135.

[Ebe97] J. Eberth *et al*., Prog.Part.Nucl.Phys. Vol. 38 (1997) 29.

[Ebe01] J. Eberth *et al*., Prog. Part. Nucl. Phys. Vol.46 (2001) 389.

[Gam88] Gammasphere Proposal '*A National Gamma-ray Facility*', ed. by M.A. Deleplanque and R.M.Diamond, March 1988, LBL.

[Gas90] GaSp Collaboration Report, INFN/BE-90/11 (1990).

[Gas01] W. Gast, *et al*., to be published in IEEE Trans. Nucl. Sci. (2001).

[Gat01] E. Gatti *et al*., Nucl. Instr. Meth. A458 (2001) 738.

[Geo93] A. Georgiev and W. Gast, IEEE Trans. Nucl. Sci., Vol. 40, No. 4, (1993) 770.

[Geo94] A. Georgiev, W. Gast, and R.M. Lieder, IEEE Trans. Nucl. Sci., Vol. 41, No. 4, (1994) 1116.

[Ger98] J. Gerl *et al*., VEGA-Proposal, GSI report (1998).

[Her85] B. Herskind et *al.,* Proc. Second Int. Conf. on Nucl. Nucl. collisions, Visby, Sweden, June 1985 and Nucl. Phys. A447 (1985) 353c.

[Jae83] M. Jääskelänen *et al.,* Nucl. Instrum. Meth. 204 (1983) 385.

[Joh71] A. Johnson, H. Ryde and J. Sztarkier, Phys. Lett. B34 (1971) 605.

[Kon98] F.G. Kondev *et al.,* Phys. Lett B (1998).

[Kro00] Th. Kröll *et al*., Proceedings Bologna2000, World Scientific (2001).

[Kro01] Th. Kröll and D. Bazzacco, Nucl. Instrum. Meth. A463 (2001) 227.

[Lee90] I.Y. Lee, Nucl. Phys. A520 (1990) 641c.

[Lie84] R.M. Lieder *et al.* Nucl. Instr. Meth. 220 (1984), 363.

[Lie01] R.M. Lieder *et al.* Nucl. Phys. A682 (2001), 279c.

[Lun00] S. Lunardi *et al*., Prog. Part. Nucl. Phys. 2000.

[Mar99] J. van der Marel and B. Cederwall, Nucl. Instr. and Meth. A 437 (1999) 538.

[Met86] V. Metag *et al.*, Nucl. Part. Phys. 16 (1986) 213.

[Mih00] L. Mihailescu, W. Gast, R.M. Lieder, H. Brands, H. Jäger, Nucl. Instr. and Meth., A 447 (2000) 350.

[Mih01] L. Mihailescu, Ph.D. thesis (2000), to be published as Jül Report (2001).

[Mor63] H. Morinaga and P.C. Gugelot, Nucl. Phys. 46 (1963) 210.

[Nol85] P.J. Nolan, D.W.Gifford and P.J.Twin, Nucl. Instrum. Meth. A236 (1985) 95, P.J.Twin *et al.,* Nucl. Phys. A409 (1983) 343c.

[Nol89] P.J. Nolan and P.J. Twin, Ann. Rev. Nucl. Part. Sci. 38 (1989) 53.

[Nol90] P.J. Nolan, Nucl. Phys. A520 (1990) 657c.

[Ott75] G. Ottaviani, C. Canali and A. Alberigi Quaranta, IEEE Trans. on Nucl. Sci. Vol. 22 (1975) 192).

[Pfü01] M. Pfützner *et al.,* accepted for publication in Phys. Rev. C (2001).

[Ram39] S. Ramo, Proc. IRE (1939) 584.

[Rag86] I. Ragnarsson, Z. Xing, T. Bengtsson and M.A.Riley, Phys. Scr. 34 (1986) 651.

[Rie80] L.L. Riedinger *et al.,* Phys. Rev. Lett. 44 (1980) 568.

[Ros93] C. Rossi-Alvarez, Nucl. Phys. News Europe 3 (3) (1993) 10.

[Sch99] G.J. Schmid *et al*., Nucl. Instr. Meth. A430 (1999) 69.

[See85 K. Seeger, Semiconductor Physics, Springer (1985).

[Sha88] J.F. Sharpey-Schafer and J.Simpson, Prog. Part. Nucl. Phys. 21 (1988) 293.

[Sim87] J. Simpson *et al.,* J.Phys. G 13 (1987) L235.

[Sim97] J. Simpson, Z.Phys. A358 (1997) 139.

[Sim00] J. Simpson *et al*., APH N.S. Heavy Ion Physics **11** (2000) 159.

[Tar87] P. Taras *et al.,* 'The 8π Proposal' October 1983, J.P. Martin *et al.,* Nucl. Instr. and Meth. A257 (1987) 301.

[Twi86] P.J. Twin *et al.,* Phys. Rev. Lett. 57 (1986) 811.

[Vet00] K. Vetter, *et al*., Nucl. Instr. and Meth., A 452 (2000) 223.